Project funded by the European Commission under the 6th (EC) RTD Framework Programme (2002- 2006) within the framework of the specific research and technological development programme “Integrating and strengthening the European Research Area”

Project UpWind
Contract No.: 019945 (SES6)

“Integrated Wind Turbine Design”

VERIFIED MATERIAL MODEL INCORPORATING PROGRESSION OF DAMAGE DUE TO STATIC LOADING AND THE EFFECT OF FATIGUE ON RESIDUAL STRENGTH AND STIFFNESS

FADAS

AUTHOR:	T. P. Philippidis
AFFILIATION:	University of Patras, Dept. of Mech. Engng & Aeronautics, Section of Applied Mechanics
ADDRESS:	P. O. Box 1401, Panepistimioupolis Rio, GR 265 04, Greece
TEL.:	+30 2610 969450, 997235
EMAIL:	philippidis@mech.upatras.gr
FURTHER AUTHORS:	E. N. Eliopoulos
REVIEWER:	
APPROVER:	

Document Information

DOCUMENT TYPE	Deliverable
DOCUMENT NAME:	Verified Material Model Incorporating Progression of Damage Due to Static Loading and the Effect of Fatigue on Residual Strength and Stiffness
REVISION:	0
REV.DATE:	08.02.2011
CLASSIFICATION:	R1: Restricted to project members
STATUS:	S0: Approved/Released

Abstract: Work described in this technical report was performed in the frame of Task 3.3 “Damage Tolerant Design Concept” of Work-Package WP3 “Rotor Structure and Materials” of the UPWIND project. A non-linear ply-to-laminate approach to analyze failure onset and damage propagation in generic laminates under multi-axial cyclic loading was presented. The FADAS (FAtigue DAmage Simulator) algorithm implements in one hand simple phenomenological models to describe strength and stiffness loss at each ply due to fatigue and on the other hand adequate failure criteria to predict damage progression triggered by different failure mechanisms. It is a distributed damage model in the sense that constitutive material response is defined in terms of meso-mechanics for the unidirectional ply. The algorithm modules for non-linear material behaviour, pseudo-static loading-unloading-reloading response, constant life diagrams and strength and stiffness degradation due to cyclic loading were implemented on a robust and comprehensive experimental database for a unidirectional Glass/Epoxy ply. The model, based on property definition in the principal coordinate system of the constitutive ply, can be used, besides life prediction, to assess strength and stiffness of any multidirectional laminate after arbitrary, constant or variable amplitude multi-axial cyclic loading. Numerical predictions were corroborated satisfactorily by test data from constant and variable amplitude fatigue data and residual static strength/stiffness after fatigue from multidirectional Glass/Epoxy laminates. The agreement was satisfactory with most of the test results.

Contents

STATUS, CONFIDENTIALITY AND ACCESSIBILITY									
Status				**Confidentiality**				**Accessibility**	
S0	Approved/Released	**X**		**R0**	General public			Private web site	**X**
S1	Reviewed			**R1**	Restricted to project members	**X**		Public web site	
S2	Pending for review			**R2**	Restricted to European. Commission			Paper copy	
S3	Draft for commends			**R3**	Restricted to WP members + PL				
S4	Under preparation			**R4**	Restricted to Task members +WPL+PL				

PL: *Project leader* **WPL:** *Work package leader* **TL:** *Task leader*

1. Introduction

When complex stress fields are developed in composite structures operating under cyclic load, life prediction becomes a formidable task especially in cases of irregular spectrum loading. The implementation of the numerical procedure for fatigue analysis consists of a number of distinct calculation modules, related to the main theme of life prediction. Some of them are purely conjectural or of semi-empirical nature, e.g. the failure criteria, others heavily rely on experimental data, e.g. S-N curves and Constant Life Diagrams (CLD).

In cases of composite laminates under uniaxial loading, leading to uniform axial stress fields, the situation might be substantially simplified since almost all relevant procedures could be implemented by experiment. On the other hand, for complex stress states, the laminated material is considered being a homogeneous orthotropic medium and its experimental characterization, i.e. static and fatigue strength is performed for both material principal directions and in-plane shear. The relevant stress parameters taken into account when comparing with strengths in the failure criteria are the stress resultants (N_x, N_y, N_s), as defined in classical plate theory.

Such a *laminate approach* is a straightforward one, in predicting fatigue strength under plane stress conditions, avoiding the consideration of damage modelling, interaction effects between the plies and stress redistribution. The experimental data set required to implement the procedure, to cover variable amplitude (VA) loading for structures such as the wind turbine rotor blades, consists of a number of S-N curves at various stress ratio, R, values, not less than three, usually taken equal to R=10, -1 and 0.1. These characteristics must be derived for both principal material directions and in-plane shear, resulting in a total of at least 7 S-N curves by assuming that in-plane shear fatigue strength is independent of stress ratio, R. The experimentally defined fatigue property set is unique for each laminate. The approach was implemented by Philippidis and Vassilopoulos [1]-[4] for a Glass/Polyester multidirectional laminate of [0/±45] stacking sequence and was shown to yield satisfactory predictions for fatigue strength under complex stress conditions for both constant (CA) and variable amplitude (VA) loading.

When the number of different stacking sequences in a structural element is limited, the *laminate approach* is a reliable alternative to a life prediction task. However, with large composite structures, composed of different components of varying structural details, numerous laminates of different stacking sequences are usually in order. The huge number of test effort to characterize fatigue strength of all different lay-ups prevents from implementing a *laminate approach* methodology. In these cases, a *ply-to-laminate approach* in which experimental characterization is performed at the basic constitutive ply level and then fatigue strength of whatever laminate configuration is numerically derived, is certainly a more effective procedure.

Nevertheless, with such an option a number of additional calculation modules needs to be developed, requiring both theoretical and experimental implementation. These are related to how damage is modelled in each lamina, what are the implications in local stress fields and also on stress redistribution in neighbouring plies. Finally, how damage propagates as a function of loading cycles.

There are relatively few works published on the subject, most of them in the last fifteen years. Based on the *Internal State Variable Approach* of Lee et al. [5] to describe stiffness degradation of a material element due to distributed damage, Coats and Harris [6] and Lo et al. [7] have presented one of the first contributions in the field. Input data for damage progression were derived experimentally and consist of crack surface area and crack density measurements by means of edge replicas and X-rays. Model predictions were only possible for tension-tension loading while experimental verification was provided so far only for stiffness degradation as a function of the applied number of cycles.

The approach followed by Harris and co-workers is of the “ply-to-laminate” type in which all constitutive formulation takes place at the ply level. Prediction of life, strength or stiffness for a laminate of any stacking sequence, composed of the building ply is in general possible. One of the most complete works of that type of approach was published by Shokrieh and Lessard [8]-[9]. They have developed a method that could be used as a design tool, predicting life, residual stiffness and strength of a laminate based on ply properties. Linear stress analysis was performed, although nonlinear effects for the shear stresses were included in their failure criteria.

Van Paepegem et al. [10]-[15] have developed a stiffness degradation based damage mechanics model, using material properties of a cross ply laminate and not of the UD ply. So, the model does not predict failure modes of the ply but the macroscopic failure of the cross ply laminate. It includes a number of parameters, fitted by experiments on a specific load case (single side displacement-controlled bending) which probably depend on the stacking sequence and the load case.

Sihn and Park [16] have presented an integrated design module for predicting strength and life of composite structures. Their analysis was based on micromechanics of failure by considering separately the composite constituents. Viscoelastic behaviour of the polymeric matrix was also taken into account. No experimental evidence on the validity of their method was presented. Although this type of approach, based on micromechanics, seems promising for the future it has also serious disadvantages related especially to the mechanical characterization of fibre and matrix interaction and the description of damage evolution laws. Further, from an engineering point of view, composite material properties are certified at the ply level and thus before a life prediction method based on micromechanics could be used, wide agreement on characterization procedures and test methods should be sought.

In this work, a continuum damage mechanics method is implemented in a *ply-to-laminate* life prediction scheme for composite laminates under cyclic CA or VA loading. According to theoretical foundations of distributed damage, e.g. as in the works by Lee et al. [5], Ladeveze [17], Renard et al. [18], Maire and Chaboche [19], instead of considering the geometric description of a type of defect induced by local failure, a set of appropriate stiffness degradation rules is applied, resulting in a modified stiffness tensor, i.e. an equivalent, homogeneous, continuum description, such that either the resulting strain field or strain energy density under the same load is similar to that of the damaged medium.

This effective medium description requires besides *sudden stiffness* degradation due to failure onset driven by the stress at a point, strength and stiffness degradation as well of a progressive character due to cycling, expressed as a function of load cycles, n. Hence, residual strength and stiffness after cycling becomes of importance for this approach of *progressive damage mechanics* and certainly requires a great experimental effort, besides efficient modelling, to cover the various loading conditions, e.g. tension-tension (T-T), tension-compression (T-C), etc., at various stress ratio values and material principal directions.

To assess conditions for incipient failure in a specific mode, compatible with certain defect type and respective stiffness degradation strategy, appropriate failure criteria considering separately the various failure modes, such as those introduced by Puck et al. [20]-[22] or Chang and Lessard [23], were implemented in the numerical procedure.

The material model consists also of the detailed description of fatigue strength in each principal material direction and in-plane shear, for the basic building ply always, for several R values to ease the implementation of CLD formulations.

A detailed load step-by-step simulation of each cycle is foreseen in the realization of the algorithm, as it performs actually, however, albeit more accurate, this could be extremely time-consuming especially when the routine is implemented in finite element formulations. Alternatively, calculations are performed in steps for a complete cycle and then after a block, Δn, of cycles again a detailed complete cycle and so forth. The size of cycle jump is defined by the user.

Non-linear response of the unidirectional (UD) ply especially under static in-plane shear and normal loading transversely to the fibres is also taken into account, introducing appropriate models derived by fitting experimental data. In the numerical analysis, non-linearity is modelled by implementing an incremental stress-strain constitutive law.

An extensive comparison of life prediction and residual stiffness/strength numerical results with experimental data from CA or VA uniaxial and biaxial cyclic testing of UD and multidirectional (MD) laminates was presented.

2. Constitutive Laws

The progressive damage simulator for life prediction under cyclic complex stress presented in this work was initially devised for Glass/Epoxy composites used in the wind turbine rotor blade industry. It relies on material data from a huge experimental effort in the frame of an EC-funded research project that resulted in a comprehensive material property database with test results from static, cyclic and residual strength experiments under axial and multi-axial loading conditions. All data is free for download in the official OPTIMAT BLADES site (http://www.wmc.eu/optimatblades.php) along with the relevant reports and publications. Additional tests for deriving material models and verification purposes were performed in the frame of UPWIND.

2.1 Ply response under quasi-static monotonic loading

The basic building block of all laminates considered is the UD ply that will be called hereafter as OB_UD Glass\Epoxy. Besides information on mechanical property characterization that was reported in the OPTIDAT database as indicated in the above, most of the data were also presented in [24]. In-plane mechanical properties of the UD ply were obtained through an extensive experimental program consisting of static tests, both parallel and transverse to the fibres and also in shear. The unique specimen geometry used in the characterization procedure has replaced the numerous ISO geometry coupons in all kind of tests, static, fatigue and residual strength. Experimental data compare very well with those produced with ISO specimens, except the case of compression along the fibres where the so-called OB-coupon suffers from buckling (ISO strength is adopted). Shear stress-strain response was still obtained through ISO procedure, while shear strength was obtained through V-notched Iosipescu tests; see Megnis and Brøndsted [25].

UD material performs linearly in the fibre direction as expected, however transversely to the fibres, mainly in compression and under in-plane shear the material behaviour is highly non-linear. To take this into account, incremental stress-strain theory is implemented, retaining the validity of the generalized Hooke law for each individual interval:

$$\begin{aligned} d\sigma_1 &= \frac{E_1}{1-\frac{E_{2t}}{E_1}\nu_{12}^2}d\varepsilon_1 + \frac{\nu_{12}E_{2t}}{1-\frac{E_{2t}}{E_1}\nu_{12}^2}d\varepsilon_2 \\ d\sigma_2 &= \frac{\nu_{12}E_{2t}}{1-\frac{E_{2t}}{E_1}\nu_{12}^2}d\varepsilon_1 + \frac{E_{2t}}{1-\frac{E_{2t}}{E_1}\nu_{12}^2}d\varepsilon_2 \\ d\sigma_6 &= G_{12t}d\varepsilon_6 \end{aligned} \tag{1}$$

In the above equations, E_1 and ν_{12} were considered constant throughout the static loading up to failure, while the tangential elastic moduli E_{2t} and G_{12t} were given by the nonlinear constitutive relation introduced by Richard and Blacklock [26]:

$$\sigma_i = \frac{E_{o_i}\varepsilon_i}{\left[1+\left(\frac{E_{o_i}\varepsilon_i}{\sigma_{o_i}}\right)^{n_i}\right]^{\frac{1}{n_i}}},\ i=2,6 \tag{2}$$

E_{o_i}, σ_{o_i} are model parameters defined by fitting the experimental data. Tangential elastic moduli were derived using the following relations:

$$E_{2t} = \frac{d\sigma_2}{d\varepsilon_2} = E_{o_2}\left[1-\left(\frac{\sigma_2}{\sigma_{o_2}}\right)^{n_2}\right]^{\frac{1}{n_2}+1}, \; G_{12t} = \frac{d\sigma_6}{d\varepsilon_6} = G_{o_{12}}\left[1-\left(\frac{\sigma_6}{\sigma_{o_6}}\right)^{n_6}\right]^{\frac{1}{n_6}+1} \quad (3)$$

The parameters $E_{o_2}, \sigma_{o_2}, n_2$ were found different in tension and compression. Numerical values for all the above constants were summarized in Table 1. The predicted stress-strain curves compare favourably to the experimental data as seen in Fig. 1 and Fig. 2.

Mean values of the ply in-plane failure stresses were given in Table 2. By X, Y and S the respective strengths in the fibre direction, transversely and in-plane shear were denoted.

Table 1: Elastic constants (in MPa). OB_UD Glass/Epoxy

E_1=37,950 ν_{12}=0.28

	E_{o_i}	σ_{o_i}	n_i
$E_{2t}^{(T)}$	15,035	75	3
$E_{2t}^{(C)}$	15,262	188	2.18
G_{12t}	5,500	67	1.3

Table 2: Strength values (in MPa). OB_UD Glass/Epoxy

X_T	X_C	Y_T	Y_C	**S**
776	686	54	165	80

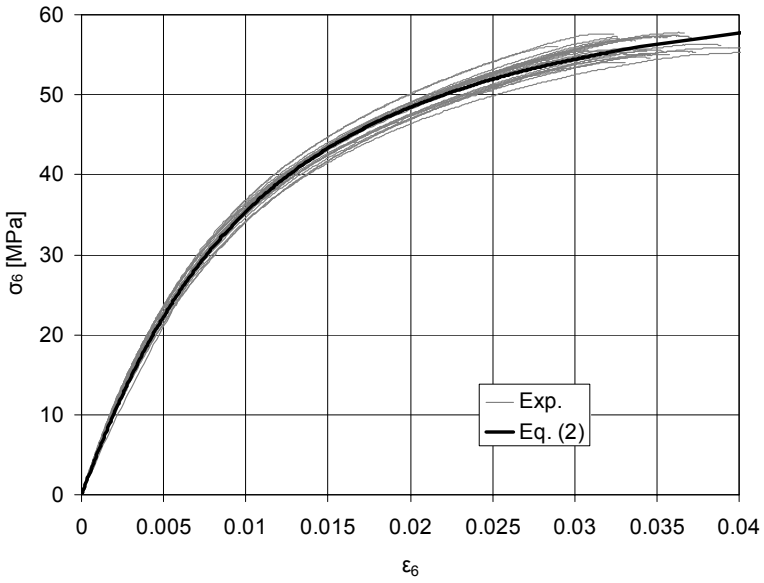

Fig. 1: In-plane shear stress-strain behaviour of OB_UD Glass/Epoxy

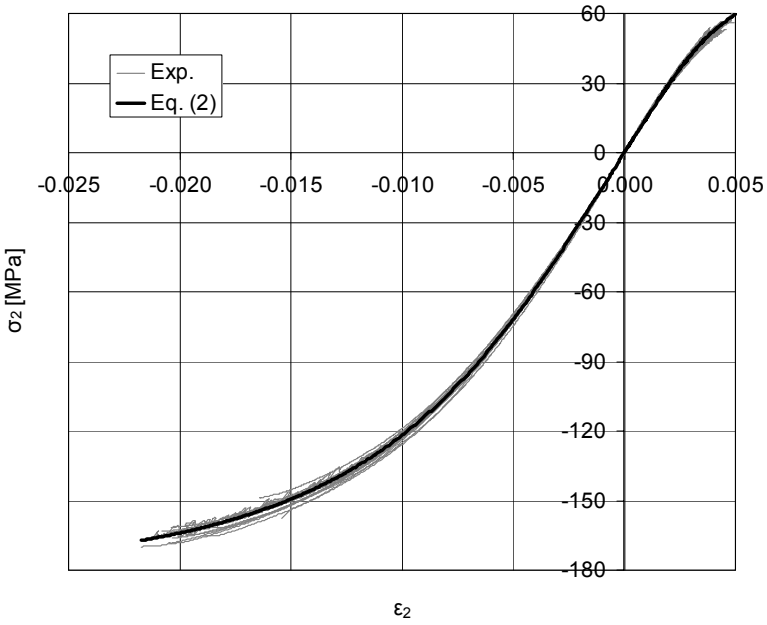

Fig. 2: Transverse Tension-Compression response. OB_UD Glass/Epoxy

2.2 Loading-unloading-reloading (L-U-R)

Engineering elastic constants appearing in the constitutive relations, Eq. (1), are valid for monotonic loading conditions. Upon unloading, the stiffness changes and must be again defined experimentally. It was further observed that stiffness decreases upon repeated L-U-R cycles, depending on the stress level previously reached. As compiled by Philippidis et al. [24], the stiffness reduction is more severe for matrix dominated response, e.g. in-plane shear and

transverse loading to the fibres. This type of stiffness degradation, although probably due to micro-cracking of the polymeric matrix possibly in the interface region with the fibres, and individual fibre breaks was considered as a constitutive tensor property of the lamina that was derived by means of dedicated experiments in the frame of UPWIND.

Two different load-controlled L-U-R test types were performed in order to study the effect of interrupting for some time between cycles. Type 1 was the interrupted test type (Fig. 3) in which the coupon remained unloaded after each loading-unloading cycle for $5t_i$, where t_i was the total duration of both loading and unloading time intervals of the i^{th} cycle. Type 2 was a continuous L-U-R test type (Fig. 4).

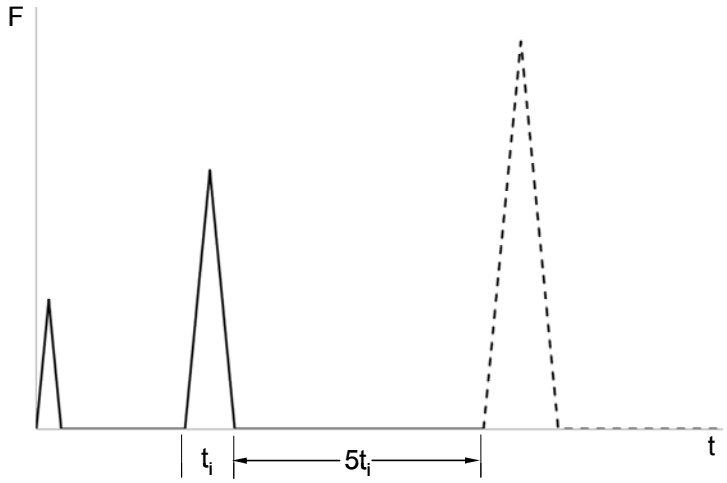

Fig. 3: Type 1 L-U-R test

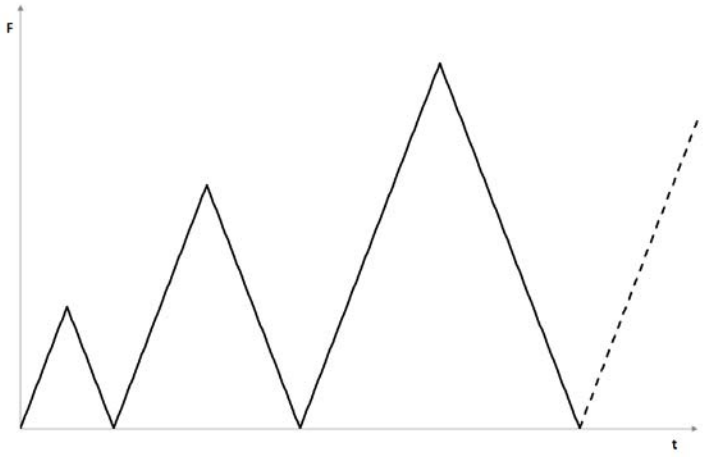

Fig. 4: Type 2 L-U-R test

The load increment and the loading and unloading rate were the same for both test types. The load increment was set at $F_{max}/20$, where F_{max} was the mean maximum load of the respective static tests [27]-[28]. The summary of the tests performed appear in Table 3. Detailed results for each series were presented in the Appendix of this report.

The loading and unloading rate was set equal to 40 kN/min for the tests on the $[0_4]_T$ laminate in both tension and compression. The stress-strain response of a tensile L-U-R test on the $[0_4]_T$

laminate which approximately lasted 4.2h appears in Fig. 5 along with the linear model for monotonic static loading (E_1 from Table 1).

Table 3: Number of coupons tested

Laminate	Test type			
	Type 1		Type 2	
	Tensile	Compressive	Tensile	Compressive
$[0_4]_T$	3	3	-	-
$[90_7]_T$	3	3	3	3
$[\pm45]_S$	3	-	1	-

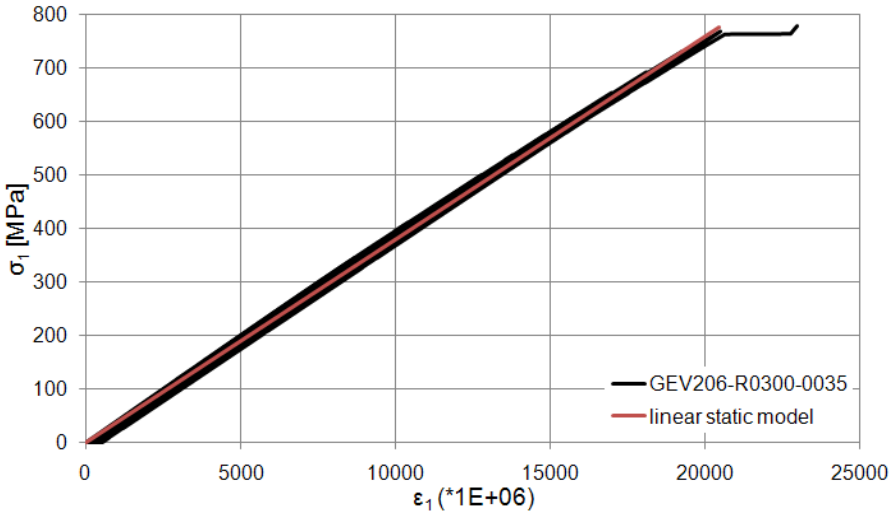

Fig. 5: Stress-strain curve of a tensile L-U-R test on the $[0_4]_T$ laminate

Strain was recorded during the L-U-R tests using strain gauges. The elastic modulus was determined as the slope of the linear regression model of each stress-strain loop. The values from a test were normalized with respect to the modulus of the first cycle and plotted vs. the normalized (with respect to the maximum stress of each test) stress level, see Fig. 6.

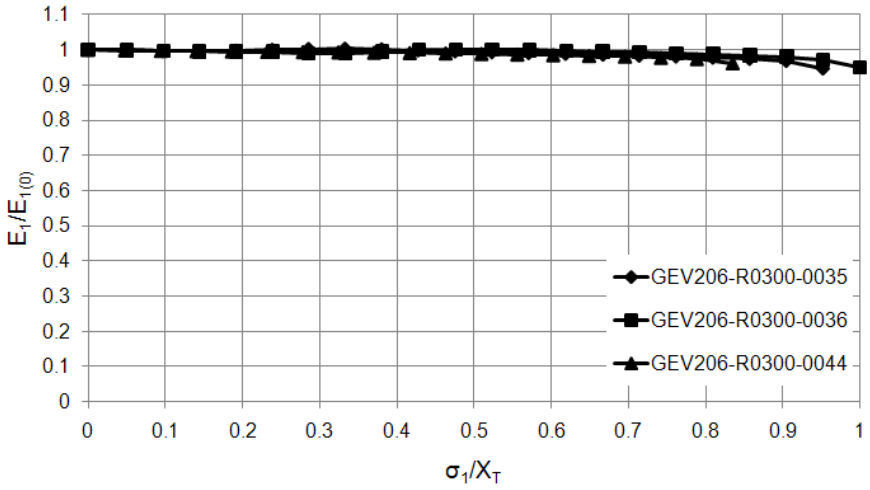

Fig. 6: Modulus degradation parallel to the fibres due to tensile L-U-R cycles

The stress-strain response of a compressive L-U-R test on the $[0_4]_T$ laminate which approximately lasted 2.4h appears in Fig. 7 and the respective modulus degradation in Fig. 8.

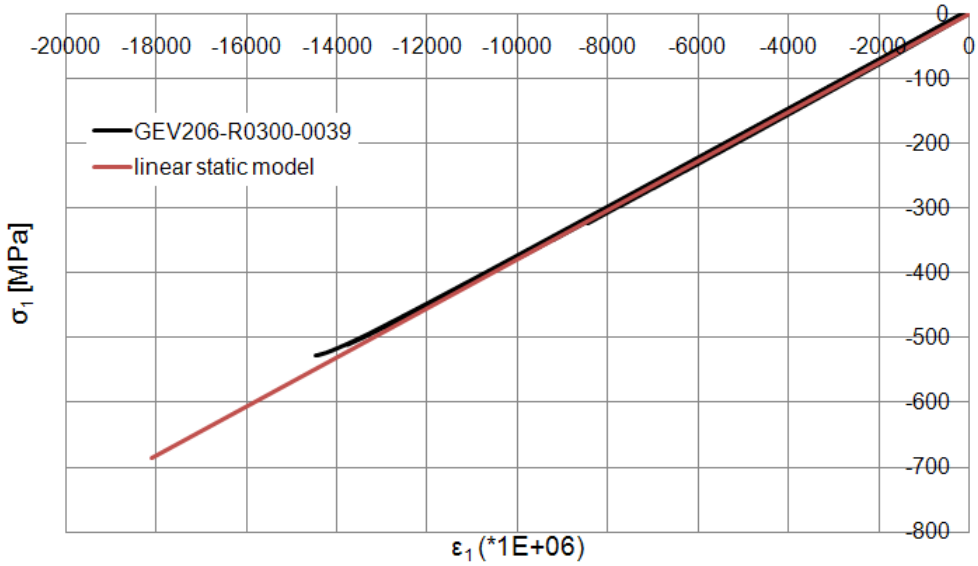

Fig. 7: Stress-strain curve of a compressive L-U-R test on the $[0_4]_T$ laminate

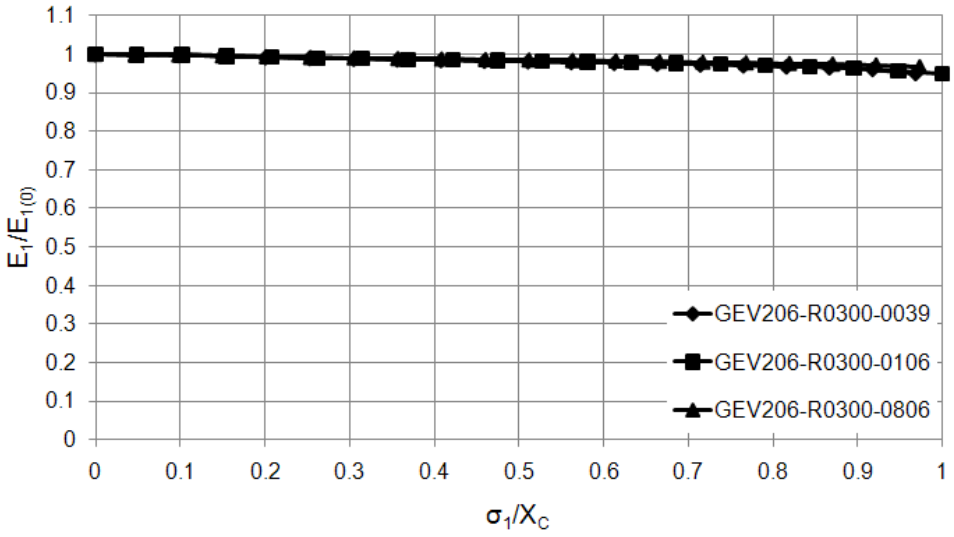

Fig. 8: Modulus degradation parallel to the fibres due to compressive L-U-R cycles

The E_1 modulus degradation due to quasi-static L-U-R cycles was not important, see Fig. 5-8 and was overlooked in the numerical model. The material behaviour can still be represented by the linear model introduced for monotonic quasi-static loading.

The loading and unloading rate was set at 25 kN/min for the tests on the $[90_7]_T$ laminate in both tension and compression. The stress-strain response of a tensile L-U-R test on the $[90_7]_T$ laminate appears in Fig. 9 along with the non-linear model for monotonic static loading, Eq. (2). The tensile tests of type 1 on the $[90_7]_T$ laminate approximately lasted 0.6h. The respective modulus degradation was shown in Fig. 10.

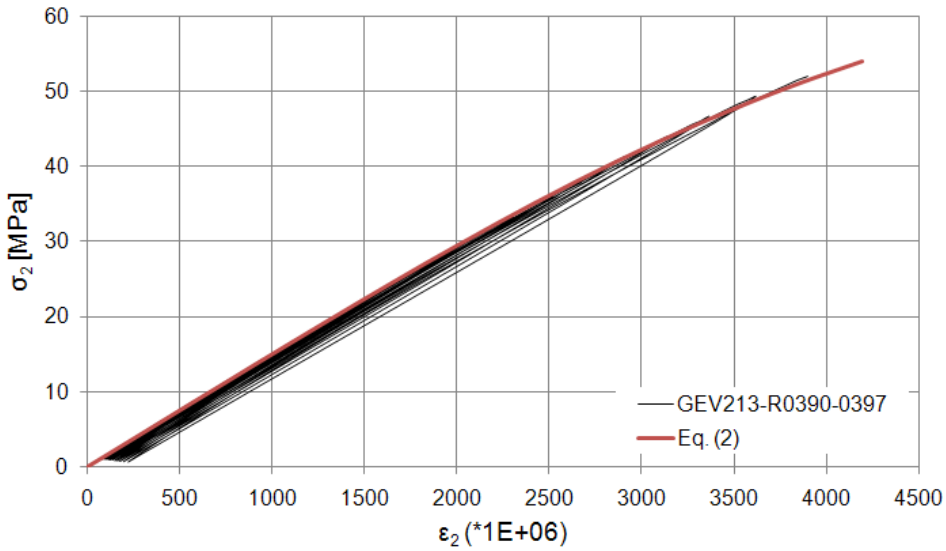

Fig. 9: Stress-strain curve of a tensile L-U-R test on the $[90_7]_T$ laminate

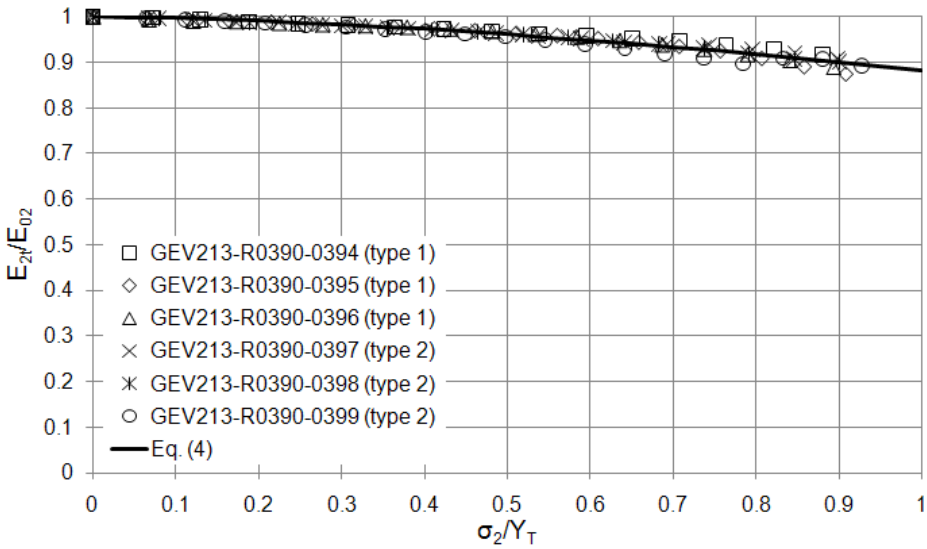

Fig. 10: Modulus degradation transversely to the fibres due to tensile L-U-R cycles

The stress-strain curves of two compressive L-U-R tests transversely to the fibres appear in Fig. 11, one of each test type. The respective modulus degradation was shown in Fig. 12.

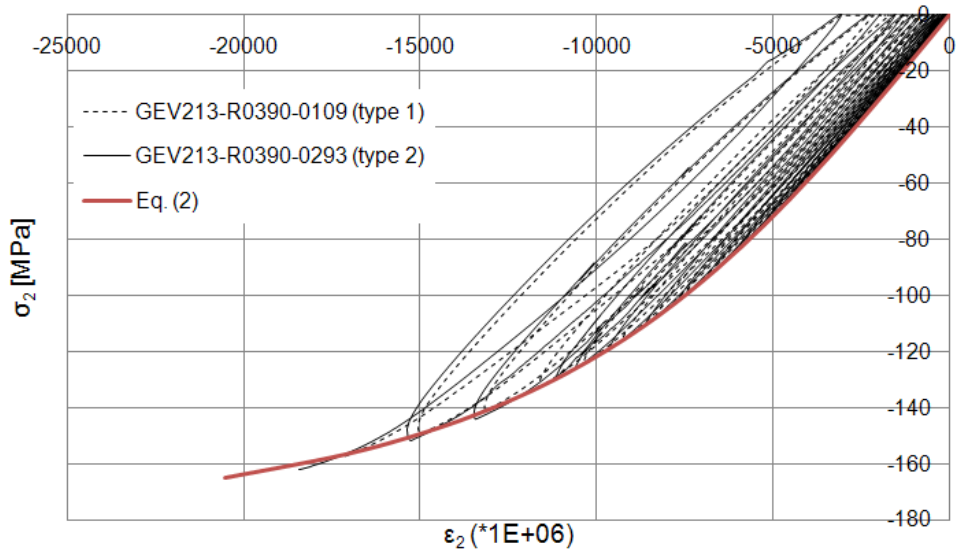

Fig. 11: Stress-strain curve of two compressive L-U-R tests on the $[90_7]_T$ laminate

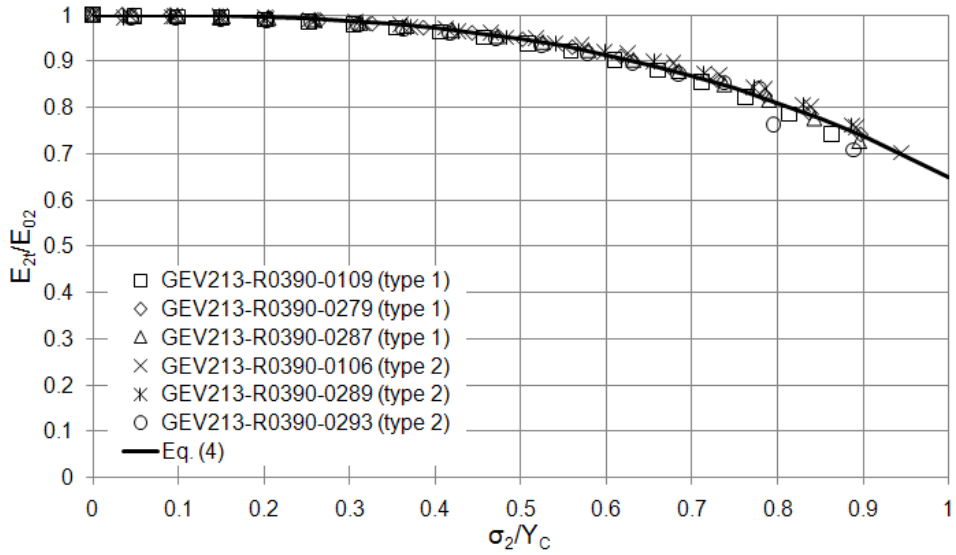

Fig. 12: Modulus degradation on the $[90_7]_T$ laminate due to compressive L-U-R cycles

Similar modulus degradation was observed for both test types in tension and compression.

For the in-plane shear modulus degradation due to L-U-R cycles, axial tensile tests were performed on ISO 14129 $[\pm 45]_S$ coupons. The loading and unloading rate was 10 kN/min. The shear stress-strain response of two tests on $[\pm 45]_S$ coupons appear in Fig. 13 and the shear modulus degradation in Fig. 14. The approximate duration of the type1 tests was 2.1h.

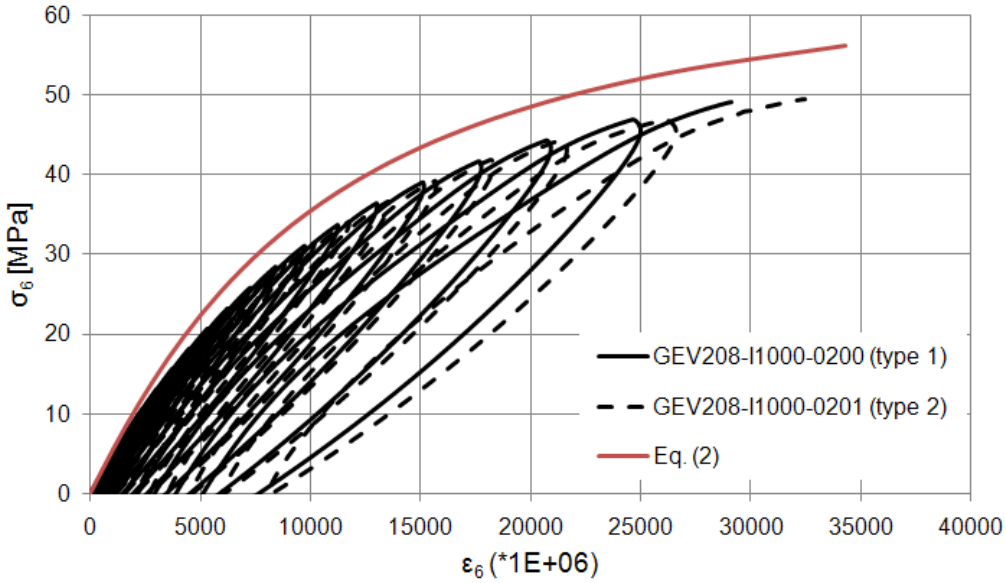

Fig. 13: Shear stress-strain curves of L-U-R tests on ISO 14129 $[\pm 45]_S$ coupons

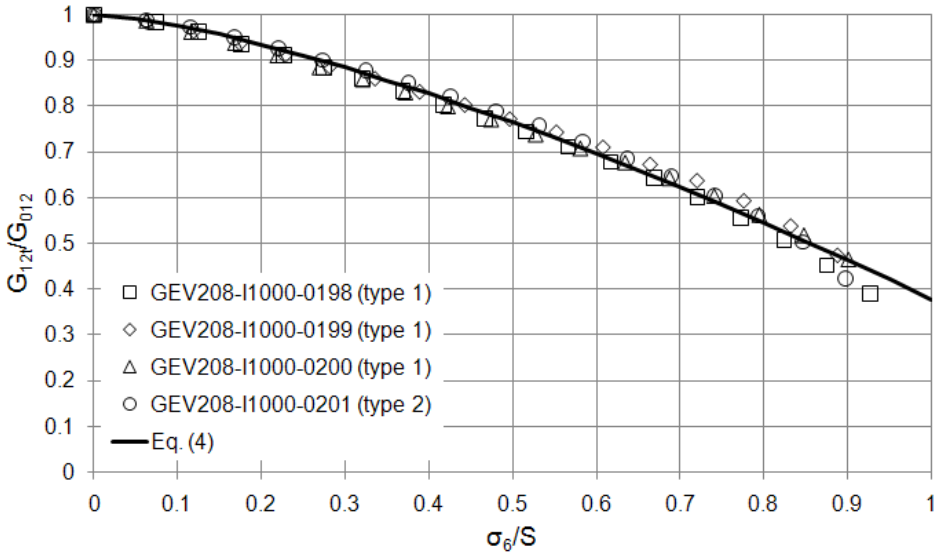

Fig. 14: Shear modulus degradation due to L-U-R cycles

Again the modulus degradation was similar for both test types. The different material behaviour between the monotonic static tests and the static L-U-R tests observed in Fig. 13 was due to the difference in the strain rate. In the load controlled L-U-R tests it was not practical to have the same strain rate with the displacement controlled monotonic tests [28] due to the high material non linearity.

The stiffness degradation models were determined with nonlinear regression applied on the normalized stiffness-stress data from all tests and given by:

$$\frac{E_{2t}}{E_{o_2}} = 1-(1-a_2)\left(\frac{\sigma_{2G_{max}}}{Y_T}\right)^{b_2},\ \frac{G_{12t}}{G_{o_{12}}} = 1-(1-a_6)\left(\frac{\sigma_{6_{Gmax}}}{S}\right)^{b_6} \quad (4)$$

By σ_{iGmax}, the global maximum stress reached during cycling was denoted while Y_T and S stand for the tensile strength transversely to the fibres and in-plane shear strength respectively. Since values of E_{o2} or G_{o12} presented slight variations for the different coupon tests, the respective values from Table 1 were implemented along with Eq. (4). The parameters a_2, b_2 were found different in tension and compression. Numerical values for all the above constants were summarized in Table 4.

Table 4: Parameter values for L-U-R stiffness degradation models, Eq. (4)

	a_i	b_i
$E_{2t}^{(T)}$	0.88	1.60
$E_{2t}^{(C)}$	0.65	2.77
G_{12t}	0.38	1.40

When the first of Eq. (4) is used to determine the compressive elastic modulus transverse to the fibres the tensile strength, Y_T, should be replaced by the corresponding compressive one, Y_C.

The elastic modulus as determined by Eq. (4) is implemented for the reloading branch. Considering a slightly greater unloading modulus, e.g. multiplying by a factor greater than unity, enables the model to take into account the permanent strains as well. The inclusion of this type of stiffness reduction in the constitutive material model is expected to affect numerical predictions, especially in cases of VA loading.

2.3 Progressive stiffness degradation

In-plane stiffness of the lamina is degrading due to several reasons, e.g. *sudden stiffness* reduction due to some kind of failure occurrence or progressive stiffness reduction due to cyclic loading. In general, the latter is non linear and several formulations were proposed in the literature to describe it. As presented by Philippidis et al. [24], during constant amplitude (CA) cyclic tests [28]-[29], load-displacement data corresponding to ca. 10 cycles were recorded periodically and were transformed to respective stress-strain data, e.g. see Fig. 15a where experimental data from CA cyclic loading of a $[90_7]_T$ coupon at a stress ratio R=-1 (T-C) were shown. The calculated strain was proved to be accurate by comparing with extensometer data for low stiffness specimens as of [28]-[29] where no tab debonding occurred during the test. The stiffness of the coupon at the first cycle of each periodically recorded block of cycles was determined as the slope of the linear regression model of the respective stress-strain loop. These stiffness values were normalized with respect to the stiffness of the first cycle and plotted vs. the normalized number of cycles with respect to the number of cycles at failure. For example, for the case of a $[90_7]_T$ coupon, said results from all available stress levels at R=0.1 and -1 were presented in Fig. 15b. Due to the high experimental scatter it was thought more appropriate to select a representative group of data for fitting the material model, e.g. in Fig 15b the solid line data corresponding to R=-1 and stress level of 24.3 MPa were chosen for the tensile transverse modulus. The stiffness degradation models were determined with nonlinear regression applied on the normalized stiffness-cycle number data from these representative load cases, Fig. 16. A similar procedure was also followed to derive the compressive modulus degradation shown in Fig. 17 and the respective one for the in-plane shear modulus (Fig. 18).

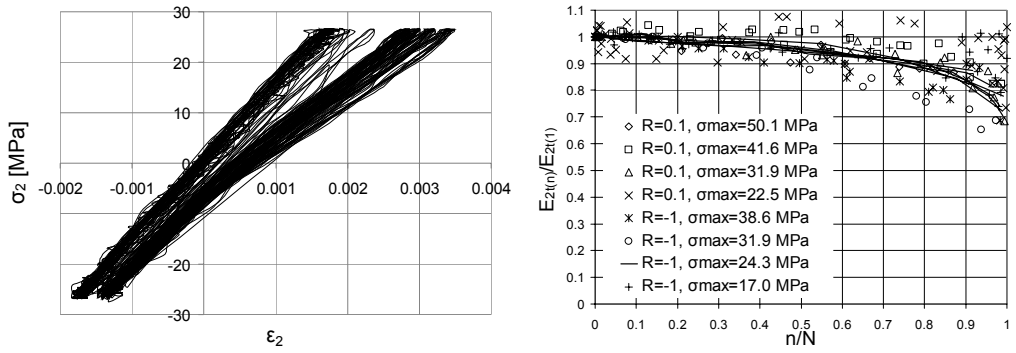

Fig. 15: (a) Stress-strain cycles under R=-1 CA fatigue transversely to the fibres, (b) Respective stiffness degradation data from R=0.1 and -1

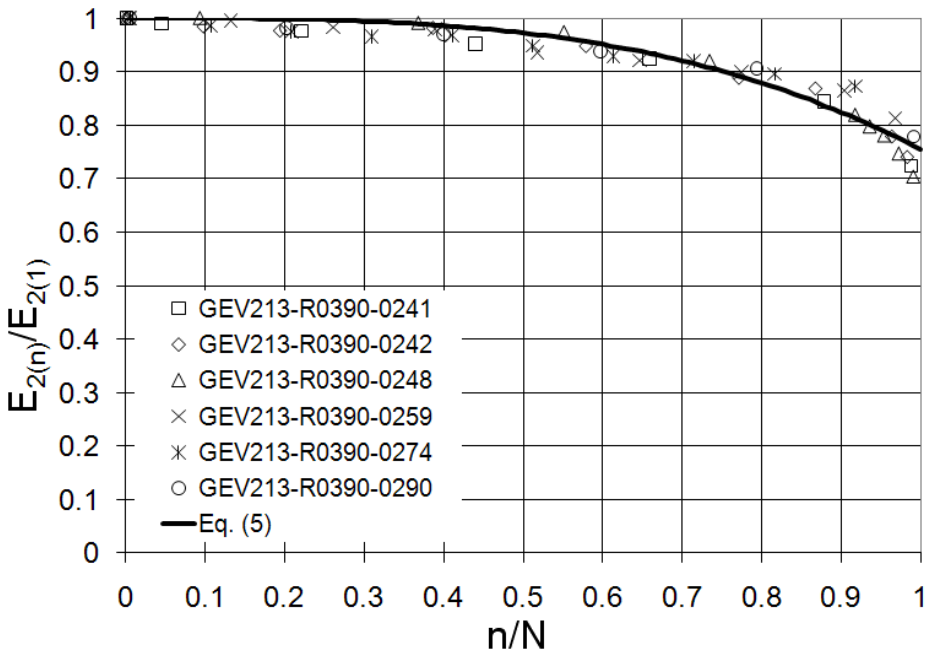

Fig. 16: Tensile transverse modulus degradation due to CA cyclic loading

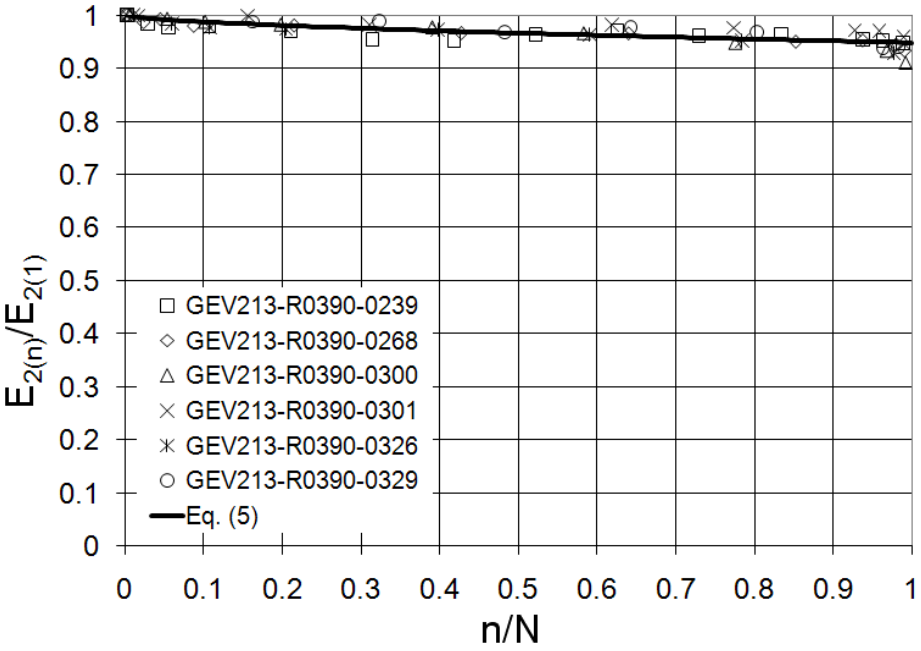

Fig. 17: Compressive transverse modulus degradation due to CA cyclic loading

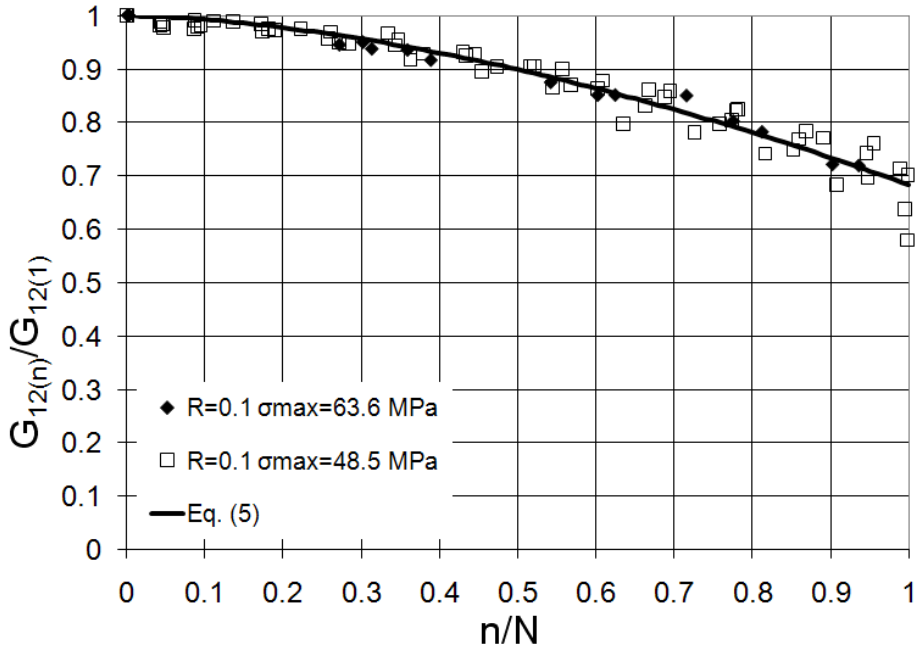

Fig. 18: Shear modulus degradation due to CA cyclic loading

In the present FADAS implementation the regression models depend only on the fatigue life fraction, i.e. the ratio of the applied cycles versus the nominal fatigue life at the current stress level. In this way, the modulus degradation depends implicitly also on the stress ratio, R, and the maximum applied cyclic stress, σ_{max}. The following functional forms were fitted to the experimental data:

$$\frac{E_{2t}(n)}{E_{2t}(1)} = 1-(1-c_2)\left(\frac{n}{N}\right)^{d_2},\ \frac{G_{12t}(n)}{G_{12t}(1)} = 1-(1-c_6)\left(\frac{n}{N}\right)^{d_6} \quad (5)$$

The parameters c_2, d_2 were found different in tension and compression; they were calculated by fitting test data from 6 tests at R=-1 and σ_{max}=24.3 MPa for the tensile E_{2t} and from 6 tests at R=10 and σ_{min}=-138.6 MPa for the compressive E_{2t}. For the in-plane shear modulus, G_{12t}, 5 tests on ISO 14129 coupons of $[\pm 45]_S$ lay-up at σ_{max}=63.6 MPa and 5 tests at σ_{max}=48.5 MPa, R=0.1, were used together as they exhibited similar stiffness degradation. Numerical values for all the above constants were presented in Table 5. Since the modulus values at the first cycle from the different coupons tested were different, $E_{2t(1)}$ and $G_{12t(1)}$ in Eq. (5) were substituted by the respective, to the stress level, reloading stiffness values as given by Eq. (4).

For CA testing in the fibre direction, axial strain was measured with extensometers in 4 UD coupons [30]. Description of this type of tests can be found in [31]. Progressive stiffness degradation during cyclic loading parallel to the fibres was not important (1-2%), as shown in Fig. 19 and thus it was neglected in the numerical model.

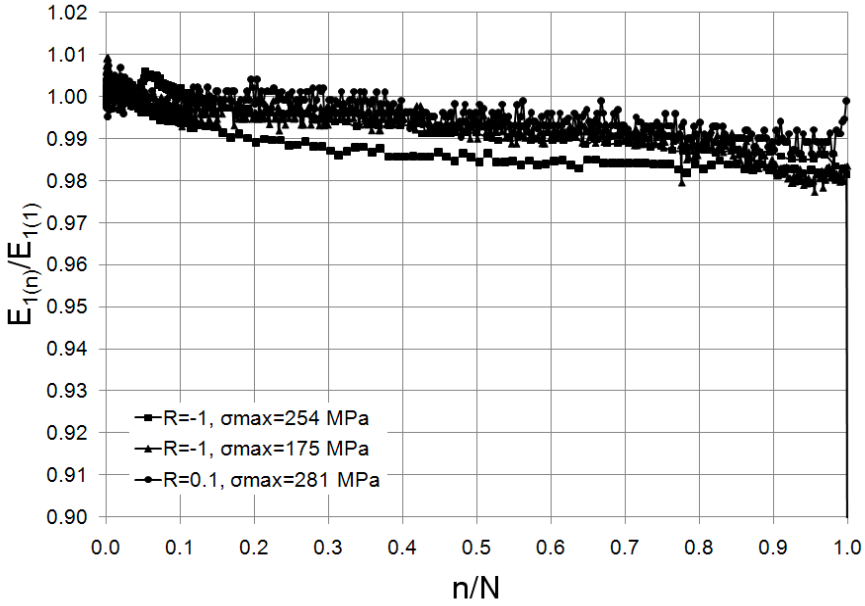

Fig. 19: Stiffness degradation of the UD ply in the fibres direction due to CA loading

Table 5: Parameter values for the progressive stiffness degradation models, Eq. (4)

	c_i	d_i
$E_{2t}^{(T)}$	0.75	3.17
$E_{2t}^{(C)}$	0.95	0.62
G_{12t}	0.68	1.65

2.3.1 Pre-failure material models

In case that no failure was detected, the simulated ply response and especially the description of stiffness evolution for VA cyclic loading were expressed by combining the constitutive relations presented in the above. For each stress tensor component at the k-th loading step it is examined if it corresponds to loading, i.e. $\left|\sigma_{i(k)}\right| \geq \left|\sigma_{i(k-1)}\right|$, i=1, 2, 6 or else to unloading.

In the former case, if $\sigma_{i(k)}$ is higher than the global maximum stress $\sigma_{i_{G\max}}$ or lower than the global minimum stress $\sigma_{i_{G\min}}$, the initial material behaviour under quasi-static loading, presented in section 2.1 is assumed. That is, constant modulus E_1 and Poisson ratio v_{12} while E_{2t} and G_{12t} are functions of $\sigma_{2(k)}$ and $\sigma_{6(k)}$ as expressed by Eq. (3). If $\sigma_{i(k)}$ lies between the global minimum and maximum stress, the reload elastic properties are used, Eq. (4), calculated at the global maximum or minimum stress, degraded according to the stiffness degradation models due to cycling, i.e. Eq. (5).

In the case of unloading, elastic properties slightly higher than in the case of reloading are used to introduce an increasing permanent strain due to cyclic loading. In the routine this is realized by multiplying by a number slightly higher than one the reloading stiffness values for E_{2t} and G_{12t}. The specific value depends on the numerical implementation.

The above was illustrated in Fig. 20:
A-B: Initial loading. Stress is always greater than its previous global maximum value, so the non-linear material behaviour under quasi-static loading is used.
B-C-D: Stress cycling under CA or VA. Stress values remain between their global minimum and maximum values, 0 and σ_{iGmax} respectively, so the reload and unload elastic properties were used, gradually degrading with increasing number of cycles.
D-E: Stress becomes greater than its previous global maximum value σ_{iGmax}, so the initial material behaviour is assumed etc.

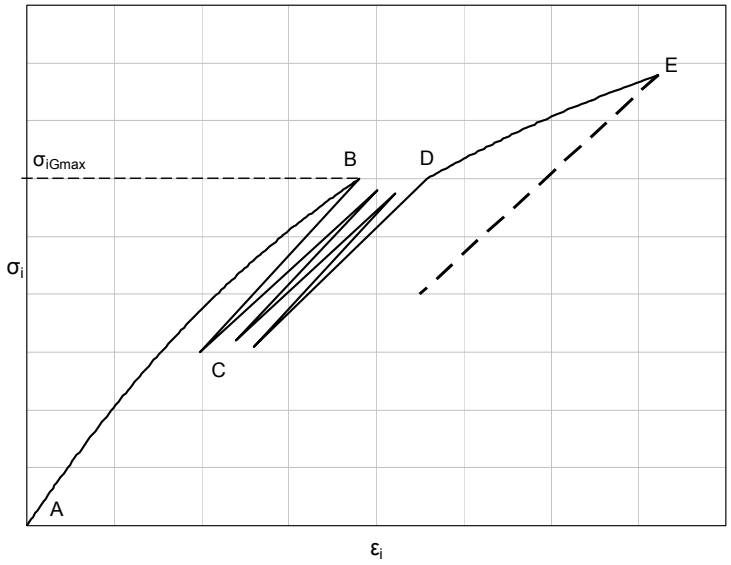

Fig. 20: Pre-failure material model for the OB_UD Glass/Epoxy

As it is seen in Fig. 20, the behaviour of the material under cyclic stress is assumed linear elastic, its stiffness depending on the global maximum stresses reached so far and also on the

applied number of cycles. However, when the applied stress level exceeds previous maxima, non-linear response is again recalled.

2.3.2 Post-failure material models

Upon failure onset in some loading step, the stiffness degrades depending on the failure mode observed and the changes apply for the next loading step. In fibres failure (FF) under either tensile or compressive stresses the three engineering elastic constants, E_1, E_{2t} and G_{12t} drop to zero. If matrix damage modes occur, also called inter-fibre failure (IFF), see section 3 for a detailed description, only E_2 and G_{12} drop to zero.

After fibres failure (FF), the unload behaviour for all three stress tensor components remains as in the virgin material, i.e. constant E_1 and degraded reload values for E_{2t} and G_{12t} multiplied by the appropriate factors mentioned earlier to take into account residual strains. If reloading occurs before any stress tensor component has changed sign, the respective modulus, i.e. E_1, E_{2t}, or G_{12t} drops to zero. If the stress has changed sign once, the corresponding modulus remains always at zero. The above was illustrated in Fig. 21:

A: Stress level at which FF mode was detected.
A-B: If $\sigma_{i(k)}$ stands for loading, the corresponding engineering elastic constant drops to zero.
B-C, C-D, E-F: Unloading using the unloading elastic properties.
C-E: If reloading is encountered before stress has changed sign, the elastic property drop to zero.
D, F: Following unloading a stress tensor component changes sign. The corresponding elastic property drops and remains henceforth at zero.

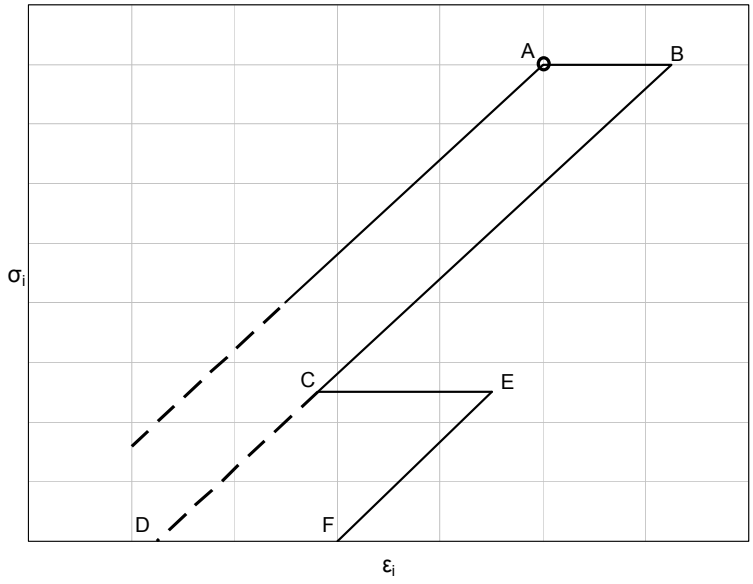

Fig. 21: Post-FF material model for the OB_UD Glass/Epoxy

In case of matrix failure (IFF damage modes), E_1 remains unaffected and only the normal stress transverse to the fibres and the in-plane shear component are taken into account in the stiffness degradation model.

Once IFF was detected, both unload and reload properties remain as for the virgin material models presented in section 2.2, unless IFF is detected again; both engineering elastic

constants E_{2t} and G_{12t} drop to zero. If only the value of the normal stress transverse to the fibres σ_2 or the in-plane shear stress σ_6 exceeds its value for which IFF has been predicted last time, the respective elastic property drops to zero (E_{2t} or G_{12t}) and the process is continued. With respect to Fig. 22, illustrating the above, the following characteristics can be noted.

A: Stress level at which IFF was first detected.
A-B: Loading is continued; both E_2 and G_{12} drop to zero.
B-C-D: No IFF is predicted again. Stress component remains lower than its value at failure. The reload and unload elastic properties of the virgin material are used, gradually degraded with the number of cycles.
D-E: IFF is predicted once more or stress σ_2 or σ_6 becomes equal or greater than its value when IFF was predicted. The corresponding elastic property drops to zero.

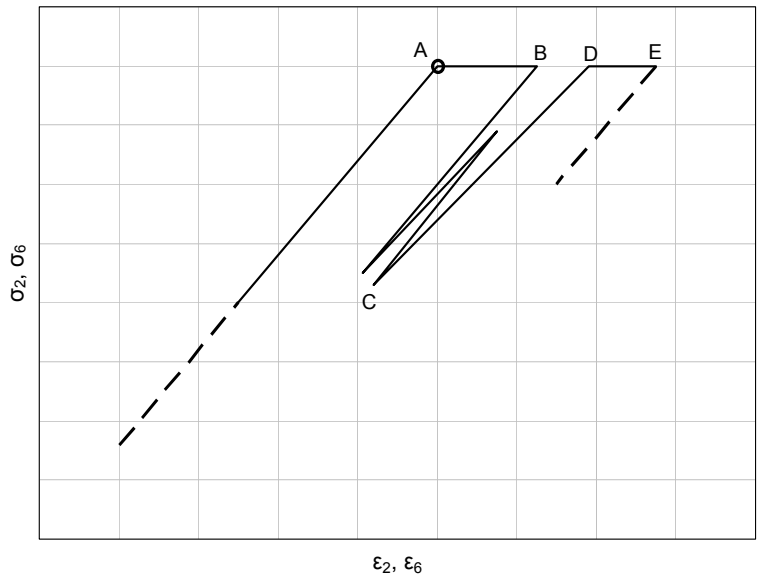

Fig. 22: Post-IFF material model for the OB_UD Glass/Epoxy

3. Failure Onset Conditions

Predicting laminate strength under cyclic complex stress states is conceptually different from predicting failure onset under monotonic loading. The latter is a First Ply Failure (FPF) approach implementing directly ply stresses in a suitable limit condition and finally suggesting the layer with the maximum risk of failure. On the other hand, fatigue strength prediction is a Last Ply Failure (LPF) procedure involving modelling of progressive damage, e.g. consideration of strength and stiffness degradation due to cyclic stresses when a ply-to-laminate approach is implemented, as by Shokrieh and Lessard [8]-[9].

The methodology used in FADAS is of the ply-to-laminate type with progressive damage modelling. In such an approach it is sufficient to use a static limit condition at the ply level where however, material strength parameters are replaced by the corresponding residual strength values which are in general functions of the number of cycles and the type of loading. For the cases studied in this work, numerical results were derived by implementing the Puck criterion in the FADAS routine.

Based on the concepts first introduced by Hashin [32] for different damage mechanisms in composite materials and the Mohr-Coulomb hypothesis for brittle materials that fracture is exclusively triggered by stresses acting on the fracture plane, the criterion of Puck [20]-[22] describes several failure modes using different equations. For 2D plane stress analysis five types of damage were assumed; two related with fibre fracture (FF), one in tension and another in compression. The other three concern matrix failure (inter-fibre fracture or IFF). Under tension ($\sigma_2 \geq 0$), cracks open transverse to the applied normal stresses ($\theta_{fp}=0^o$, the angle subtended by the fracture plane and the vertical one to the layer plane), described as mode A. In compression, closed cracks are formed either transverse to the applied normal stresses ($\theta_{fp}=0^0$), described as mode B, or an oblique rupture occurs with the fracture plane forming an angle θ_{fp} between $\pm 45^o$ and $\pm 55^o$, described as mode C.

Fibre and matrix failure effort or stress exposure factor, $f_{E(FF)}$ and $f_{E(IFF)}$ respectively, can be calculated as follows. For fibre failure (FF) under tensile loading:

$$f_{E(FF)}^{T} = \frac{1}{X_T}\left[\sigma_1 + \left(\frac{\mathrm{E}_1}{\mathrm{E}_{f1}} v_{f12} m_{\sigma f} - v_{12}\right)\sigma_2\right] \leq 1 \; if \; [...] \geq 0 \tag{6}$$

Respectively, for fibre failure (FF) under compressive loading:

$$f_{E(FF)}^{C} = \frac{1}{X_C}\left|\left[\sigma_1 + \left(\frac{\mathrm{E}_1}{\mathrm{E}_{f1}} v_{f12} m_{\sigma f} - v_{12}\right)\sigma_2\right]\right| \leq 1 \; if \; [...] < 0 \tag{7}$$

For Mode A, IFF condition, for which the fracture plane is vertical to the layer plane ($\theta_{fp}=0^o$):

$$f_{E(IFF)}^{A} = \sqrt{\left(\frac{\sigma_6}{S}\right)^2 + \left(1 - p_{\perp\parallel}^{(+)}\frac{Y_T}{S}\right)^2\left(\frac{\sigma_2}{Y_T}\right)^2} + p_{\perp\parallel}^{(+)}\frac{\sigma_2}{S} + \left(0.9 f_{E(FF)}\right)^6 \leq 1 \; if \; \sigma_2 \geq 0 \tag{8}$$

For transverse compression and moderate in-plane shear, Mode B, IFF condition, for which again the fracture plane is vertical to the layer plane ($\theta_{fp}=0^o$):

$$f_{E(IFF)}^{B} = \frac{1}{S}\left[\sqrt{\left(\sigma_6\right)^2 + \left(p_{\perp\parallel}^{(-)}\sigma_2\right)^2} + p_{\perp\parallel}^{(-)}\sigma_2\right] + \left(0.9 f_{E(FF)}\right)^6 \leq 1 \; \text{if} \; \sigma_2 < 0 \; and \; 0 \leq \left|\frac{\sigma_2}{\sigma_6}\right| \leq \frac{R_{\perp\perp}^{A}}{\left|\sigma_{6c}\right|} \tag{9}$$

Finally, for the explosive mode C, IFF condition, the fracture plane forms an oblique angle with the vertical to the ply plane ($\theta_{fp}\neq 0^o$):

$$f^{C}_{E(IFF)} = \left[\left(\frac{\sigma_6}{2\left(1+p^{(-)}_{\perp\perp}\right)S}\right)^2 + \left(\frac{\sigma_2}{Y_C}\right)^2\right]\left(\frac{Y_C}{\left(-\sigma_2\right)}\right) + \left(0.9\, f_{E(FF)}\right)^6 \leq 1 \; if \;\; \sigma_2 < 0 \; and \; 0 \leq \left|\frac{\sigma_6}{\sigma_2}\right| \leq \frac{\left|\sigma_{6c}\right|}{R^A_{\perp\perp}} \qquad (10)$$

E_{f1} and v_{f12} are the elastic modulus and the Poisson ratio of the fibres. The term $m_{\sigma f}$ accounts for a stress magnification effect caused by the different moduli of fibres and matrix which leads to an uneven distribution of the transverse stress σ_2 from a micromechanical point of view; in the fibres it is slightly higher than in the matrix. For the variety of parameters implemented in the above relations, guidelines and typical values were explicitly presented by Puck et al. [22]. The values used in the present version are given by:

$$E_{f1} = 72.45 \text{ GPa},\; \nu_{f12} = 0.22,\; m_{\sigma f} = 1.3,\; p^{(+)}_{\perp\parallel} = 0.3,\; p^{(-)}_{\perp\parallel} = 0.25$$

$$p^{(-)}_{\perp\perp} = \frac{1}{2}\sqrt{1+2p^{(-)}_{\perp\parallel}\frac{Y_C}{S}} - 1,\; \sigma_{6c} = S\sqrt{1+2p^{(-)}_{\perp\perp}},\; R^A_{\perp\perp} = \frac{Y_C}{2\left(1+p^{(-)}_{\perp\perp}\right)} \qquad (11)$$

When the criterion is used for cyclic stresses, the lamina strength values X_T, X_C, Y_T, Y_C, S given in Table 2 must be replaced by the corresponding residual strength values, see section 4.

4. Strength Degradation Due to Cyclic Loading

Static strength degradation or residual strength after fatigue in composites has been intensively investigated the last 30 years. Numerous research groups have developed a variety of models; an appraisal of their effectiveness has been presented by Philippidis and Passipoularidis [33]. The majority of the work concerns modelling of residual tensile strength in the laminate level, under axial loading and in most cases at a single R-ratio, usually in the tension-tension region. Very limited are the experimental data sets concerning complex stress states. The model introduced by Shokrieh and Lessard [34]-[35] is perhaps one of the first phenomenological approaches to examine damage evolution and failure due to multi-axial fatigue in a composite laminate in terms of the strength and stiffness degradation of the building ply.

On the other hand, only few tests under limited loading conditions have been performed for models evaluation, without any investigation on more complex issues e.g. residual tensile strength after compression-compression fatigue. In general, the lack of detailed experimental data, under various fatigue conditions and for a single material has restricted the study of residual strength based models to limited loading conditions and to specific lay-ups.

To link existing knowledge and promote the modelling of static strength degradation due to stress cycling, a comprehensive experimental program was undertook in the frame of the European research project OPTIMAT BLADES in order to study, amongst other things, the static strength, fatigue life and residual strength behaviour of wind turbine rotor blade materials. These properties have been in particular studied in the symmetry directions of an orthotropic UD Glass/Epoxy material (OB_UD), i.e. along and transverse to the fibres and under in-plane shear. Regarding residual strength, it was studied in detail –for the first time- both the tensile and compressive residual strength under different stress ratios of fatigue loading, for all the principal directions of the specific lamina, using a single coupon geometry for tensile, compressive tests under either static or fatigue loads, in an effort to keep results unbiased of different coupon geometries, use of anti-buckling devices etc. The investigation considered stress ratios in the range of those experienced at different points of blades during operation, i.e. tension-tension, reversed loading as well as compression-compression fatigue.

From the processing of the experimental data, Philippidis and Passipoularidis [36], main conclusions were derived and formulated as guidelines for further development. First, the residual strength in both principal material directions is not affected when cyclic stress of the opposite sign is applied, i.e. tensile strength is not reduced under purely compressive cycles and vice versa. A similar trend was also observed by Nijssen [37] from tests in the fibre-dominated direction of a $[(\pm 45/0)_4/\pm 45]_T$ laminate, made also of the OB_UD Glass/Epoxy, under various loading conditions (R ratios).

The tensile and the in-plane shear static strength experienced degradation of up to 40% when tested at a nominal life fraction of 80%. The compressive residual strength on the other hand did not show significant degradation in all types of loading and material directions. Concerning the many theoretical models considered in this investigation, only a few corroborated satisfactorily with the majority of the experimental data, Passipoularidis and Philippidis [38]. It was demonstrated in a clear manner that the complexity of a model is not related to the accuracy of its predictions. In addition, it was also proved by Passipoularidis and Philippidis [39] that life prediction results under VA loading are not very sensitive to which residual strength model, of these few validated of course, is used as damage metric.

Therefore, the models used herein to describe the phenomenon are two: For the modelling of tensile residual strength along the principal material directions, under T-T or T-C cyclic loading, as well as under in-plane shear, the linear degradation model proposed by Broutman & Sahu [40] was implemented. Besides being the simplest one available, it requires no residual strength

testing while at the same time it has been proven by Philippidis and Passipoularidis [33] to produce always safe residual strength predictions under various stress conditions and lay-ups.

It is described respectively by the following equations:

$$X_{T_r} = X_T - \left(X_T - \sigma_{1max}\right)\left(\frac{n}{N_1}\right) \quad Y_{T_r} = Y_T - \left(Y_T - \sigma_{2max}\right)\left(\frac{n}{N_2}\right) \quad S_r = S - \left(S - \sigma_{6max}\right)\left(\frac{n}{N_6}\right) \tag{12}$$

X_{Tr} and Y_{Tr} is the tensile residual strength parallel and transverse to the fibres respectively, while S_r is the residual shear strength. σ_{1max}, σ_{2max} and σ_{6max} are the maximum cyclic stresses applied for n cycles and N_i, i=1, 2, 6, the corresponding fatigue life at the specific stress level. Although the three relations of Eq. (12) seem to depend only on the applied stress level, they also depend on the stress ratio through the fatigue life N_i, obtained for a specific stress ratio through the constant life diagram (CLD) used, see section 5.1. The model can be implemented once the static strength and fatigue S-N curves at arbitrary R-ratios are known.

The compressive strength, both parallel and transversely to the fibres has been shown not to degrade significantly due to fatigue, especially when the specimens were subjected to tensile cyclic stress. Nevertheless, in modelling the compressive residual strength under C-C or T-C cyclic loading, a degradation equation simulating constant strength throughout the life with a sudden drop near failure (sudden death) of the following form was implemented:

$$X_{C_r} = X_C - \left(X_C - \left|\sigma_{1min}\right|\right)\left(\frac{n}{N_1}\right)^k \quad Y_{C_r} = Y_C - \left(Y_C - \left|\sigma_{2min}\right|\right)\left(\frac{n}{N_2}\right)^k \tag{13}$$

A summary of experimental evidence on the effectiveness of Eq. (12), (13) in modelling the residual strength behaviour in the principal material directions of the OB_UD Glass/Epoxy was presented in Figs. 23 to 28. In each of these figures, static strength data, tensile, compressive or in-plane shear were plotted in the ordinate axis which was moved to N=10 or 100 for increased resolution.

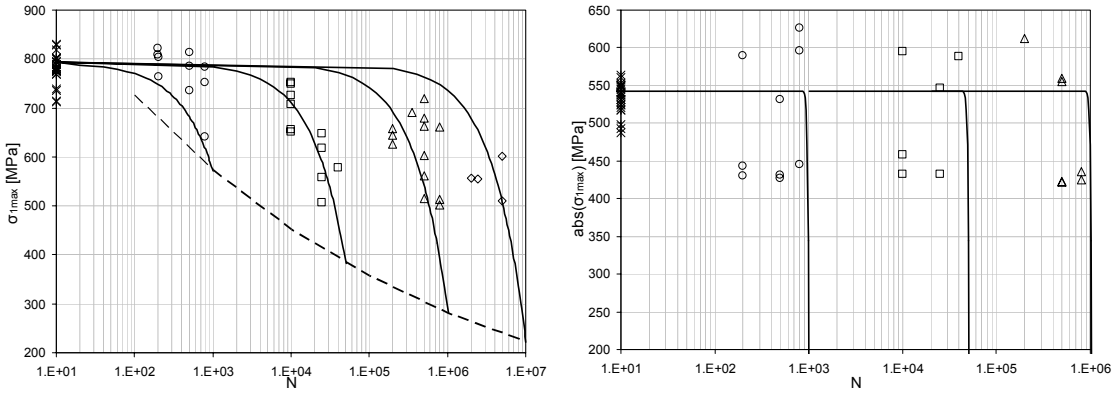

Fig. 23: Strength degradation of OB_UD in the fibre direction under R=0.1. (Tensile residual strength: left, compressive residual strength: right)

The corresponding S-N curve was also shown as dashed line, where appropriate, e.g. under T-T loading at R=0.1 it appears in the picture for the residual tensile strength whereas for compressive R=10 loading it is plotted along with the residual compressive strength.

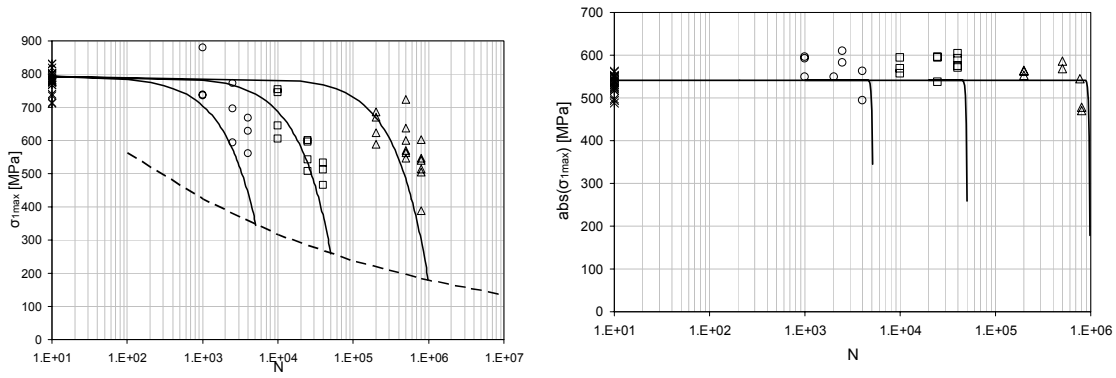

Fig. 24: Strength degradation of OB_UD in the fibre direction under R=-1. (Tensile residual strength: left, compressive residual strength: right)

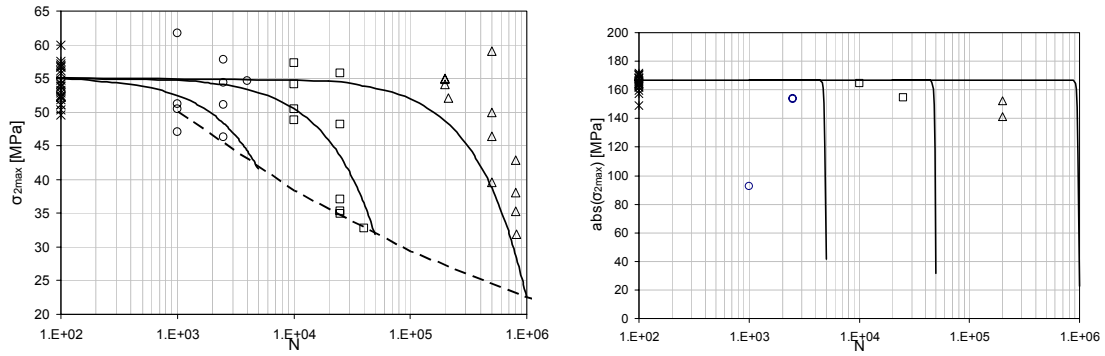

Fig. 25: Strength degradation of OB_UD transversely to the fibres. R=0.1. (Tensile residual strength: left, compressive residual strength: right)

The solid lines appearing in Figs. 23 to 28 are theoretical predictions from Eq. (12) or Eq. (13) for the residual compressive strength. The exponent k for the latter case was set equal to 50. Different data point sets were also displayed that correspond to three different stress levels while for each set data correspond to coupons cycled up to 20%, 50% or 80% of their nominal life. Details for all these tests were reported by Philippidis and Passipoularidis [36].

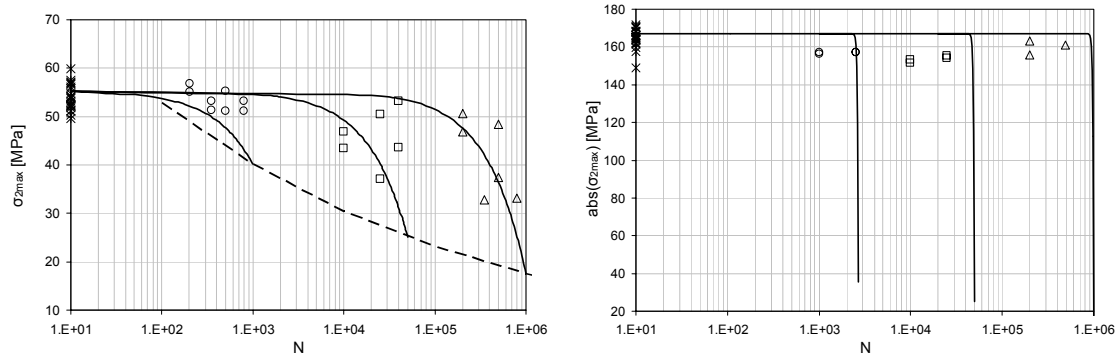

Fig. 26: Strength degradation of OB_UD transversely to the fibres. R=-1. (Tensile residual strength: left, compressive residual strength: right)

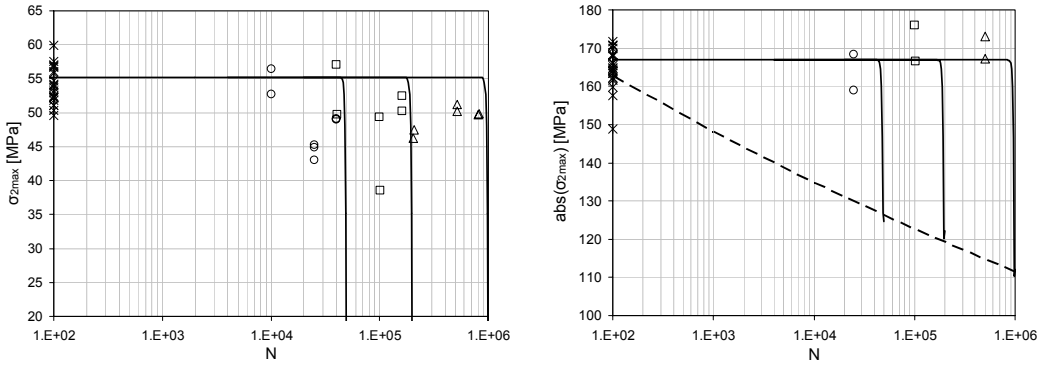

Fig. 27: Strength degradation of OB_UD transversely to the fibres. R=10. (Tensile residual strength: left, compressive residual strength: right)

Initially tests were planned for three stress ratios, both parallel and transversely to the fibres. Nevertheless, compressive tests at R=10 in the fibre direction were skipped due to the very flat S-N curve derived at this stress ratio that made the definition of stress levels for specific fatigue lives very sensitive to even slight variations of applied load. That has also introduced uncertainty on the quality of the results and also caused many premature failures. Concerning the residual shear strength tests, they were performed using the ISO 14129 standard $[\pm 45]_S$ tensile coupon. For this reason only cyclic tests at R=0.1 were possible.

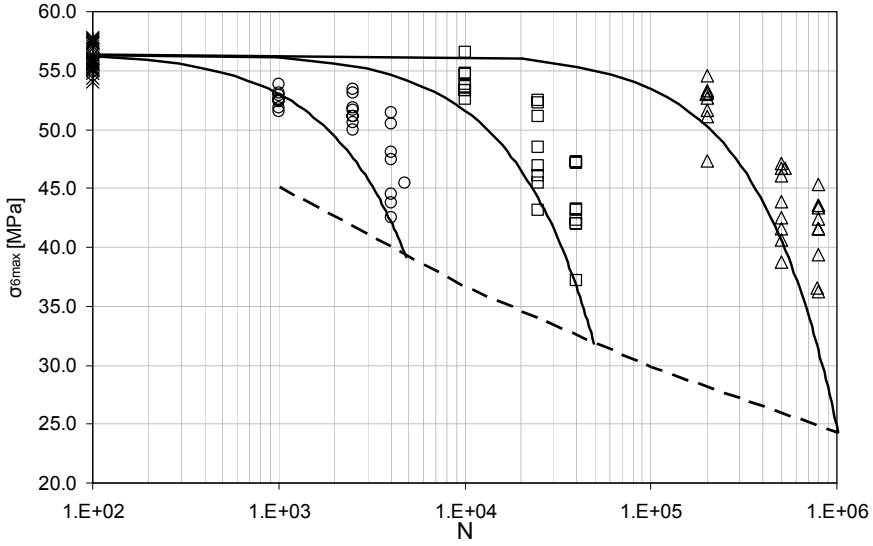

Fig. 28: In-plane shear strength degradation of OB_UD. R=0.1

Summarizing the above, the residual strength model in the symmetry directions of the unidirectional glass/epoxy layer, and also for in-plane shear, due to cyclic loading is given by a different set of equations, depending on the value of the cyclic stress ratio, R. As it is well known from the representation of constant life diagrams (CLD) in the (σ_a-σ_m) plane of the alternating, σ_a, and mean stress, σ_m, characteristics of the cyclic loading, radial lines emanating from the origin of the coordinates system correspond to stress states with constant R values. Then, with respect to Fig. 29, the following sets of equations are valid for purely tensile (T-T) cyclic loading:

$$X_{T_r} = X_T - \left(X_T - \sigma_{1max}\right)\left(\frac{n}{N_1}\right),\ X_{C_r} = X_C$$
$$Y_{T_r} = Y_T - \left(Y_T - \sigma_{2max}\right)\left(\frac{n}{N_2}\right),\ Y_{C_r} = Y_C \qquad 0 \le R < 1 \qquad (14)$$
$$S_r = S - \left(S - \sigma_{6max}\right)\left(\frac{n}{N_6}\right).$$

For negative R values, corresponding to compressive σ_{min} and tensile σ_{max} values, where however the tensile stresses are of greater magnitude, (T-C):

$$X_{T_r} = X_T - \left(X_T - \sigma_{1max}\right)\left(\frac{n}{N_1}\right),\ X_{C_r} = X_C - \left(X_C - |\sigma_{1min}|\right)\left(\frac{n}{N_1}\right)^k$$
$$Y_{T_r} = Y_T - \left(Y_T - \sigma_{2max}\right)\left(\frac{n}{N_2}\right),\ Y_{C_r} = Y_C - \left(Y_C - |\sigma_{2min}|\right)\left(\frac{n}{N_2}\right)^k \qquad -1 \le R < 0 \qquad (15)$$
$$S_r = S - \left(S - \sigma_{6max}\right)\left(\frac{n}{N_6}\right).$$

For compression dominated cyclic loading (C-T) in the range of negative R values, the same set of Eq. (15) is valid with the exception of the relation for the residual shear strength which is now given by:

$$S_r = S - \left(S - |\sigma_{6min}|\right)\left(\frac{n}{N_6}\right) \qquad R \in [-1, -\infty) \qquad (16)$$

Finally, the residual strength equations for purely compressive cyclic loading (C-C) are given by:

$$X_{T_r} = X_T,\ X_{C_r} = X_C - \left(X_C - |\sigma_{1min}|\right)\left(\frac{n}{N_1}\right)^k$$
$$Y_{T_r} = Y_T,\ Y_{C_r} = Y_C - \left(Y_C - |\sigma_{2min}|\right)\left(\frac{n}{N_2}\right)^k \qquad R \in [1, +\infty) \qquad (17)$$
$$S_r = S - \left(S - |\sigma_{6min}|\right)\left(\frac{n}{N_6}\right).$$

In all the above equations for compressive residual strength, expressed by the “sudden death” relation, the exponent k assumes a great value, ca. 50.

As explained in section 2.3.2, after a fibre failure mode has been predicted, the post-failure model is strict, leading all stress components to zero. On the other hand, after a matrix failure mode has been predicted, the post-failure model is not strict, allowing normal stress in the transverse direction and shear stress reaching the stress level when failure occurred unless failure is predicted at lower stress level. Since strength degradation due to cyclic loading is meaningless after failure has been predicted, the transverse and shear strength are degraded with a degradation factor when matrix failure is predicted, considering that, besides stiffness degradation, failure has caused strength degradation as well, and remain constant from this point forward:

$$Y_{T_r}^{PF} = f \cdot Y_{T_r}^{F}$$
$$Y_{C_r}^{PF} = f \cdot Y_{C_r}^{F} \qquad (18)$$
$$S_r^{PF} = f \cdot S_r^{F}$$

$Y_{T_r}^{PF}$, $Y_{C_r}^{PF}$, S_r^{PF} are the post failure residual strengths, $Y_{T_r}^{F}$, $Y_{C_r}^{F}$, S_r^{F} are the residual strengths when matrix failure was predicted for the first time and f is the strength degradation factor. The selected values of this factor for the different implementations of the algorithm are reported below.

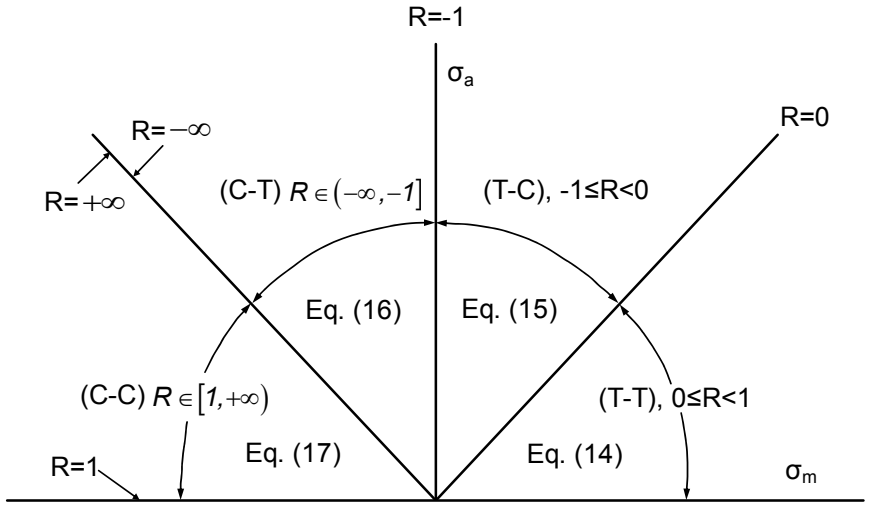

Fig. 29: (σ_a, σ_m)-plane notation and region of validity for residual strength models

5. Constant Life Diagrams and S-N Curves

The life prediction methodology presented herein, although it can be used for any glass/epoxy laminate under any type of cyclic loading, it has been initially introduced for wind turbine rotor blade applications where VA fatigue under various R ratios spanning the entire (σ_a, σ_m)-plane, see Fig. 29, is the case. Therefore, characterization of fatigue behaviour in the principal coordinate system of the orthotropic UD ply must take place for several R-values and then by using an appropriate interpolation scheme define the "Constant Life Diagram" or else define the number of cycles to failure, N, for every pair (σ_a, σ_m).

A great number of CA cyclic tests were performed and the respective S-N curves parallel, transversely to the fibre and in shear, at three stress ratios R were obtained. All test details and results can be found at the OPTIMAT BLADES site, cited earlier, either in the OPTIDAT database or reports by Philippidis et al. [29], [31]. The R-ratios for which tests were performed are R=0.1, -1 and 10 which apart from being proposed by wind turbine rotor blade certification bodies as GL or DNV cover a minimum range of fatigue conditions, both in tension and compression. For in-plane shear fatigue strength tests were performed only for R=0.1 and the common assumption that shear strength in the principal material system does not depend on the sign of the shear stress along with the Goodman approach led to a symmetric CLD.

Experimental results from CA tests parallel, transverse to the fibres and under in plane shear were presented in Fig. 30, 31 and 32 respectively. The S-N curves drawn in these figures are given by:

$$\sigma_a = \sigma_o N^{\left(-\frac{1}{k}\right)} \tag{19}$$

In the above relation, σ_a stands for the alternating component of the cyclic stress, N for the number of cycles to failure while constants σ_o and k, depending on the R-ratio and the stress component were given in Table 6.

Table 6: S-N curve parameters for the OB_UD glass/epoxy

	σ_1		σ_2		σ_6	
R	σ_o	k	σ_o	k	σ_o	k
0.1	500.8	10.03	50.2	8.63	38.1	11.06
-1	972.2	8.05	87.5	8.43	N/A	N/A
10	289.5	26.08	88.5	24.32	N/A	N/A

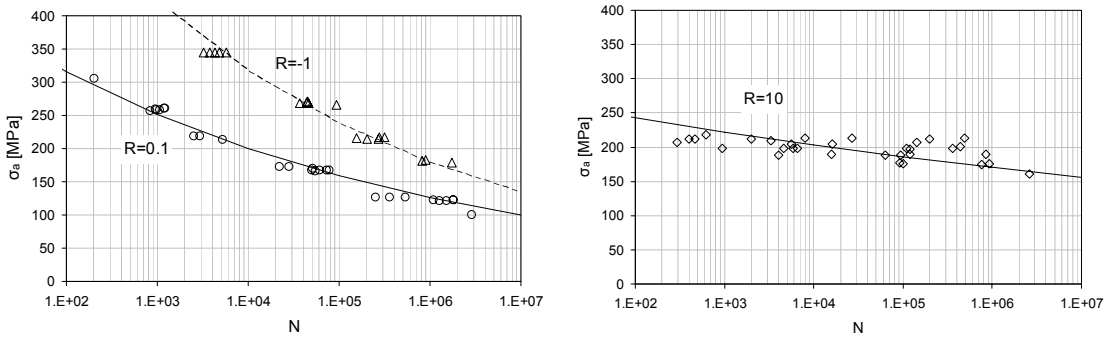

Fig. 30: S-N curves for the OB_UD glass/epoxy in the fibre direction

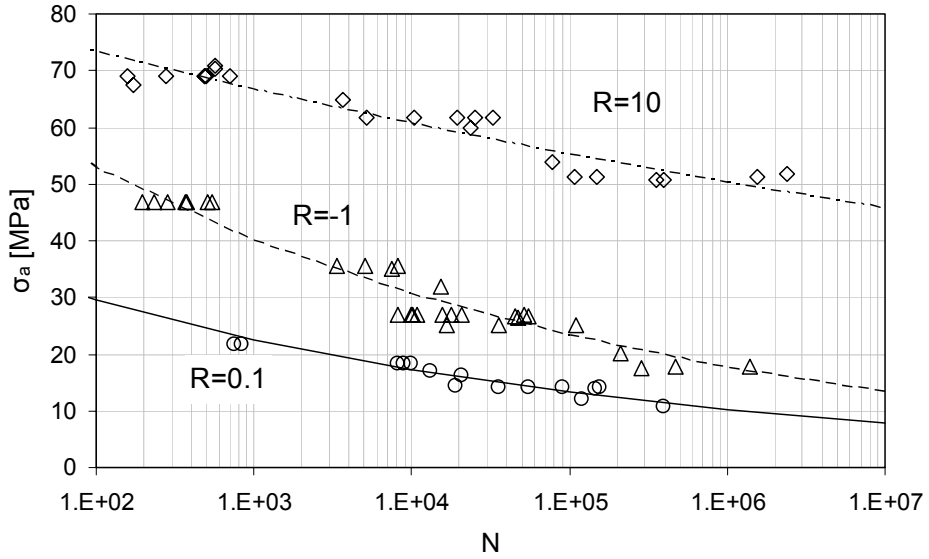

Fig. 31: S-N curves for the OB_UD glass/epoxy transverse to the fibres

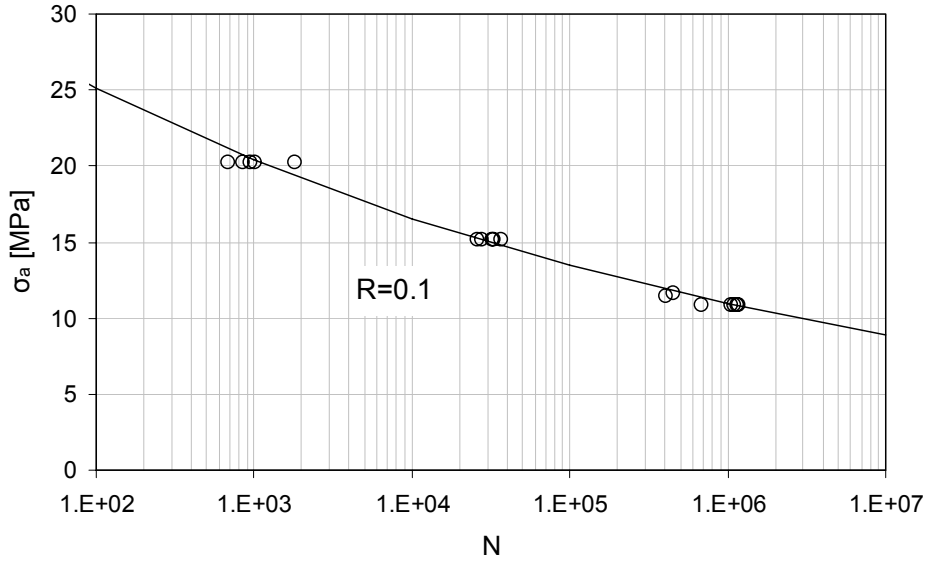

Fig. 32: S-N curve under in-plane shear for the OB_UD glass/epoxy

Fatigue behaviour at different stress ratios were obtained by linear interpolation between the already known S-N curves as described by Philippidis and Vassilopoulos [4]. Alternative formulations, e.g. the interpolation model by Harris [41], were already developed for the OB_UD glass/epoxy material, see Passipoularidis and Philippidis [39], but not used in deriving the results presented herein.

The constant life diagrams for axial loading parallel or transverse to the fibres and in-plane shear were presented in Fig. 33, 34 and 35 respectively.

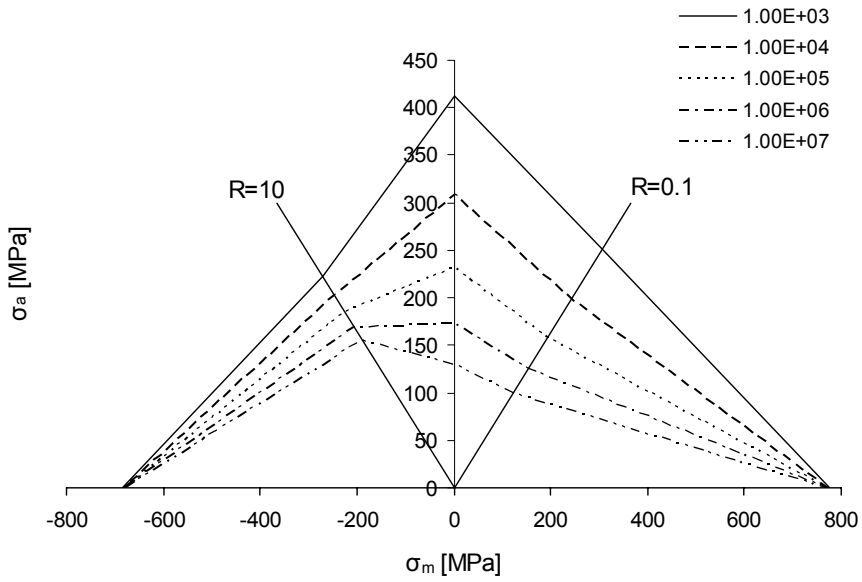

Fig. 33: CLD for the OB_UD glass/epoxy (parallel to the fibres)

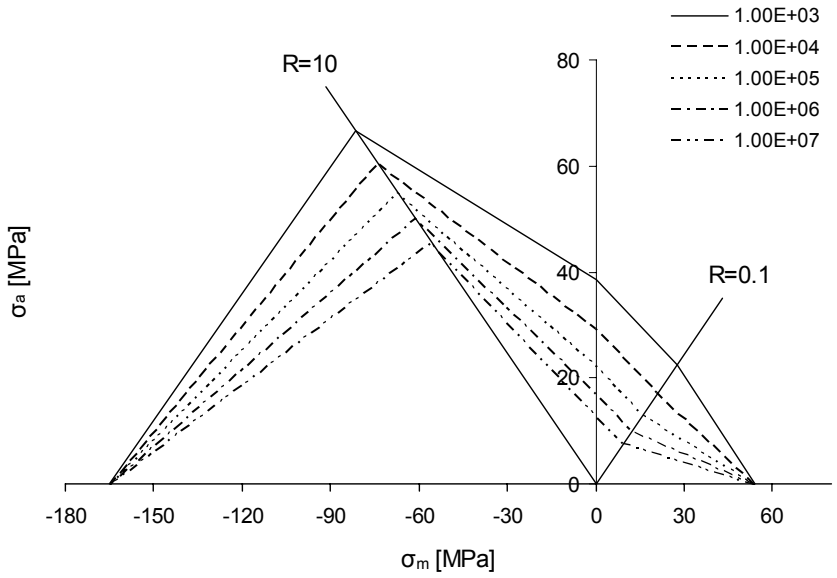

Fig. 34: CLD for the OB_UD glass/epoxy (transverse to the fibres)

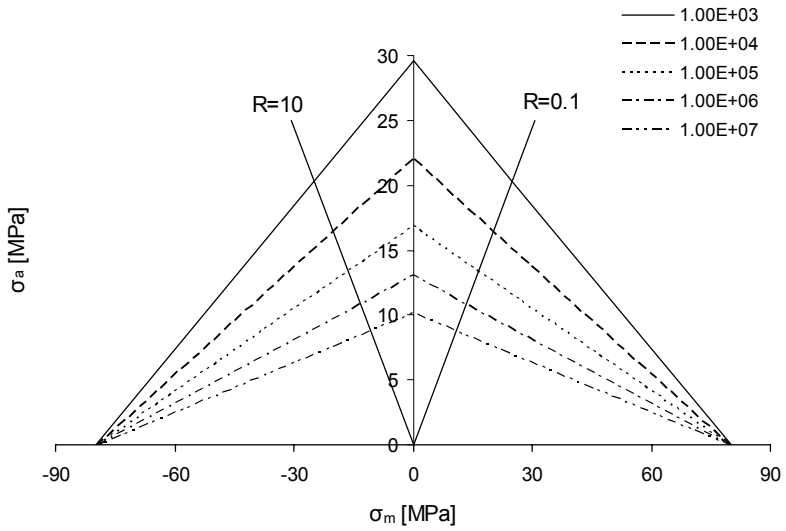

Fig. 35: CLD under in-plane shear for the OB_UD glass/epoxy

6. FAtigue DAmage Simulator (FADAS)

The FADAS methodology developed for life prediction of composite shell structures under VA complex cyclic loading, e.g. wind turbine rotor blades, considers a basic orthotropic UD lamina to be the constitutive element of the multidirectional (MD) lay-up. Application of the model requires in-plane mechanical properties of the ply, i.e. on-axis, transversely to the fibre and in shear to be experimentally derived.

The elastic behaviour is assumed non-linear, as already presented in section 2.1. Elasticity is subject to a gradual degradation due to the fatigue loading, which is accounted for through the simple models presented in section 2.3. Adequate formulations for degradation of tensile, compressive and shear static strength due to fatigue, both in tension and compression, were also taken into account. Residual static strength is used as the damage accumulation metric. Complex cyclic stress states are combined by means of the failure criterion to predict life of the component.

Two implementations of the algorithm have been developed. The first was implemented in MATLAB [42] and the algorithm proceeds by means of CLT assumptions for the stress and strain calculations. In the second, implemented in ANSYS, the stress analysis is performed using a Reissner-Mindlin shell FE formulation [43]-[44]. An earlier linear version of the method based on CLT assumptions was presented by Passipoularidis et al. [45].

6.1 MATLAB implementation of FADAS

The stress and strain components at the principal coordinate system of each ply are calculated by means of CLT assumptions for the current external load segment (peak-trough pair) in the MATLAB implementation of FADAS. With stresses known, the Failure Criterion is applied. If failure occurs in some ply, its stiffness is modified as presented in section 2.3.2. After failure events are accounted for, the algorithm progresses with calculation of the gradual strength and stiffness degradation due to fatigue: The stress amplitude and R-ratio of each stress component are defined and the corresponding fatigue life, N_f is derived using appropriate CLD data. A general flowchart of the algorithm is shown in Fig. 36. Further details on the operation of the various modules shown in the diagram are given below.

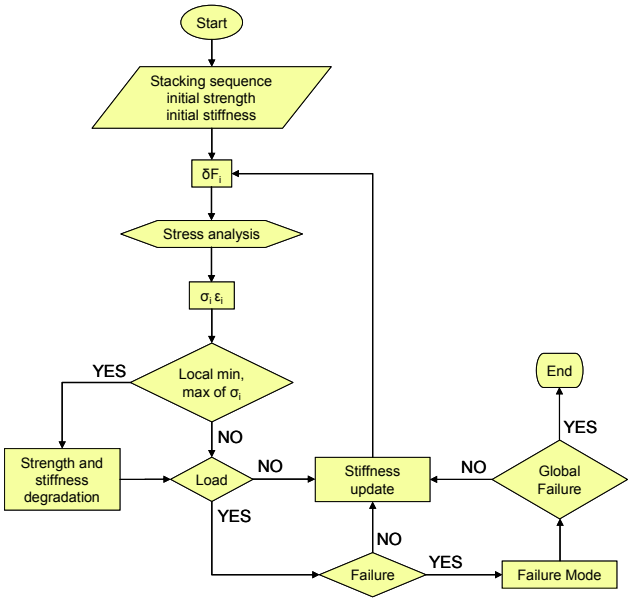

Fig. 36: Flowchart of the FADAS algorithm

6.1.1 Calculation under VA cyclic stresses

The model simulates any load sequence presented as input cycle by cycle, or more specifically segment by segment with a number of load steps per segment. Even external loading of constant amplitude causes cyclic stress components of variable amplitude at each ply due to nonlinearity, reload stiffness and stiffness degradation. The latter being driven by cyclic loading and local failures, causes stress redistribution.

While a load segment is incrementally applied, the maximum and minimum values of each component of stress at each ply are determined. When a local min or max stress component σ_i is detected, the corresponding stress ratio R_i, and stress amplitude σ_{ia} can be calculated by:

$$R_i = \frac{\sigma_{i_{min}}}{\sigma_{i_{max}}},\ i = 1,2,6 \tag{20}$$

$$\sigma_{ia} = \frac{\sigma_{i_{max}} - \sigma_{i_{min}}}{2},\ i = 1,2,6 \tag{21}$$

For the calculated R_i, the stress amplitude values σ_{ia} for number of cycles to failure, N, equal to 10^3, 10^4, 10^5 and 10^6 are calculated as described in section 5 by linear interpolation from the CLD corresponding to each stress component. Then, with linear regression on these four data points on a double logarithmic scale, the S-N curve is derived for the specific stress ratio, and thus finally, the number of cycles to failure for the developed stress range is calculated.

The obtained N_i is required for the calculation of the cumulative life fraction for each stress component that is used in the stiffness degradation models:

$$\sum \frac{n_i}{N_i}\bigg|_{(\lambda+1)} = \sum \frac{n_i}{N_i}\bigg|_{(\lambda)} + \frac{0.5}{N_i},\ i = 1,2,6 \tag{22}$$

Indices into parentheses in the above relation, e.g. (λ), (λ+*1*), denote the stress segment number, hence the term 0.5 in the second term of the right hand side denoting half a cycle, i.e. a stress segment. In the stiffness degradation models of Eq. (5) presented in section 2.3, the ratio *n/N* for the case of VA cyclic stress has to be replaced by the cumulative live fraction given by Eq. (22).

The calculated N_i, i=1,2,6 are also used with the strength degradation models presented in section 4. When a local min or max value for the σ_1 stress component is detected, the residual tensile strength in the fibres direction $X_{T_r(\lambda+1)}$ is reduced by using an adapted form for VA cyclic stress of the Broutman & Sahu model, Eq. (12), only if the maximum stress is positive. Otherwise, it remains unchanged.

The residual strength at the (λ+*1*) segment of magnitude σ_{1max} can be readily proved to be given by:

$$X_{T_r(\lambda+1)} = X_T - (X_T - \sigma_{1max})\left[\frac{X_T - X_{T_r(\lambda)}}{X_T - \sigma_{1max}} + \frac{0.5}{N_1}\right] \tag{23}$$

The term added in $0.5/N_1$ in the brackets is the equivalent number of cycles, n_{eq}/N_1, which is the CA number of cycles at the actual stress level of σ_{1max} that would reduce the static strength down to the value of $X_{T_r(\lambda)}$, see Schaff and Davidson [46].

For the compressive residual strength in the fibres direction, the use of the sudden death model given by Eq. (13) might be prohibited (numerical precision problems) for high values of the exponent of the equation due to very small reduction of strength. In such cases an alternative formulation based on a modified linear model, Eliopoulos [47], is implemented:

$$X_{C_r(\lambda+1)} = X_C - \beta(X_C - |\sigma_{1min}|)\left[\frac{X_C - X_{C_r(\lambda)}}{\beta\left(X_C - |\sigma_{1min}|\right)} + \frac{0.5}{N_1}\right] \tag{24}$$

The constant β is a small positive number, e.g. 10^{-3}, 10^{-6}. Its value is not of importance provided that the term $(1-\beta)X_C$ is greater than the largest $|\sigma_{1min}|$ in the time series. Nevertheless, the values suggested in the above were efficiently used for the verification examples presented in this work. The degradation model is supplemented by the following logical statement:

$$\text{If } X_{C_r(\lambda+1)} \le (1-\beta)X_C + \beta|\sigma_{1min}| \text{ then } X_{C_r(\lambda+1)} = |\sigma_{1min}| \tag{25}$$

The degradation scheme for the compressive residual strength formed of the two Eq. (24) and (25) has a numerically stable sudden death response. Therefore, under C-C and T-C cyclic loading the compressive strength degradation is calculated by means of Eq. (24) and (25). Otherwise it remains unchanged.

Implementation in the routine of the residual strength models for the transverse to the fibres direction and in-plane shear is performed in a similar way as for the fibre direction. The value of the degradation factor f of Eq. (18) was set at 0.5 in the MATLAB implementation of FADAS.

The values of ply engineering constants E_{2t} and G_{12t} for unloading are calculated by multiplying the respective reloading properties, given by Eq. (4), with 1.00001.

6.1.2 Computational procedure

As it was mentioned in previous sections, an incremental stress-strain analysis was performed and to that end external loading was also applied incrementally. The load series presented as input must be in the form of peaks and troughs, so previous treatment of continuous time series might be necessary. For the examples of MD laminates made of the OB_UD glass/epoxy ply included herein, the range between successive peak and trough values was divided into 20 load steps. The first two are very small, e.g. 1E-03 times the respective peak or trough value, so as the detection of any change of the loading condition, loading or unloading, was performed at an early stage with negligible stress and strain variation. 18 equal loading steps were used to span the remaining of the stress range.

With this resolution, the application of an irregular loading spectrum with 1E+05 load reversal points results in 2E+06 load steps for just one pass. For the simulation of the fatigue behaviour of the MD laminates treated in this work an average CPU time was 0.06s per cycle. More specifically, for the MD laminate, $[(0/\pm45)_4/\pm45]$ with 14 plies, it took 0.08s per cycle while only 0.04s for the bi-directional (BD) $[\pm45]_S$ coupon (4 layers). The above were derived by evaluating the performance of this FADAS version in an Intel Core 2 Quad CPU Q6600 @ 2.4 GHz and 4 GB of RAM.

6.1.3 Final failure

While ply failure in one or more different modes might occur even from the first load steps of the first cycle, depending on the stress level, the routine continues the calculations without stopping until the stiffness matrix of the laminate looses its positive definiteness, which practically might

not occur. However, near the final laminate failure a drastic stiffness loss is observed and for this reason the coupon is considered to have failed when at least one strain component of its middle plane ε_x^o, ε_y^0 or ε_s^0 exceeds in a disproportional manner its previous values.

As an example, the last cycles near final failure for a $[(0/\pm45)_4/\pm45]$ coupon under R=-1 reversed uniaxial loading and for a $[/\pm45]_S$ under T-T, R=0.1, were presented in Fig. 37. The cases shown correspond to low-cycle fatigue stress levels, nevertheless the same trend was clearly also observed for all max stress values. Note that the real strain value at failure, for both graphs of Fig. 37, was considerably decreased to enhance resolution. If plotted with its real value then the oscillating part of the curve appears as a bold horizontal line. In fact, these strain values were 0.246 for the MD laminate while several orders of magnitude greater values were reached by the BD lay-up.

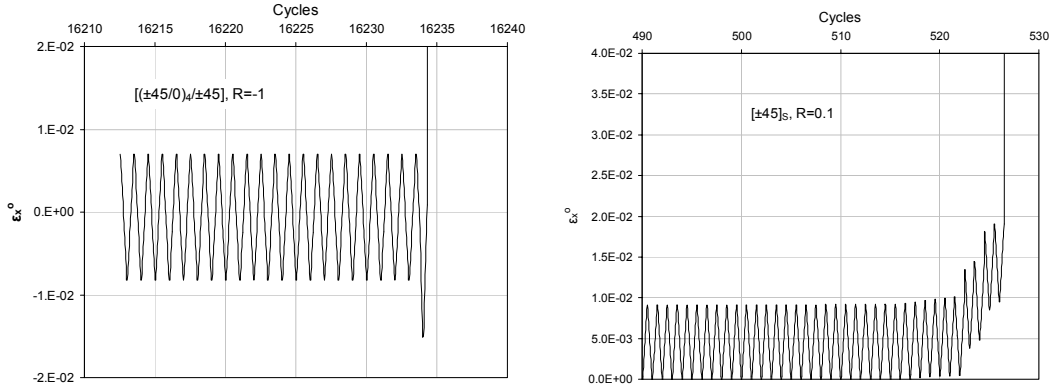

Fig. 37: Axial strain in the loading direction as a function of the applied number of cycles

6.2 ANSYS implementation of FADAS

The FADAS routine has been successfully integrated in ANSYS commercial code and has been adapted to various element formulations; plane strain, 3D brick and shell. For the validation cases presented in this work, all results were derived using the SHELL181 element [48], governed by the Mindlin-Reissner shell theory. It is a 4-node layered element with six degrees of freedom at each node. The reduced integration option was selected with 1 integration point location at the area of the element and 3 integration points through the thickness of each layer. Non-linear geometry effects were also included.

The user defined material constitutive model was implemented in a FORTRAN routine [49] which was compiled with ANSYS core code and a new executable ANSYS file was created, reducing the solution time a lot, since calculations of the elastic properties for each successive load step were performed at the same time with the stress-strain calculations and not externally later, e.g. using APDL commands. Static analysis was performed, considered to be valid for low strain rate loading cases. A general flowchart of the algorithm is shown in Fig. 38.

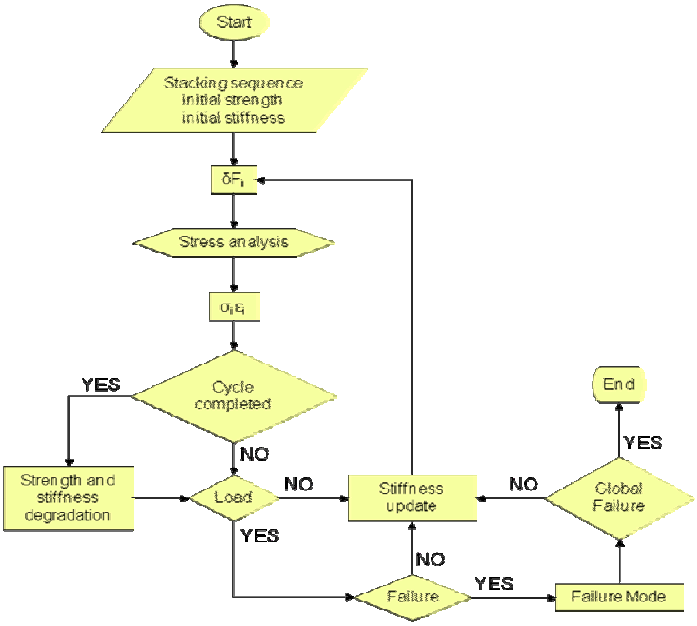

Fig. 38: Flowchart of the FADAS algorithm

6.2.1 Calculation under CA cyclic stresses

In the FE implementation, the simulation time for each load step is much higher. In fact it is a multiple of the number of integration points of the entire FE model, since all calculations are performed separately for each one of them. An alternative approach was followed when the applied loading was of CA. For the time being and for moderate CPU resources, it is not practical to simulate applications of VA spectrum loading with the actual FE version of FADAS. Nevertheless, even external loading of CA generates VA cyclic stress components in each ply due to strength and stiffness degradation driven by cyclic loading and local sudden failures, causing stress redistribution.

While the external load is incrementally applied, the max and min values of each component of stress in each ply are determined. The stiffness and strength degradation calculations are performed when a cycle of the external load is completed. The value 0.5 in Eq. (22)-(24) is replaced with Δn which is an arbitrary block of CA cycles defined by the user considered to be of the same mean and range as the simulated one.

At the present FADAS implementation, this parameter, Δn, was left fixed for programming simplicity. For each case, after several numerical experiments, it was selected as a compromise between accuracy and realistic computational effort to have Δn such as to simulate ca. 10 to 20 full cycles (distant by Δn) in the life span of the coupon. Max and min prediction values presented in the graph results are related to the range Δn of the applied block of cycles, i.e. when failure is predicted at the beginning of a simulated cycle it is not known in which exactly cycle from the Δn has occurred.

The values of ply engineering constants E_{2t} and G_{12t} for unloading are calculated by multiplying the respective reloading properties, given by Eq. (4), with 1.001. As the full cycle of external load is simulated for a limited number of times, this value is known to predict very limited increasing permanent strain values. However, even with this value the resulting strain would be different for another user selected Δn block of cycles number but this is not expected to affect

FADAS predictions even for matrix dominated lay-ups, concerning number of cycles to failure, residual strength and stiffness since all material models and failure conditions are stress rather than strain based. Since no reliable experimental data were available for deriving accurate permanent strain models or implementing existing theoretical models, this was the simplest way to introduce increasing permanent strain due to cyclic loading since permanent strain due to increasing stress level and/or local failure was already included in the routine, Eq. (4) and post-IFF model respectively.

The value of the degradation factor f of Eq. (18) was set at 0.8 in the ANSYS implementation of FADAS.

6.2.2 FE models

The prismatic coupons were modelled with three different FE models because of different coupon geometry and stacking sequences of the specimens tested. The standard OB UD specimens, of a coupon geometry, Fig. 39, developed and used in the OPTIMAT BLADES project, were modelled with 704 elements and 1 layer, the ISO 14129 $[\pm 45]_S$ specimens with 1920 elements and 4 layers and the standard OB MD specimens with 768 elements and 14 layers. Displacements along x and z axes of all nodes located at the left tab area, Fig. 39, except those at the internal edge of the tab were constrained. In addition, the y-displacements of all nodes located on the centreline were also constrained. However, all other nodes of the left tab were left free to move in the y-direction to simulate Poisson contraction of the laminate under the compliant tab material. Axial load in the x-direction was equally shared by all the nodes located on the right tab area except those at the internal edge CD of the tab, Fig. 39. Nodal displacements of the centreline of the same tab were also constrained in the y- and z-direction.

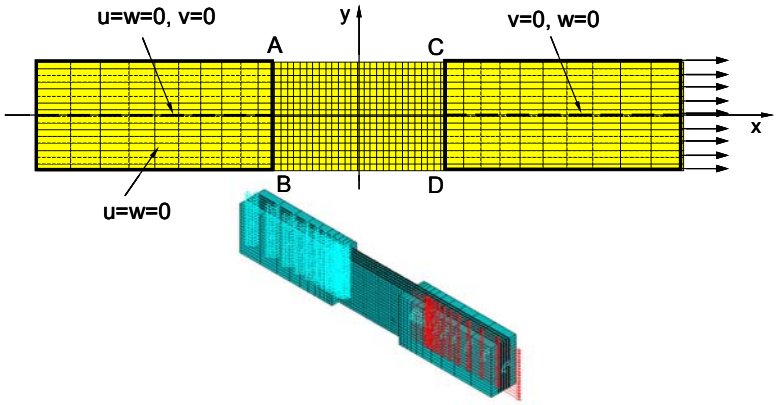

Fig. 39: Boundary conditions shown on prismatic OB coupon geometry

The tubular specimens were modeled with 2176 elements for all loading cases, adopting a cylindrical coordinate system to define the boundary conditions, see Fig. 40. All displacements in the radial, hoop and axial directions were restricted in the gripping area attached to the fixed part of the test rig. Also rotations about the hoop and axial directions were constrained. At the other tube end, attached to the moving head of the test rig, radial displacements were constrained. Forces in the axial and hoop directions were applied to simulate tensile or compressive axial load and torsion respectively. Forces were evenly distributed in all nodes of the tab area.

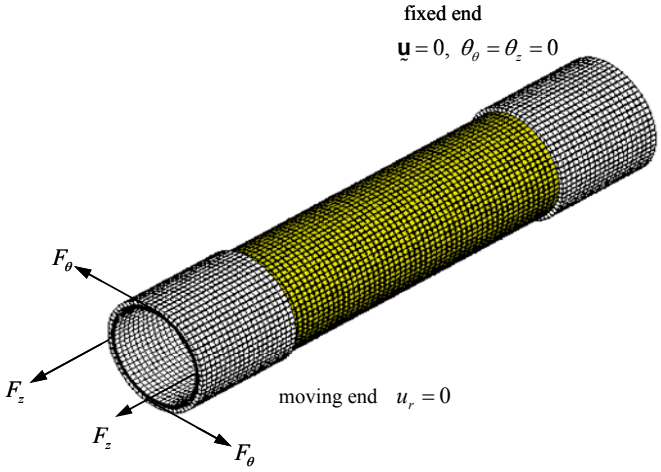

Fig. 40: FE model of cylindrical specimen

Independent rotational degrees of freedom about the radial axis, θ_r, compatible with the formulation of the shell element implemented, were restricted along specimen length, avoiding ANSYS default penalty method that relates them with in-plane displacement components [48]. Tube laminate was modelled as a $[\pm 45]_2$ lay-up, without simulating ply overlap. The same modelling was also followed in [50].

A mesh of 1039 elements simulated the cruciform specimens [51], Fig. 41. Since it was assumed that loads were smoothly transferred through laminate sections, and in order to save computational time and memory resources, only a part of the specimen arms was simulated. Excluding gripping areas, 90 mm out of total 250 mm were modeled in both directions, Fig. 41a. The milled region was simulated with drop-off layer technique, as illustrated in Fig. 41b.

Forces were evenly distributed on the upper and right arm edge nodes, Fig. 41a, also being forced to displace equally, thus simulating the test gripping boundary conditions. The edge node displacements were restricted along y and x-axis respectively in the left and the lowest arm, Fig. 41a.

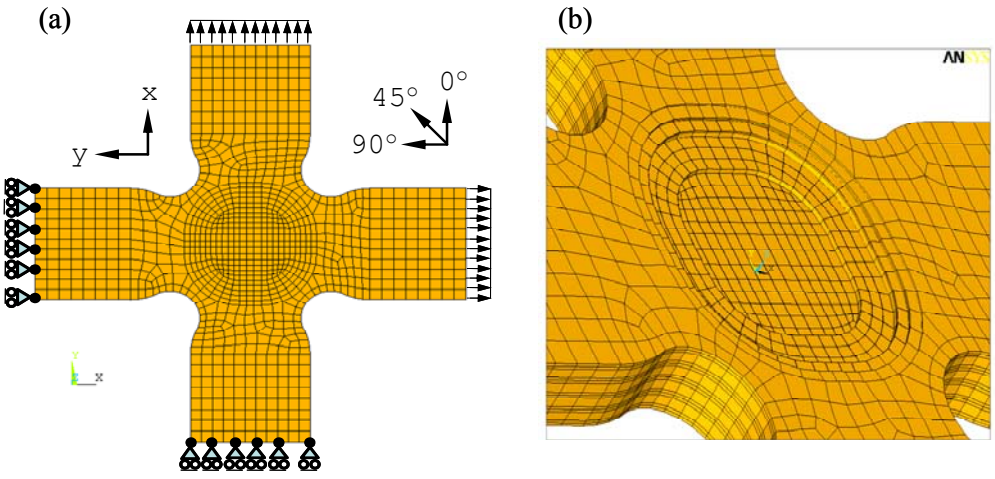

Fig. 41: FEM model of the cruciform specimen. Coordinate systems and boundary conditions

6.2.3 Computational procedure (FEM)

The number of load steps per cycle at different stress ratios was optimized as follows. Under T-C loading (R=-1, R=-0.4, R=-2.5) 60 load steps were foreseen; 40 loading (20 tensile and 20 compressive) and 20 unloading (10 tensile and 10 compressive). Under pure tensile and compressive loadings, R=0.1 (T-T), R=0.5 (T-T) and R=10 (C-C) respectively, 30 load steps were realized per cycle; 22 loading and 8 unloading. Upon unloading the material behaviour was assumed linear, so fewer steps were needed. The two load steps after the end of loading or unloading segments are much smaller, e.g. 2 to 3 orders of magnitude less than the other, so as the change of loading condition was detected with negligible stress and strain variation.

For the residual static strength predictions, the FE model was first subjected to CA cyclic loading until the desired life fraction. Then, static loading up to failure was imposed with the load increment being 5 MPa for the $[(\pm 45/0)_4/\pm 45]_T$ model and 1 MPa for that of the $[\pm 45]_S$.

The CPU time needed for each simulation depends of course on the number of elements and layers of the FE model but also on the cycle block number Δn defined by the user. For the MD and the ISO $[\pm 45]_S$ prismatic coupons, the CPU time was 6s per load step. Total time for each simulation was a couple of hours in an Intel Core 2 Quad CPU Q6600 @ 2.4 GHz and 4 GB of RAM.

6.2.4 Global failure

Again the routine continues the calculations without interruption until positive definiteness of the laminate stiffness matrix is lost. This might not occur in practice; however, near the final laminate failure a drastic stiffness loss is observed and for this reason the coupon is considered to have failed when any nodal displacement of the model in any direction exceeds in a disproportional manner its previous values.

6.3 Experimental data

FADAS has been implemented with ply properties derived for the OB_UD glass/epoxy composite. For the verification of the numerical predictions, extensive comparison with experimental data was performed. Unidirectional (UD) and multidirectional (MD) laminates made of the basic ply material were subjected to various loading conditions consisting of static loading, CA cyclic loading of different stress ratios, simple VA cyclic loading, irregular spectrum loading and finally of static residual strength tests on coupons previously subjected to cyclic loading at various stress levels and life fractions. Both uniaxial tests on prismatic coupons and biaxial tests on tubular and cruciform specimens were simulated.

Details on the experimental procedure, measurements and results discussed in this section can be found in the OPTIDAT database and dedicated reports in the OPTIMAT BLADES site and the UPWIND site (http://www.upwind.eu/CPS/default.aspx).

6.4 Results and discussion

6.4.1 Prismatic coupons

The UD ply thickness was set equal to 0.94 mm except for the +45° and -45° layers of the $[(\pm 45/0)_4/\pm 45]_T$ laminate where a thickness of 0.33 mm was used. The reason is that for this laminate a bidirectional stitched fabric of ±45 orientations was used instead of discrete layers from the basic OB_UD composite.

6.4.1.1 CA tests on UD in the fibre direction $[0_4]_T$

With an analytical method considering homogenous stress field like the MATLAB implementation of FADAS, it is obvious that the predicted results for a case that was also used as input in the method are exact. In FE simulation however, possible stress concentrations can affect the results, as the macroscopically applied stress is lower than the value at a stress concentration, from where failure initiates causing stress redistribution. After that the failure accumulates in a larger area until global failure of the specimen.

The CA tests on UD coupons were reported in [31].The reversed cyclic loading, R=-1, of the UD laminate in the fibre direction $[0_4]_T$ was simulated with the ANSYS implementation of FADAS at four stress levels and namely at σ_{max}=412, 338, 254 and 175 MPa corresponding to expected number of cycles to failure equal to N=1000, 5000, 50000 and $1 \cdot 10^6$ respectively. The predicted S-N curves along with the respective test data were shown in Fig. 42. The results are 20-30% conservative as the predicted number of cycles (min-max) to failure for the aforementioned stress levels were 700-750, 3500-3750, 35000-37500 and 750000-800000 respectively. The analysis by means of FE reveals stress concentrations at the corners of the gauge length area, where failure initiates, see Fig. 43. The predicted S-N curves were derived by means of linear regression on a double logarithmic scale of the results of the simulated stress levels.

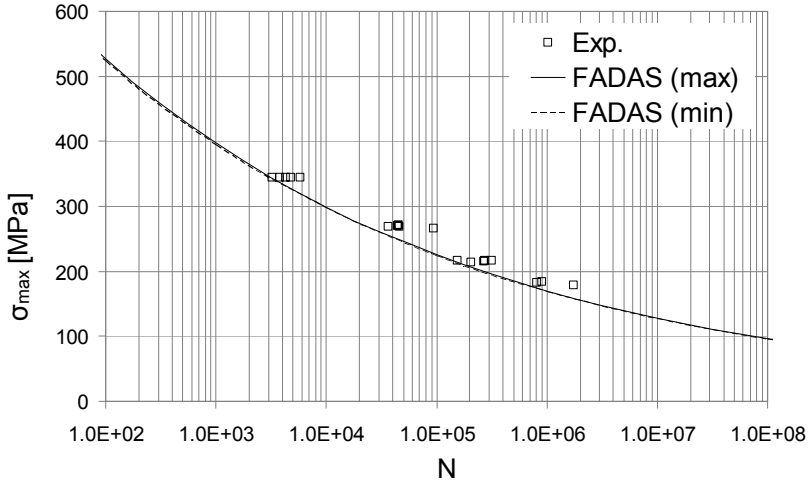

Fig. 42: Comparison between simulation results and exp. data, $[0_4]_T$ under R=-1

The different colours in Fig. 43 correspond to different failure modes. FF_T and FF_C stand for fibre fracture in tension and compression respectively while IFF_A, IFF_B and IFF_C for inter-fibre fracture modes A, B and C respectively, see Puck et al. [20].

The simulation at four stress levels at R=0.1 corresponding to the same expected number of cycles to failure gave similar results, i.e. 25-35% conservative, Fig. 44. The UD laminate in the fibre direction $[0_4]_T$ was also simulated at four stress levels at R=10 corresponding to the same expected number of cycles giving conservative results by 65-70%, Fig. 45. This was due to the flat S-N curve of the UD material in the fibre direction at R=10 resulting in high variation in the predicted number of cycles to failure for low variation of the applied maximum stress.

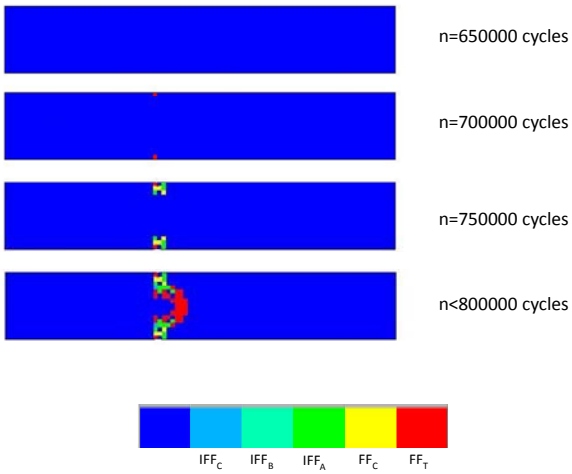

Fig. 43: Failure modes of the UD laminate $[0_4]_T$ under R=-1, σ_{max}=175 MPa

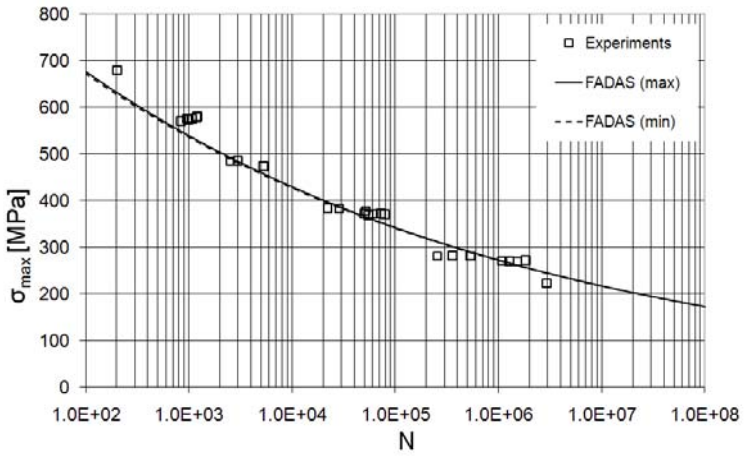

Fig. 44: Comparison between simulation results and exp. data, $[0_4]_T$ under R=0.1

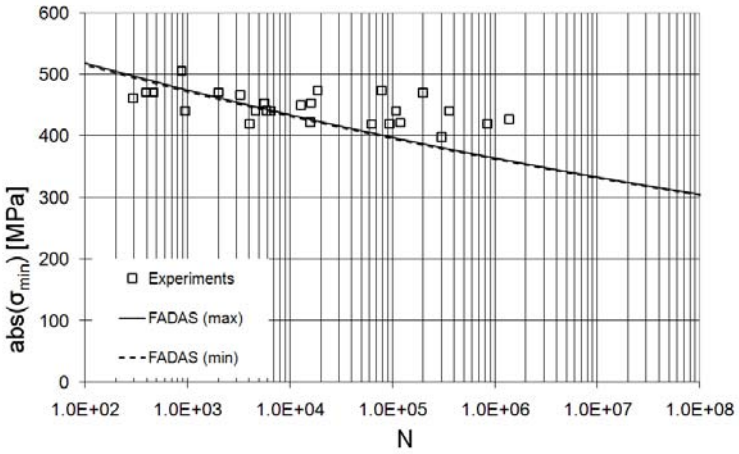

Fig. 45: Comparison between simulation results and exp. data, $[0_4]_T$ under R=10

6.4.1.2 CA tests on UD transversely to the fibres $[90_7]_T$

Reversed (R=-1) loading of the UD laminate in the transverse to the fibres direction [29] $[90_7]_T$ was simulated at four stress levels σ_{max}=38.6, 31.9, 24.3 and 17.0 MPa corresponding to the same expected number of cycles as previously, see Fig. 46. The numerical predictions were 950-1000, 4750-5000, 47500-50000 and 950000-1000000 cycles respectively. For the case of T-T loading (R=0.1) the same exactly results were derived, Fig. 47, while for R=10 the results were conservative by 20-25%, Fig. 48. Failure initiates in the corners of the gauge length area as for the UD [0] cases but the damage modes were obviously different, Fig. 49.

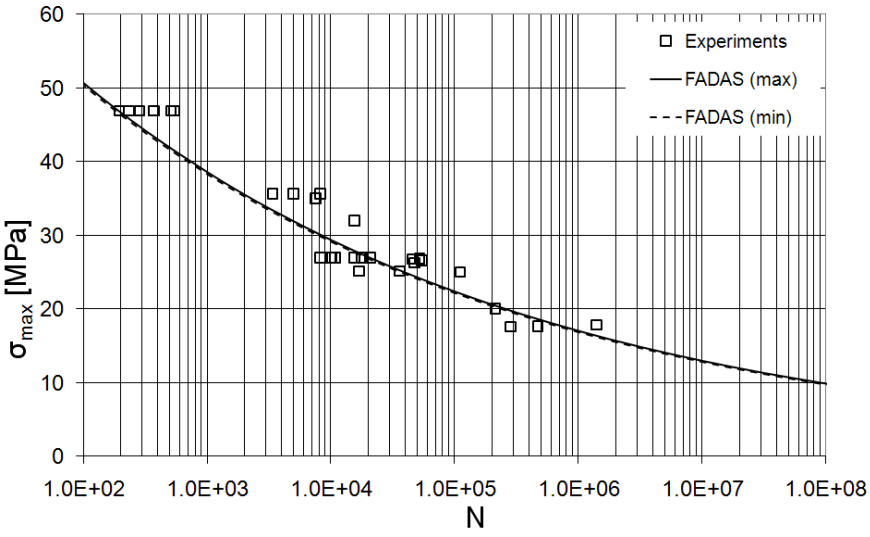

Fig. 46: Comparison between simulation results and exp. data, $[90_7]_T$ under R=-1

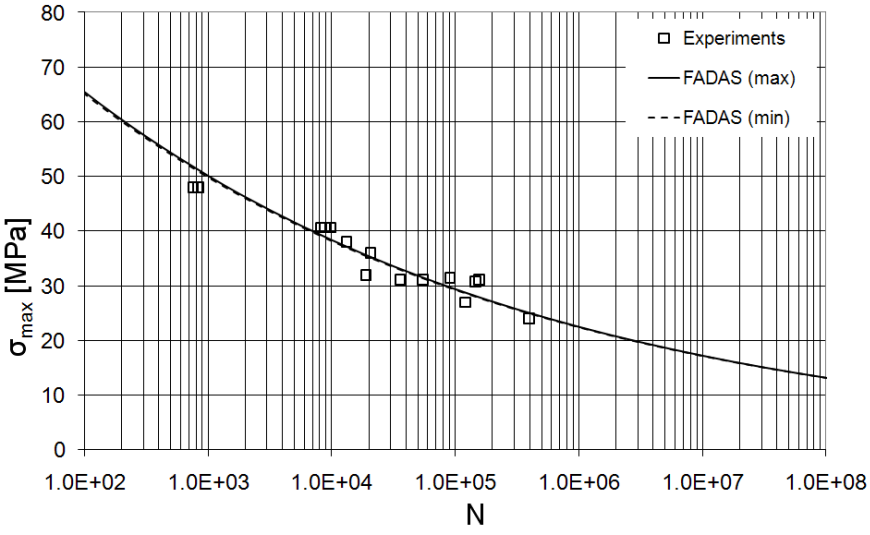

Fig. 47: Comparison between simulation results and exp. data, $[90_7]_T$ under R=0.1

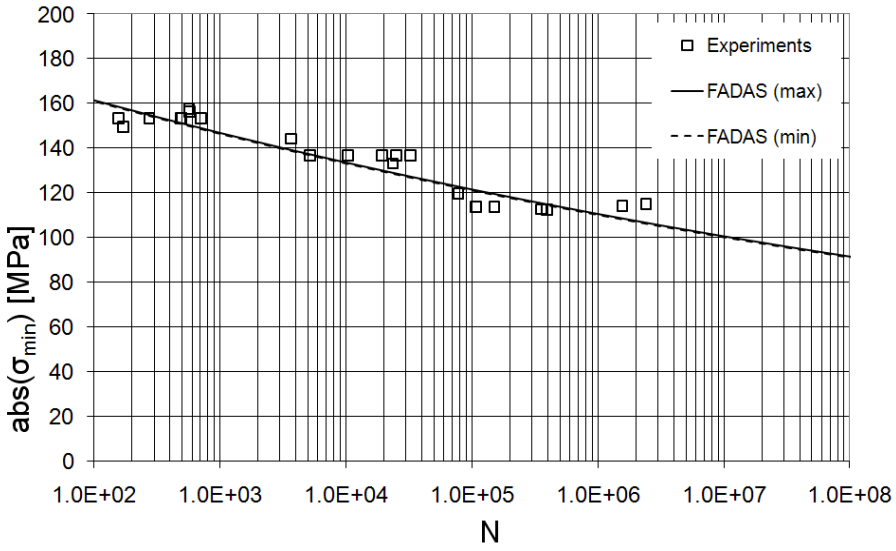

Fig. 48: Comparison between simulation results and exp. data, $[90_7]_T$ under R=10

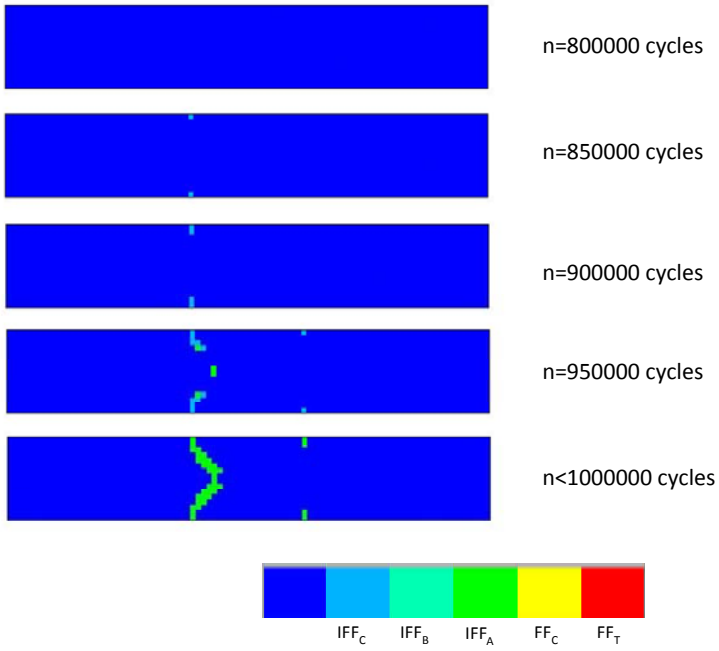

Fig. 49: Failure modes of the UD laminate $[90_7]_T$ under R=-1, σ_{max}=17 MPa

6.4.1.3 CA tests on ISO 14129 $[\pm 45]_S$ coupons

Tensile (R=0.1) CA loading of the $[\pm 45]_S$ laminate was simulated at three stress levels σ_{max}=90.6, 63.6 and 48.5 MPa corresponding to expected number of cycles to failure equal to 1000, 50000 and $1 \cdot 10^6$ respectively with both implementations of FADAS. The predicted numbers of cycles were 450-500, 37500-40000, and 900000-950000 respectively with the ANSYS implementation of FADAS and 483, 37743, and 830705 respectively with the MATLAB implementation; they were compared with test data reported by Philippidis et al. [28] in Fig. 50.

The results are more conservative for the higher stress level and improve at the lower ones. Although failure initiates very early, the final failure delays, Fig. 51, since the stiffness degradation rules for matrix failure are not strict.

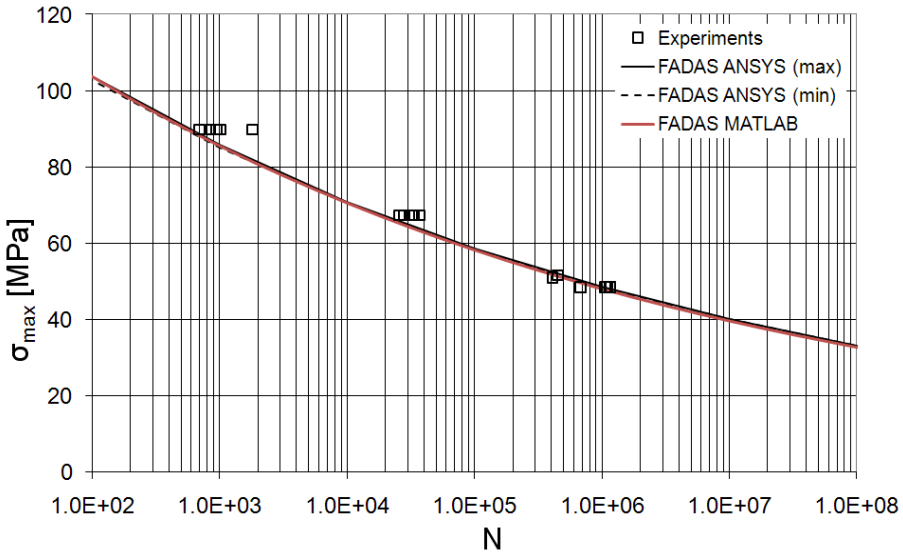

Fig. 50: Comparison between simulation results and exp. data, $[\pm 45]_S$ under R=0.1

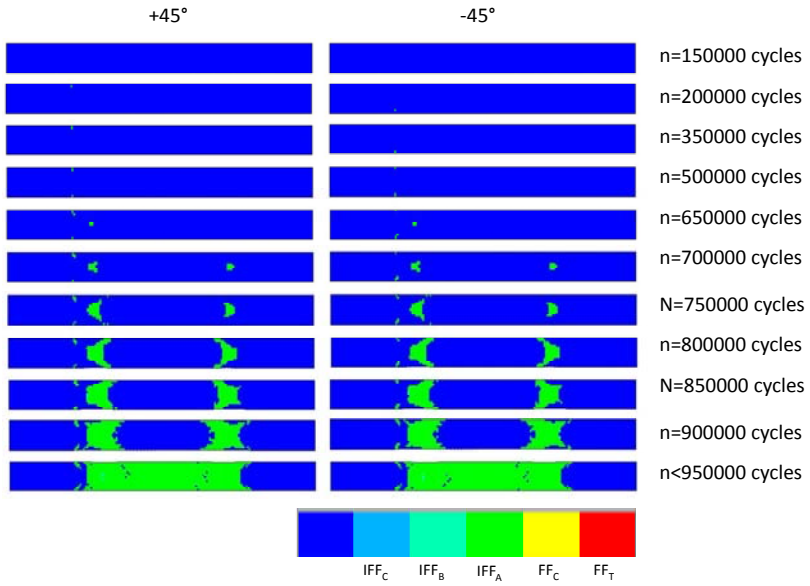

Fig. 51: Failure modes of the ISO $[\pm 45]_S$ coupon under R=0.1, σ_{max}=49 MPa

The predicted axial stiffness degradation of the coupon with ANSYS was compared to the experimental one in Fig. 52. The experimental stiffness was derived by end displacement data, while the predicted one was determined using the axial displacement of the two most distant nodes on the centreline of the FE model at the edges of the gauge length. The stiffness degradation is predicted to be higher for the lower stress levels following the trend of the experimental data. Nevertheless, simulation results are corroborated by the respective experimental data although more stiff in general.

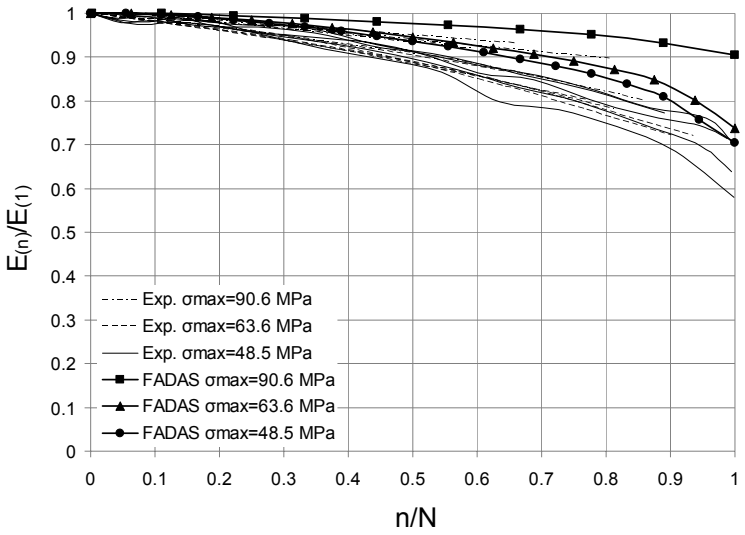

Fig. 52: Validation of stiffness degradation predictions. $[\pm 45]_S$ under R=0.1

The residual static strength of ISO 14129 $[\pm 45]_S$ coupons after CA loading up to a certain life fraction was also predicted with ANSYS and the results were compared to the respective experimental data (RS exp.) from [52]-[53] and the macroscopic residual strength model of Broutman-Sahu (BR) in Fig. 53. The experimental S-N curve, the static strength (ST exp.) of the intact coupon and the prematurely failed coupons (pr. fail.) during the residual strength test program also appear in the same figure. Tests and simulation were performed at 4 stress levels σ_{max}, namely 78.3 MPa (expected N to failure 5000 cycles), 63.6 MPa (50000 cycles), 55.6 MPa (220000 cycles) and 48.5 MPa ($1 \cdot 10^6$ cycles) for several life fractions, i.e. 0.2, 0.5 and 0.8.

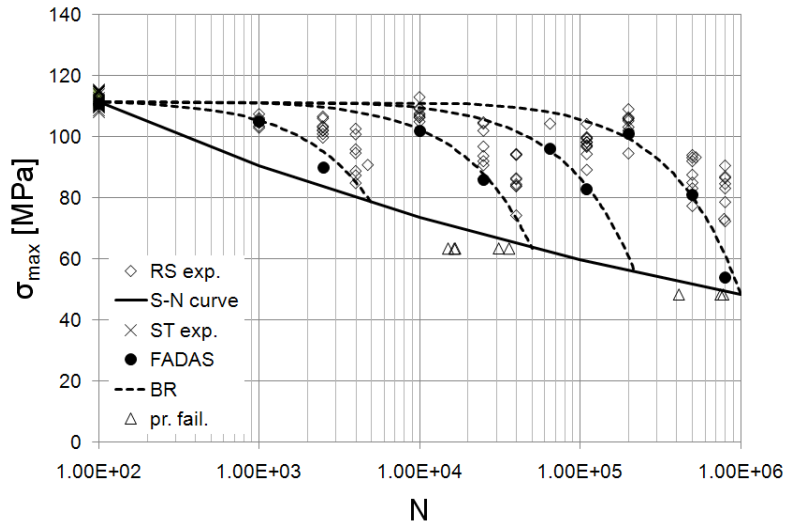

Fig. 53: Residual strength predictions for $[\pm 45]_S$ coupons after CA loading under R=0.1

The predictions are in good agreement with the macroscopic residual strength model BR and are corroborated satisfactorily by the experimental data. As also noticed previously, they improve for the lower stress levels. Some numerical results are not displayed because FADAS predicted failure during the CA loading suite.

6.4.1.4 CA tests on UD off-axis $[60_7]_T$

Tensile (R=0.1) CA loading of the $[60_7]_T$ laminate was simulated at three stress levels σ_{max}=52.2, 42.0 and 31.6 MPa with ANSYS. The results were compared to tests [54] in Fig. 54.

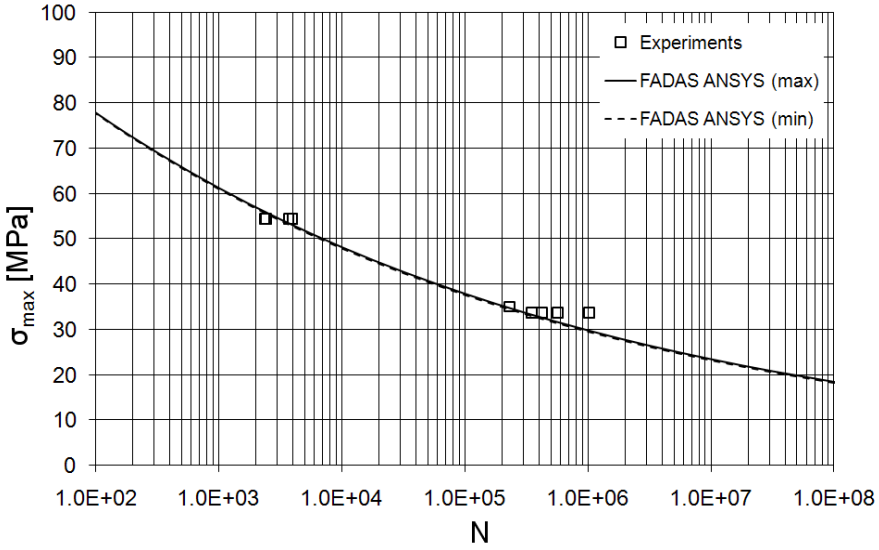

Fig. 54: Comparison between simulation results and exp. data, $[60_7]_T$ under R=0.1

6.4.1.5 CA tests on MD laminate $[(\pm45/0)_4/\pm45]_T$ on-axis loaded

Simulations were performed for the MD laminated coupons, on- and off-axis loaded, under a great variety of stress ratios, i.e. R=-0.4, -2.5, 0.5, 0.1, -1 and 10 and the numerical results were compared to the respective CA [54]-[55] and residual strength test data [56]-[58].

For the MD laminate, $[(\pm45/0)_4/\pm45]_T$, under CA reversed loading, R=-1, calculations were performed for three σ_{max} levels, namely 220, 172 and 126 MPa corresponding to expected number of cycles to failure equal to 5000, 50000 and $1 \cdot 10^6$ respectively with ANSYS and σ_{max}=250, 150 and 125 MPa, with MATLAB.

The first impression from the visual comparison of the numerical predictions and the test data in Fig. 55 is that a very good agreement was achieved. Nevertheless, when looking at the discrete values, it is concluded that the predictions are conservative. The numerical predictions were equal to N=3000-3250, 25000-27500 and 300000-325000 respectively with ANSYS. It should be noticed with respect to Fig. 55 that all available data points from the OPTIDAT database were shown and not only the earlier test results from which the S-N curve definitions [59] were derived and used for the calculation of the expected number of cycles to failure at some stress level. Nevertheless, the fact that the numerical predictions lie in the safe side is advantageous for design purposes.

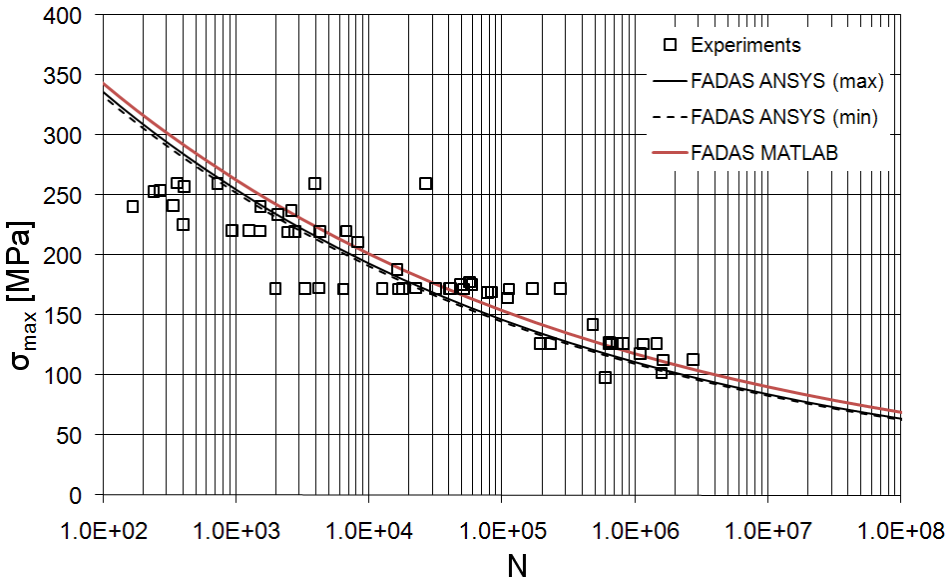

Fig. 55: Comparison between simulation results and exp. data, $[(\pm 45/0)_4/\pm 45]_T$, R=-1

Matrix failure at the off-axis layers was predicted very early. The entire gauge length area of the [±45] layers has matrix cracks from the first simulated cycles, see Fig. 56. The final failure is predicted when fibre failure spreads at an extended area of the [0] layers.

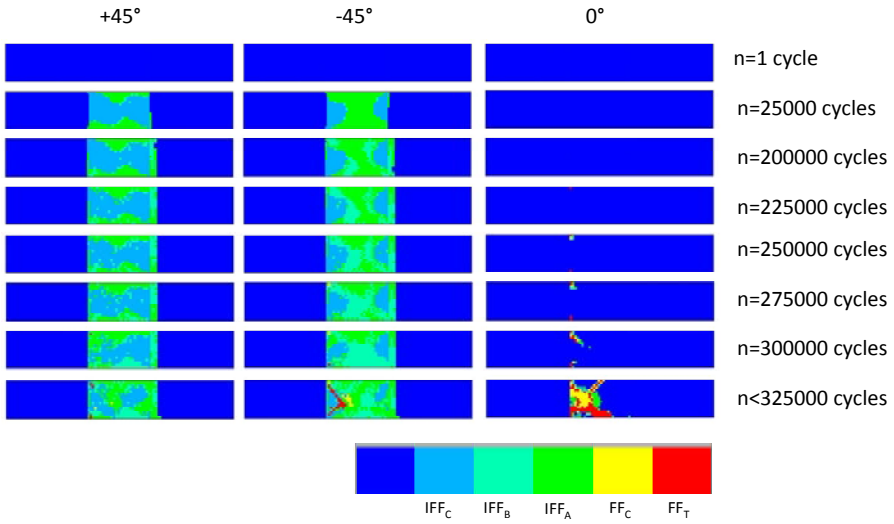

Fig. 56: Failure modes of the $[(\pm 45/0)_4/\pm 45]_T$ coupon under R=-1 at σ_{max}=126 MPa

The strain range was measured with an extensometer of 25 mm gauge length for 2 of these tests [30]. The laminate stiffness was determined by dividing the stress range of each cycle to the respective strain range and was normalized with respect to the stiffness of the first cycle. These data (Exp.) were compared to the respective FADAS predictions (Fig. 57). The predicted stiffness was determined as the slope of the linear regression model of the entire stress-strain loop, with the strain calculated using the axial displacement results from two nodes on the centreline of the FE model distant by 25 mm and was normalized with respect to the stiffness of the first simulated cycle.

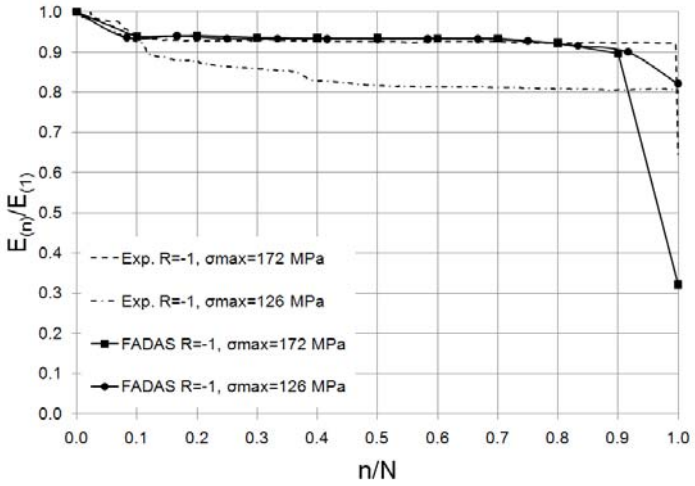

Fig. 57: Comparison between stiffness degradation exp. data and FADAS predictions, $[(\pm 45/0)_4/\pm 45]_T$, R=-1

The experimental data show the typical three-stage stiffness degradation of the composite MD laminates reported by several researchers, i.e. rapid stiffness degradation at the beginning of the cyclic loading followed by moderate stiffness degradation for the most of the fatigue life and a drastic stiffness drop near the final failure. It is also observed that the stiffness degradation is higher for the lower stress levels (high-cycle fatigue), which was also observed in other works, e.g. CA fatigue tests on Glass/Polyester MD coupons by Philippidis and Vassilopoulos [60]. FADAS predicts the three-stage stiffness degradation. The early predicted matrix cracks cause early stiffness degradation, no additional failures are predicted for most of the fatigue life and thus the stiffness is slightly degraded until the fibres failure is predicted near the final failure of the model causing drastic stiffness degradation. FADAS also predicts higher stiffness degradation for lower stress levels but the difference is negligible at R=-1 while the experimental data show significant difference.

Residual tensile and compressive strength tests were performed for the stress levels used in simulation with ANSYS for several life fractions (0.2, 0.35, 0.5, 0.8). The FADAS predictions with ANSYS agree satisfactorily with the experimental data and the macroscopic predictions, as seen in Fig. 58 where the sudden death model (SD) also appears. It should be noted that the macroscopic residual strength models (BR and SD) appearing in Fig. 58 require the knowledge of the S-N curve of the case considered while FADAS does not as it is based only on UD ply properties. The tensile residual strength predictions are in fair agreement with the BR model and even more conservative but the fact that the numerical predictions lie in the safe side is also advantageous for design purposes, since the amount of the premature failures was significant. The compressive residual strength predictions show insignificant strength degradation which is also the case for the tests.

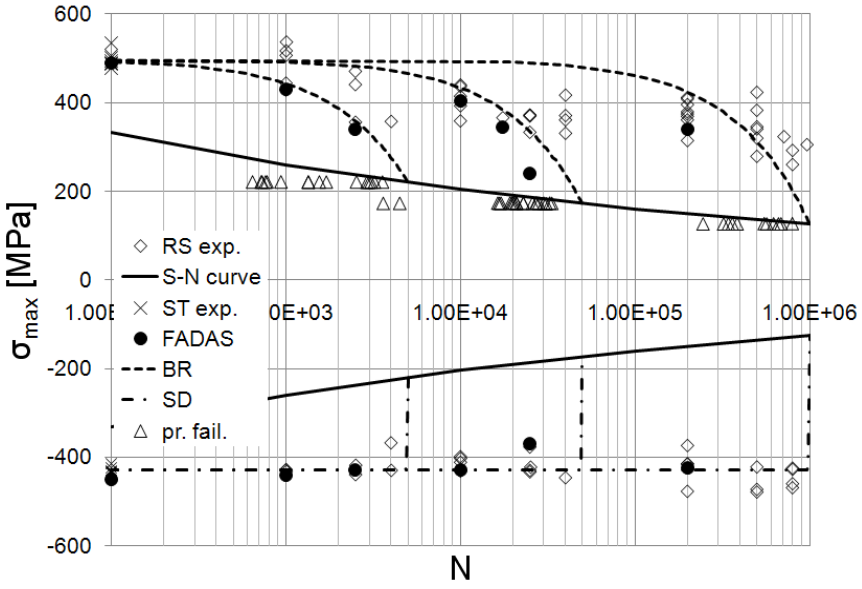

Fig. 58: Residual strength predictions of the $[(\pm 45/0)_4/\pm 45]_T$ laminate at R=-1

The predicted damage progression of the intact coupon subjected to static tensile loading up to final failure appears in Fig. 59. First ply failure (FPF) was predicted at the [±45] plies at 155 MPa with IFF mode A. Until 250 MPa IFF mode A has been spread at the entire gauge length of the [±45] plies. Fibre failure initiation is predicted at the [0] plies at 440 MPa. Fibre failure has been spread at an extended area of the [0] plies when final failure was predicted at 490 MPa.

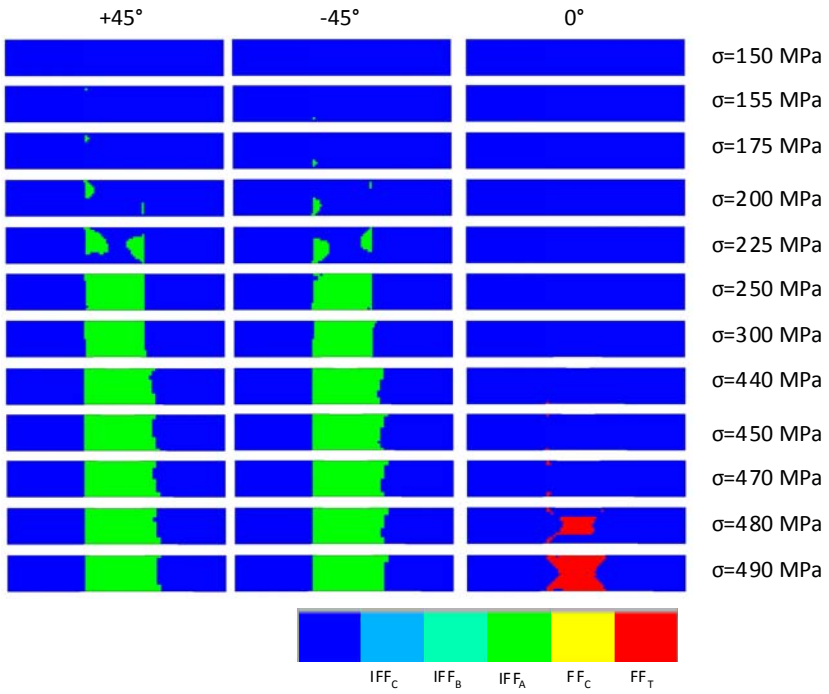

Fig. 59: Failure modes prediction of the static tensile loading of the intact coupon

The predicted damage progression of the coupon subjected to static tensile loading after CA fatigue at σ_{max}=220 MPa for life fraction of 20% appears in Fig. 60. This time the entire gauge length of the coupon is predicted to have IFF of various modes at the [±45] plies, caused by the cyclic loading, before static loading has started. The failure progression at the [0] plies is similar

to the one of the former case of the intact coupon with fibre failure initiation and final failure taking place at lower loads, at 335 MPa and 430 MPa respectively.

After life fraction of 50% at the same stress level, fibre failure at the [0] plies has been predicted during the cyclic loading (Fig. 61). The failure progression at the [0] plies is not different however and the final failure is predicted at 340 MPa.

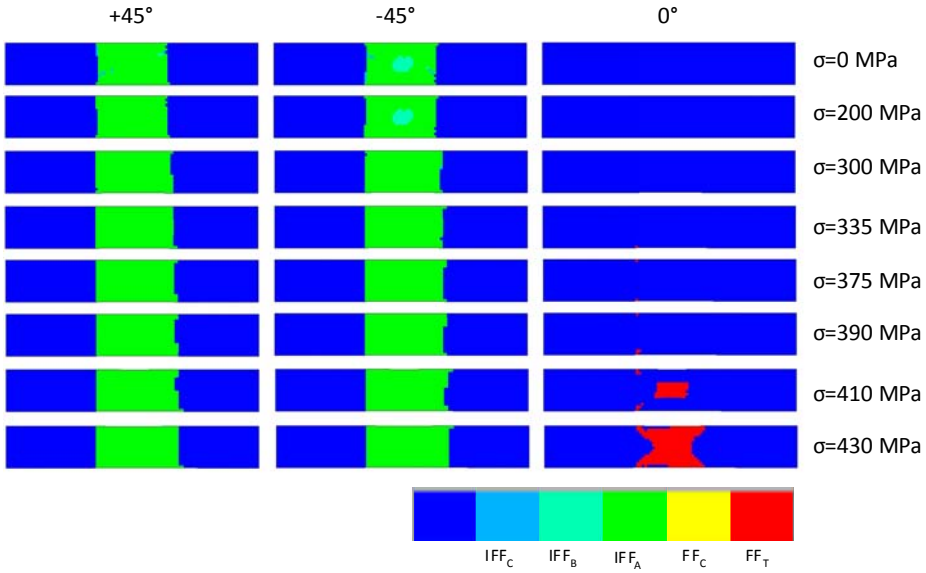

Fig. 60: Failure modes prediction of the static tensile loading of the coupon after CA fatigue at σ_{max}=220 MPa for life fraction of 20%

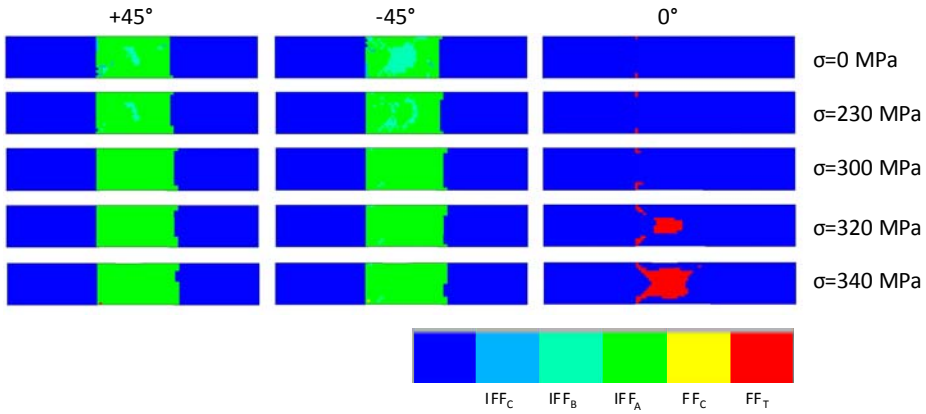

Fig. 61: Failure modes prediction of the static tensile loading of the coupon after CA fatigue at σ_{max}=220 MPa for life fraction of 50%

The predicted damage progression of the coupon after CA fatigue at σ_{max}=172 MPa for life fraction of 20% (Fig. 62) is similar to the one at σ_{max}=220 MPa with fibre failure initiation at the [0] plies and final failure being predicted at 280 MPa and 405 MPa respectively.

After life fraction of 50% at the same stress level, fibre failure at the [0] and the [±45] plies has been predicted during the cyclic loading (Fig. 63). This time the laminate is more heavily damaged from the cyclic loading and when the final failure is predicted at 240 MPa, fibre failure at the [0] plies has been spread at a smaller area of the gauge length.

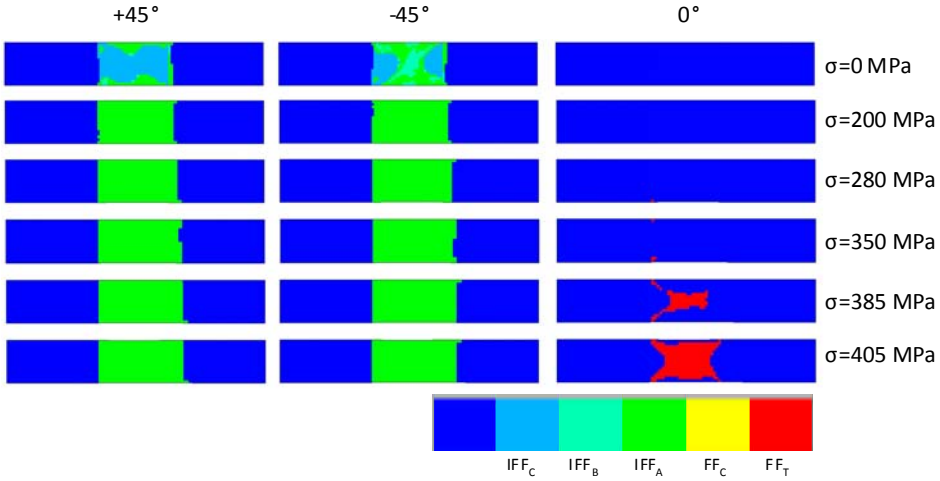

Fig. 62: Failure modes prediction of the static tensile loading of the coupon after CA fatigue at σ_{max}=172 MPa for life fraction of 20%

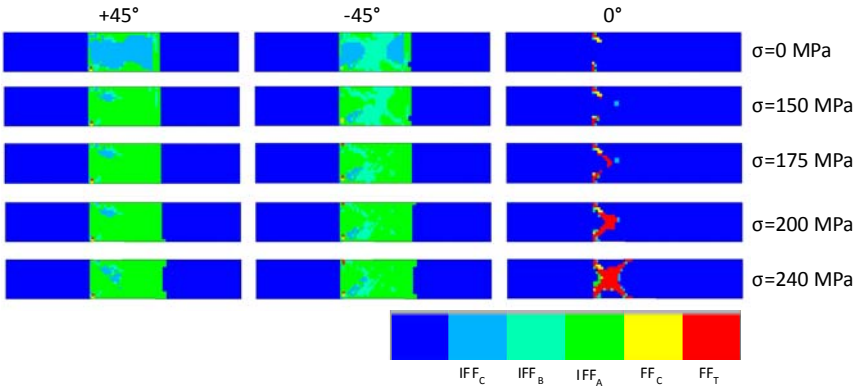

Fig. 63: Failure modes prediction of the static tensile loading of the coupon after CA fatigue at σ_{max}=172 MPa for life fraction of 50%

Simulation results for the case of T-T (R=0.1) CA loading were presented in Fig. 64 along with test data for comparison. Calculations were performed at three stress levels, σ_{max}= 317, 252 and 186 MPa with expected number of cycles to failure equal to 5000, 50000 and $1 \cdot 10^6$ respectively with ANSYS. The corresponding numerical predictions were equal to N=2000-2250, 27500-30000 and 600000-650000.

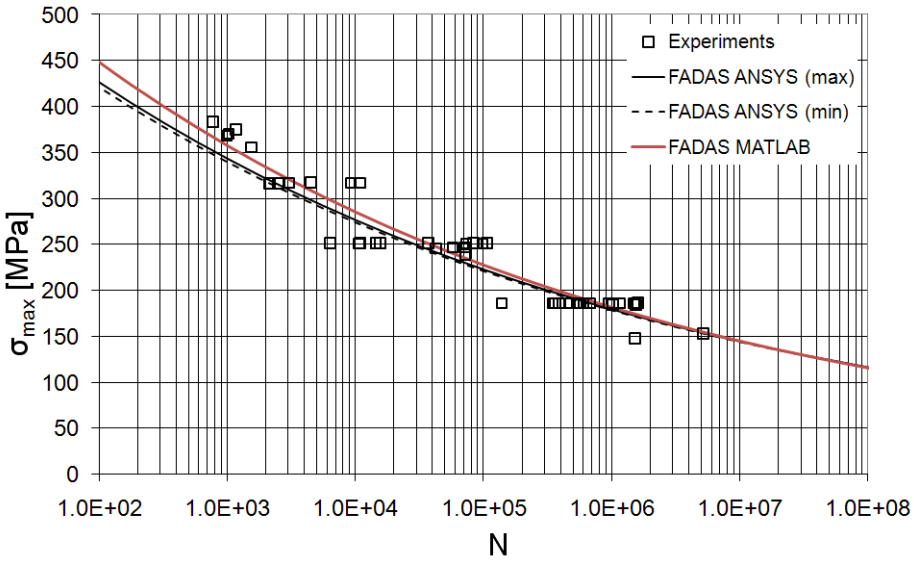

Fig. 64: Comparison of simulation results and test data, $[(\pm 45/0)_4/\pm 45]_T$, R=0.1

Failure sequence and damage modes for each ply were presented in Fig. 65. As it is seen, matrix failure initiates at the [±45] layers from the first simulated cycle.

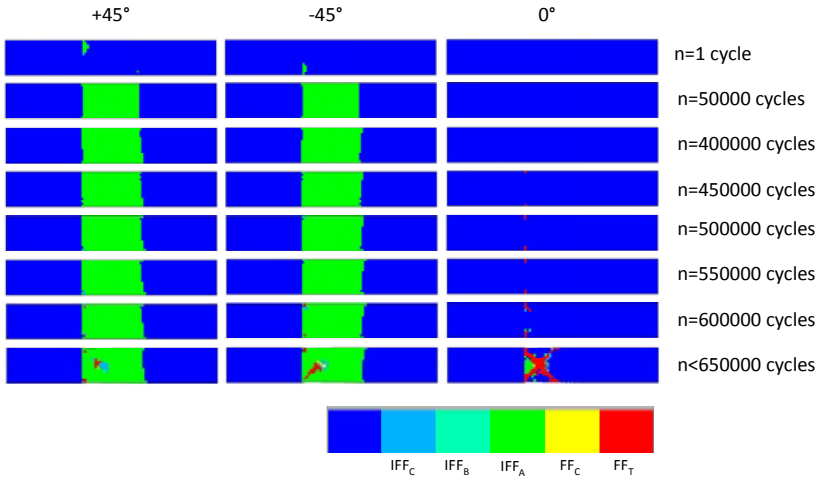

Fig. 65: Failure modes of the $[(\pm 45/0)_4/\pm 45]_T$ laminate. R=0.1, σ_{max}=186 MPa

Concerning stiffness degradation measurements, the strain was measured for 10 coupons at R=0.1; 3 at σ_{max}= 317 MPa, 4 at σ_{max}= 252 MPa and 3 at σ_{max}= 186 MPa [30]. These data (Exp.) were compared to the respective FADAS predictions (Fig. 66).

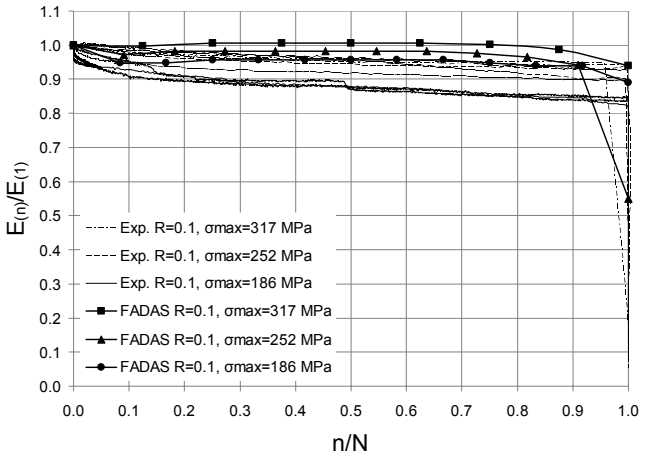

Fig. 66: Validation of stiffness degradation predictions. $[(\pm 45/0)_4/\pm 45]_T$, R=0.1

The experimental data also show the typical three-stage stiffness degradation of the composite MD laminates. FADAS predicts as well the trend of the three-stage stiffness degradation which is higher for lower stress levels although the difference is less pronounced than in the experimental data. Lower stiffness degradation was predicted for the higher stress levels because at higher stress levels the matrix cracks at the [±45] layers were spread at a larger area of the gauge length of the model during the first simulated cycle causing the predicted stiffness of the first cycle to be lower. Furthermore, the stiffness degradation predictions are lower in general than the experimental values.

Tensile and compressive residual strength tests were performed after CA cyclic loading at three stress levels, namely 372 MPa (expected N=1000 cycles), 252 MPa (50000 cycles) and 186 MPa ($1 \cdot 10^6$ cycles) for three life fractions, 20%, 50% or 80%. The residual strength predictions of the $[(\pm 45/0)_4/\pm 45]_T$ laminate at R=0.1 were compared to the experimental data in Fig. 67.

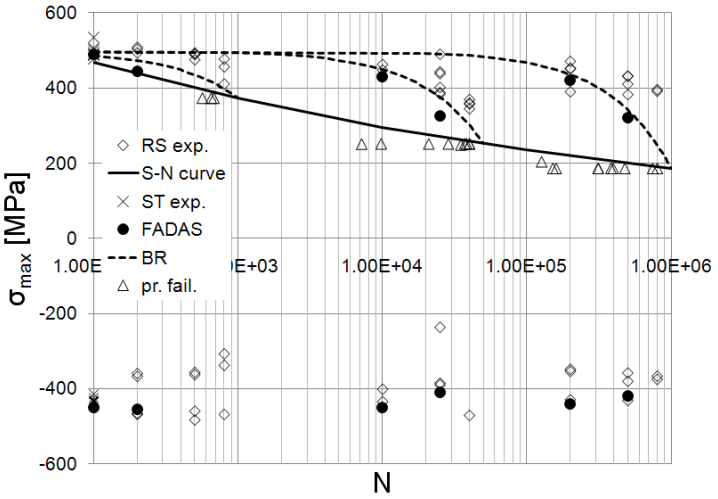

Fig. 67: Residual strength of the MD laminate after CA loading under R=0.1

The tensile residual strength results are in good agreement with the macroscopic BR model at the lower stress levels while they are more conservative at the higher one. The compressive residual strength predictions show insignificant strength degradation which is also the case for the tests.

It is interesting to note that the residual compressive strength after tension-tension cyclic loading cannot be predicted with macroscopic models such as the sudden death described by Eq. (13) while it can be efficiently predicted with FADAS.

The same trend of an overall satisfactory agreement between test data and theoretical results, with the numerical predictions being moderately conservative, was also observed for the cases of pure compressive, R=10, CA loading. Comparison of simulation and experimental results was presented in Fig. 68. The calculations for all stress levels were for the same expected number of cycles to failure as for the other stress ratios already presented with ANSYS. Simulations were performed for $|\sigma_{min}|$=300, 277 and 250 MPa. The corresponding results for the numbers of cycles to failure were N=3750-4000, 32500-35000 and 600000-650000.

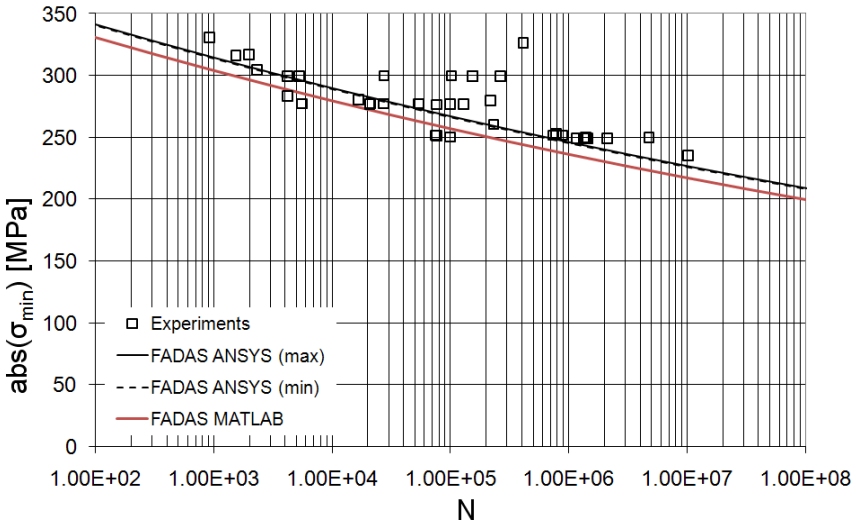

Fig. 68: Comparison between simulation results and test data, $[(\pm 45/0)_4/\pm 45]_T$, R=10

The failure sequence and damage modes were quite different in this case, see Fig. 69. Failure initiates with tensile matrix cracks at the [0] plies from the first simulated cycles. Matrix failure of various damage modes follows at the [±45] layers and final failure is caused by compressive fibre failure at the [0] plies.

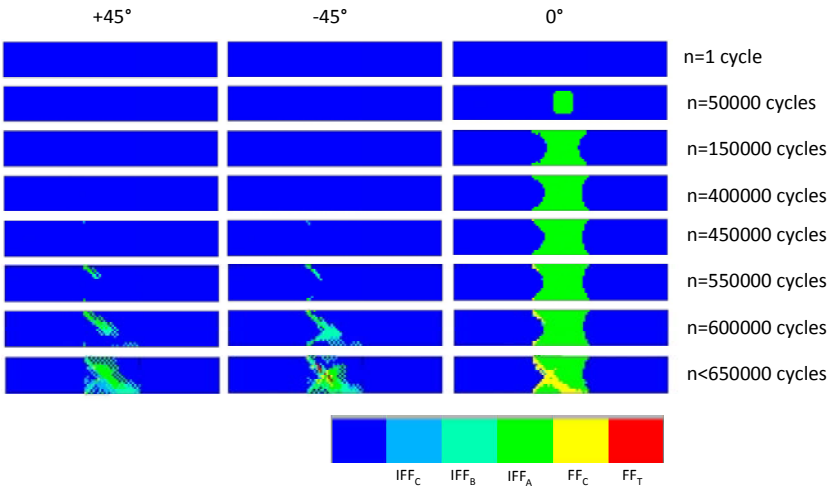

Fig. 69: Failure modes of the $[(\pm 45/0)_4/\pm 45]_T$ laminate. R=10, $|\sigma_{min}|$=250 MPa

The residual strength tests of the $[(\pm 45/0)_4/\pm 45]_T$ laminate after CA fatigue under R=10 at the same stress levels show insignificant strength degradation in both tension and compression for all life fractions and was well predicted by FADAS, as shown in Fig. 70. Likewise the former case at R=0.1, the tensile residual strength cannot be predicted with the macroscopic models.

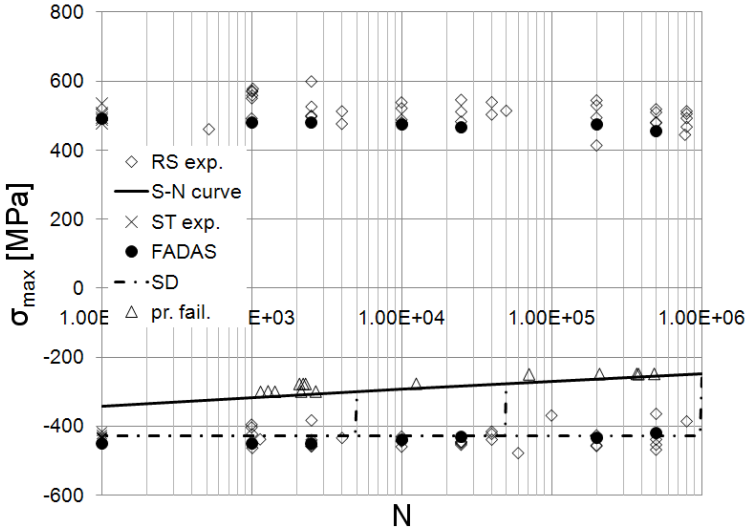

Fig. 70: Residual strength predictions of the $[(\pm 45/0)_4/\pm 45]_T$ laminate at R=10

The numerical predictions of CA cyclic loading on the $[(\pm 45/0)_4/\pm 45]_T$ laminate were also compared to experimental data for R=-0.4 in Fig. 71, R=-2.5 in Fig. 72 and R=0.5 in Fig. 73 showing satisfactory agreement. For R=0.5 the numerical results are optimistic. This was due to the selected CLD of the UD ply in the fibre direction, see section 5, which is probably not representing the actual material behaviour appropriately for the region close to the R=1 line, see [39].

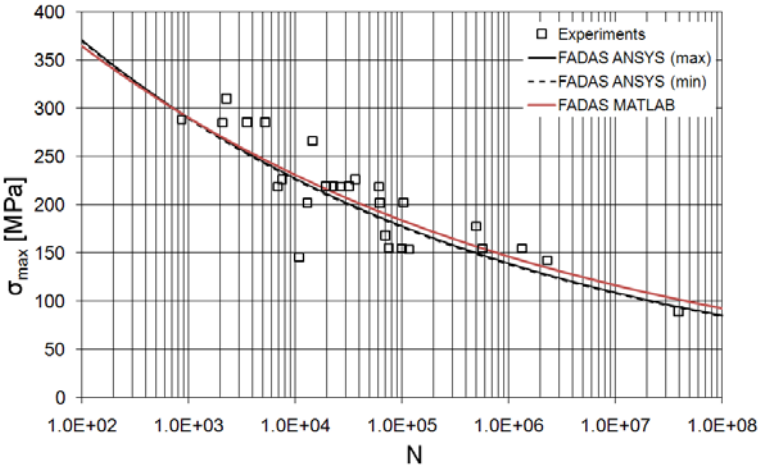

Fig. 71: Comparison of simulation results and test data, $[(\pm 45/0)_4/\pm 45]_T$, R=-0.4

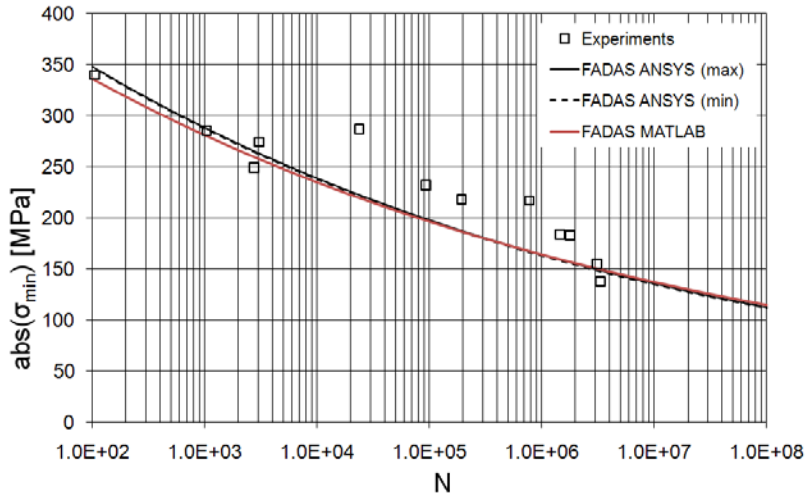

Fig. 72: Comparison of simulation results and test data, $[(\pm 45/0)_4/\pm 45]_T$, R=-2.5

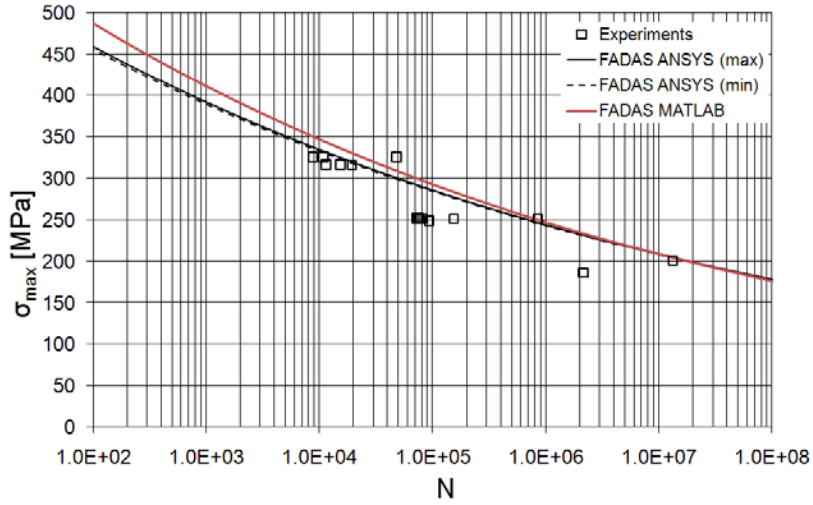

Fig. 73: Comparison of simulation results and test data, $[(\pm 45/0)_4/\pm 45]_T$, R=0.5

The predicted S-N curves for all the above stress ratios R (0.5, 0.1, -0.4, -1, -2.5, 10) and the static strength predictions of both implementations of FADAS were used to form the predicted CLD of the $[(\pm 45/0)_4/\pm 45]_T$ MD laminate and was compared to the CLD formed by the respective experimental data [55], [61] in Fig. 74. The experimental S-N curves were derived by all tests appearing in Fig. 55, 64, 68, 71, 72 and 73. They were presented in Table 7, see Eq. (19).

Table 7: Experimental S-N curves of the $[(\pm 45/0)_4/\pm 45]_T$ MD laminate

R	σ_0 (MPa)	k
0.5	198.7	10.46
0.1	350.2	9.28
-0.4	609.5	7.23
-1	520.7	9.27
-2.5	393.0	11.99
10	225.1	19.19

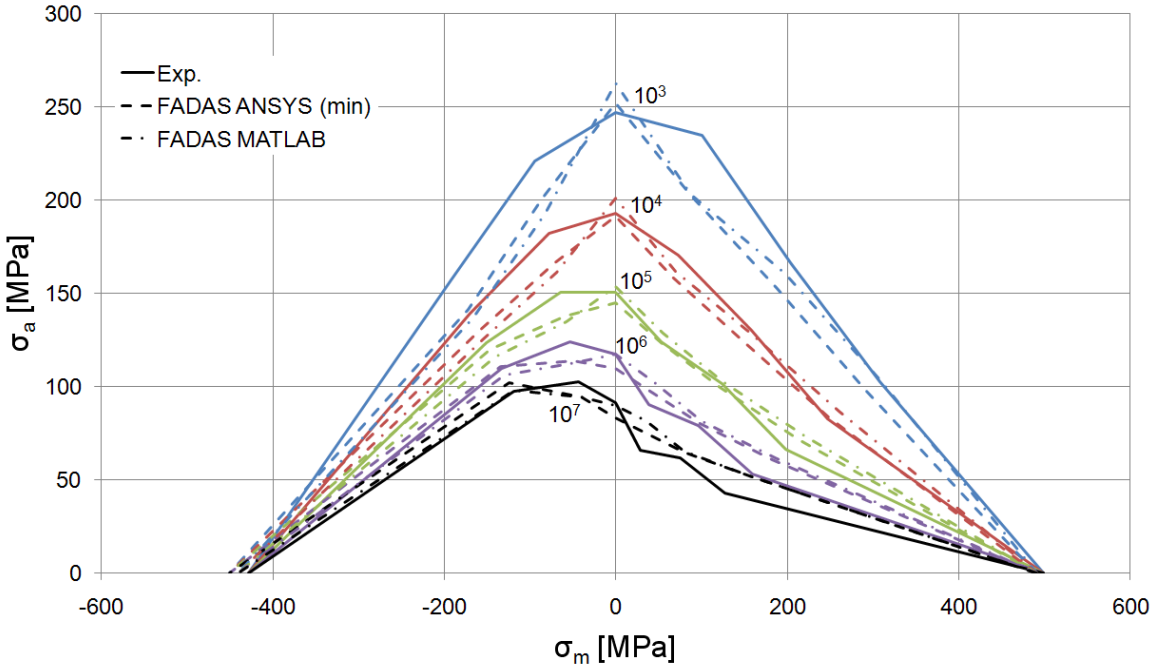

Fig. 74: Comparison between the predicted and experimental CLD, $[(\pm 45/0)_4/\pm 45]_T$

6.4.1.6 CA tests on MD laminate $[(\pm 45/0)_4/\pm 45]_T$ off-axis loaded

Two more data sets from CA cyclic testing of coupons cut off-axis at 10º and 60º from the $[(\pm 45/0)_4/\pm 45]_T$ laminate were reported by Philippidis et al. [54]. This test series was aiming to generate different complex stress states in the layers of the MD lay-up and investigate the effect on numerical life prediction of lay-ups without fibres in the load direction. The stacking sequence of these off-axis coupons was given by $[(55/-35/10)_4/55/-35]_T$ and $[(-75/15/60)_4/-75/15]_T$ respectively.

Tests were performed at two stress levels, high and low, under reversed loading, R=-1. Experimental results along with FADAS numerical predictions for both lay-ups were presented in Fig. 75-76. For the $[(55/-35/10)_4/55/-35]_T$ coupons, numerical simulations were performed for σ_{max}=230, 172 and 114 MPa while σ_{max}=105, 87 and 54 MPa were the corresponding levels for the MD [60]-off-axis coupons.

The agreement between numerical predictions and experimental data is not as good as for the previously presented S-N curves for the MD and the $[\pm 45]_S$ laminates. Final failure was dominated in both cases by fibre fracture of the [10] or [15] plies of the 10º and 60º off-axis MD laminates while all their other plies failed very early at various matrix damage modes, see Fig. 77, 78.

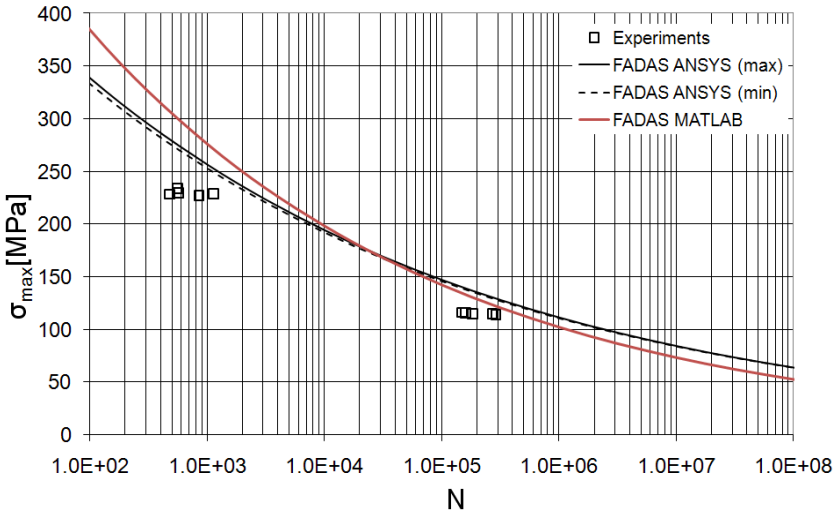

Fig. 75: Fatigue strength of the $[(55/-35/10)_4/55/-35]_T$ MD coupons under R=-1

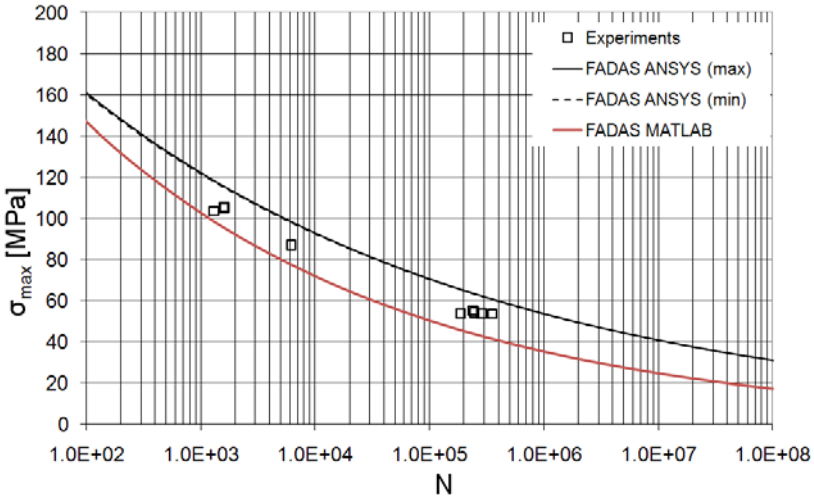

Fig. 76: Fatigue strength of the $[(-75/15/60)_4/-75/15]_T$ MD coupons under R=-1

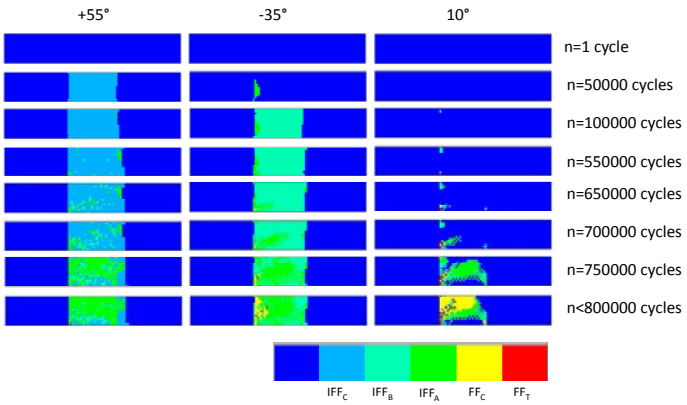

Fig. 77: Damage progression in the $[(55/-35/10)_4/55/-35]_T$ laminate. R=-1, σ_{max}=114 MPa

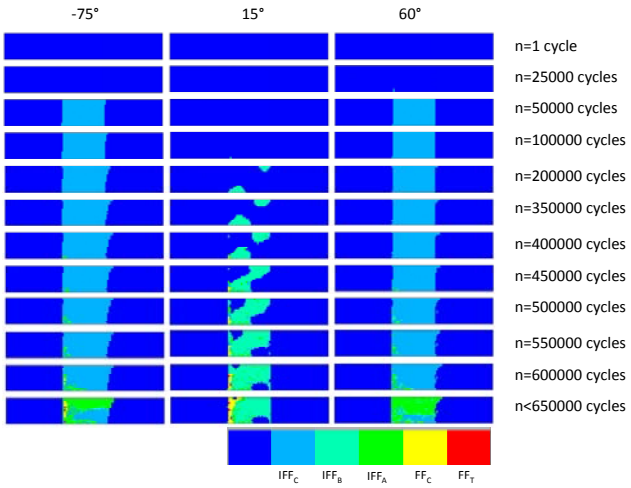

Fig. 78: Damage progression in the $[(-75/15/60)_4/-75/15]_T$ laminate. R=-1, σ_{max}=54 MPa

The predicted failure modes of the $[(55/-35/10)_4/55/-35]_T$ laminate at final failure, corresponding to n<800,000 cycles of Fig. 77, were compared visually to a failed coupon, see Fig. 79. The outer visible [-35] ply appears to have matrix cracks at most of the gauge length area. Compressive fibre fracture can be also observed along with fibre splitting and delaminated bundles. Explosive IFF mode C in the [55] ply underneath has probably contributed to this debonding. Besides matrix cracks at the entire gauge length area of the [-35] and [55] plies, FADAS has also predicted compressive fibre fracture extending along the width of the [-35] and [10] layers. Predictions were in fair agreement with the visual observations, although a damage mode such as delamination cannot be predicted with the actual FE shell element implementation of the routine.

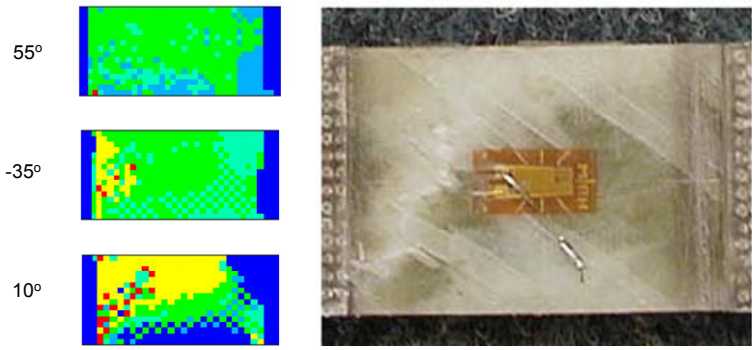

Fig. 79: Comparison of the predicted failure modes for the $[(55/-35/10)_4/55/-35]_T$ laminate with a failed coupon. R=-1, σ_{max}=114 MPa

Concerning the $[(-75/15/60)_4/-75/15]_T$ coupon, see Fig. 80, FADAS predicted matrix failure at all plies and fibre fracture at the [-75] and [15] plies near the left tab at final failure. As it can be seen in the top surface of the failed coupon, matrix cracks spread at the entire gauge length of the outer [-75] ply along with compressive fibre fracture near the left tab, validating the numerical predictions.

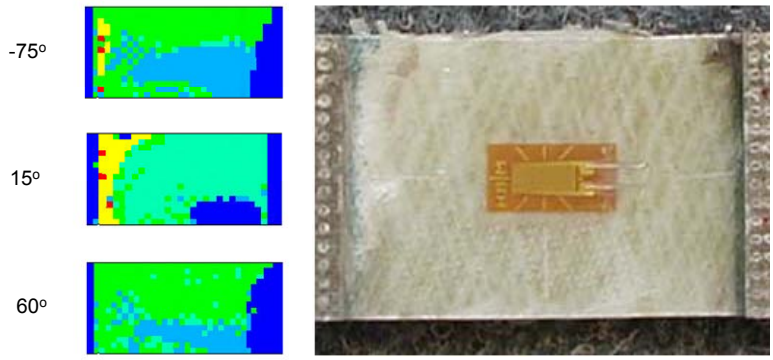

Fig. 80: Comparison of the predicted failure modes for the $[(-75/15/60)_4/-75/15]_T$ laminate with a failed coupon. R=-1, σ_{max}=54 MPa

6.4.1.7 VA tests on MD laminate $[(\pm45/0)_4/\pm45]_T$ on-axis loaded

VA tests on the MD laminate $[(\pm45/0)_4/\pm45]_T$ using simple two CA block loading [62] were simulated with both FADAS implementations. The stress levels (SL) nomenclature and the corresponding number of cycles to failure were shown in Table 8.

Table 8: Stress levels of OPTIMAT BLADES project

SL	N
1	1E+03
1b	5E+03
2	5E+04
3	1E+06

The stress levels for R=0.1, -1 and 10 were calculated from S-N curves derived at an earlier stage of the project [59], so they were not include all test data presented above. These S-N curves, Eq. (26) appear in Table 9.

$$\sigma_{\max} = \sigma_0 N^{-\frac{1}{k}} \tag{26}$$

Table 9: Early experimental S-N curves of the $[(\pm45/0)_4/\pm45]_T$ MD laminate

R	σ_0 (MPa)	k
0.1	744.9	9.96
-1	539.2	9.49
10	403.0	28.82

In the two-block tests the coupon was first subjected to the first CA block until the 50% of the nominal fatigue life and then subjected to the second block until failure. These tests were compared to the results of the ANSYS implementation of FADAS in Fig. 81-91, HL is high-low stress level. Some results were not displayed because FADAS predicted failure during the first block. The stress level σ_{max} and abs(σ_{min}) appearing in Fig. 81-91 is the stress level of the second block.

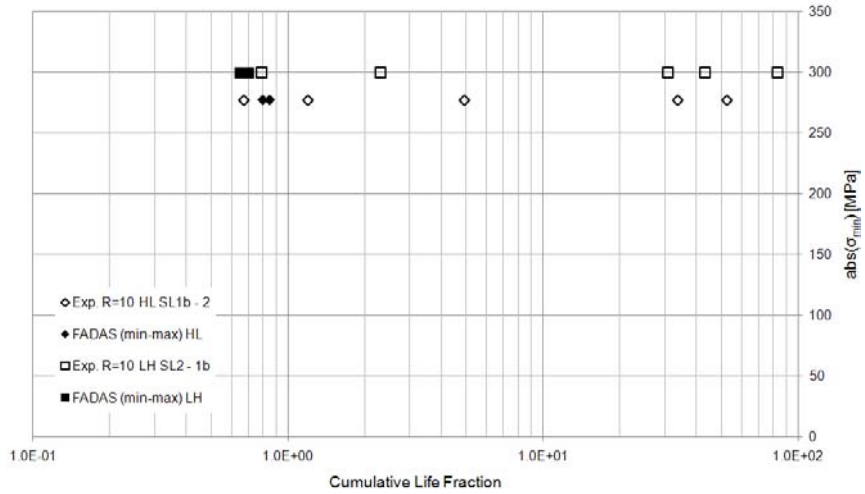

Fig. 81: Two-block tests at R=10, SL 1b and 2

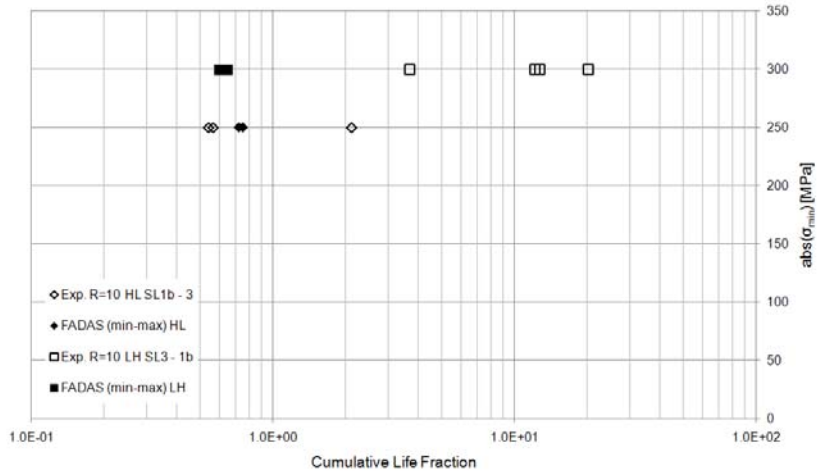

Fig. 82: Two-block tests at R=10, SL 1b and 3

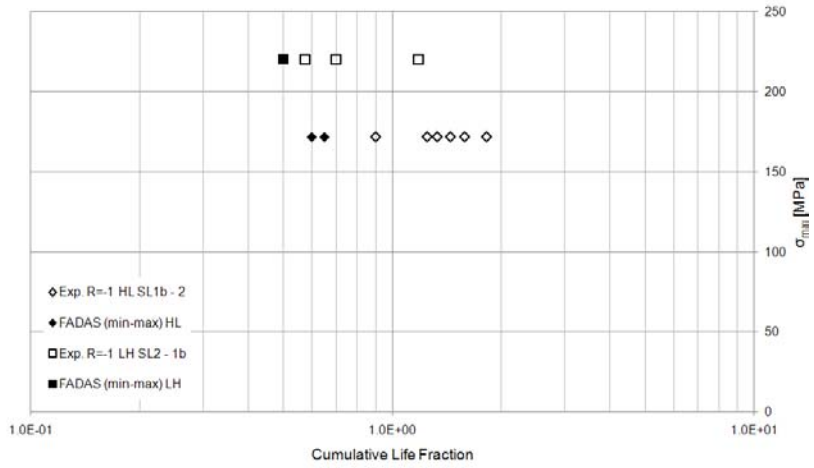

Fig. 83: Two-block tests at R=-1, SL 1b and 2

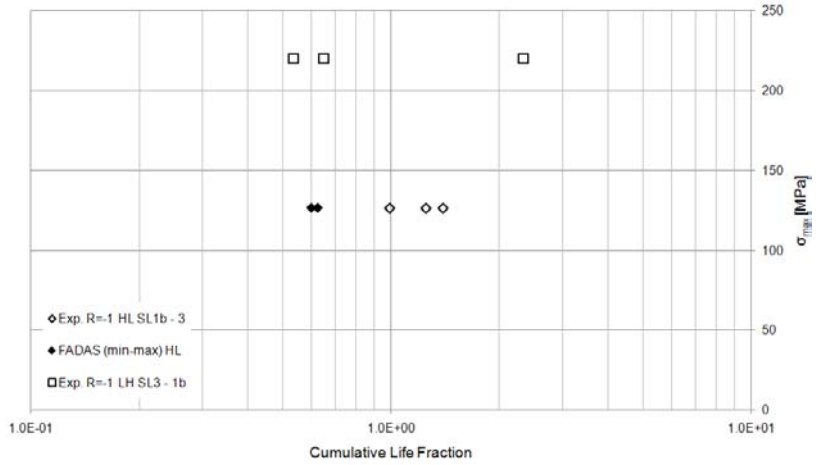

Fig. 84: Two-block tests at R=-1, SL 1b and 3

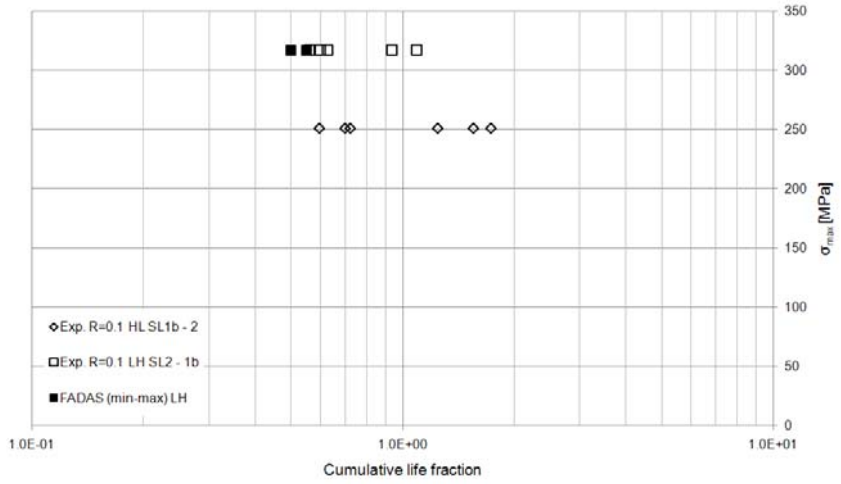

Fig. 85: Two-block tests at R=0.1, SL 1b and 2

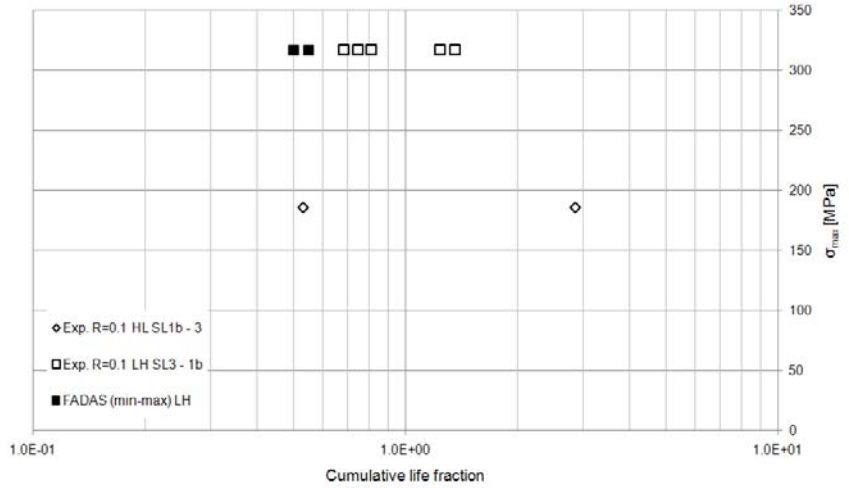

Fig. 86: Two-block tests at R=0.1, SL 1b and 3

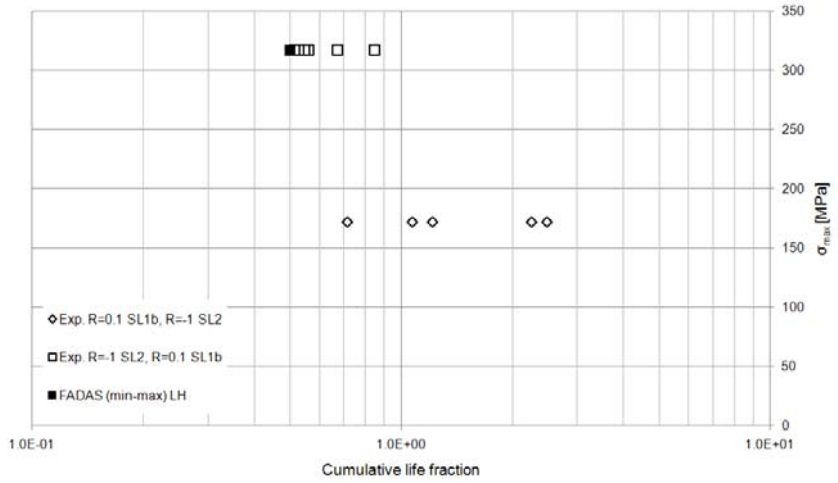

Fig. 87: Two-block tests, R=0.1 SL1b, R=-1 SL2

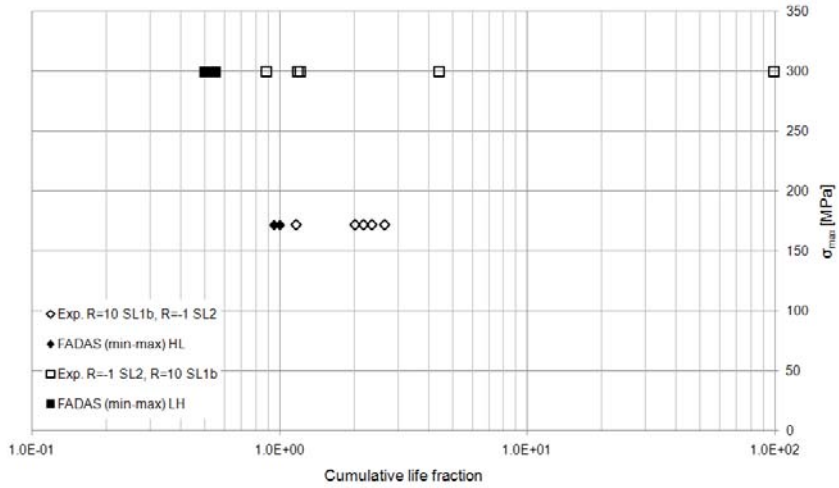

Fig. 88: Two-block tests, R=10 SL1b, R=-1 SL2

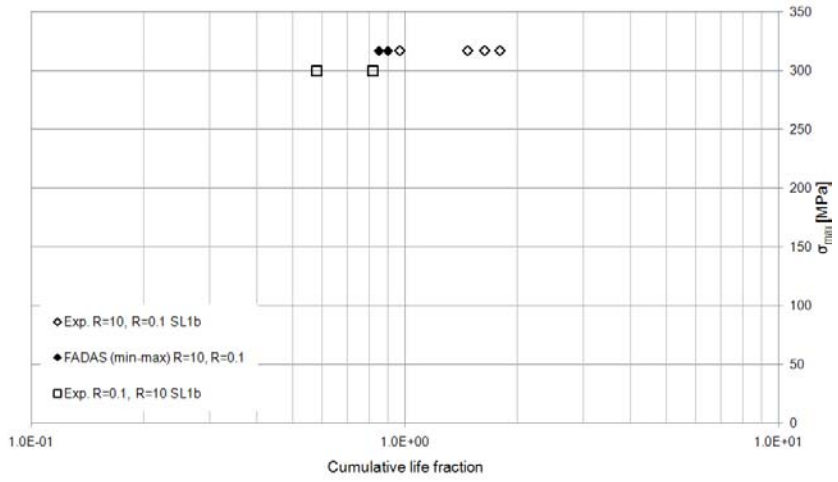

Fig. 89: Two-block tests, R=10, R=0.1 SL1b

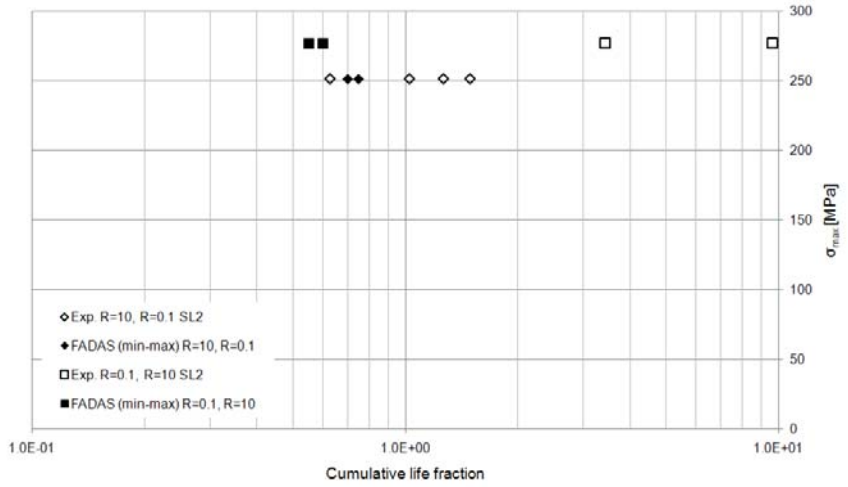

Fig. 90: Two-block tests, R=10, R=0.1 SL2

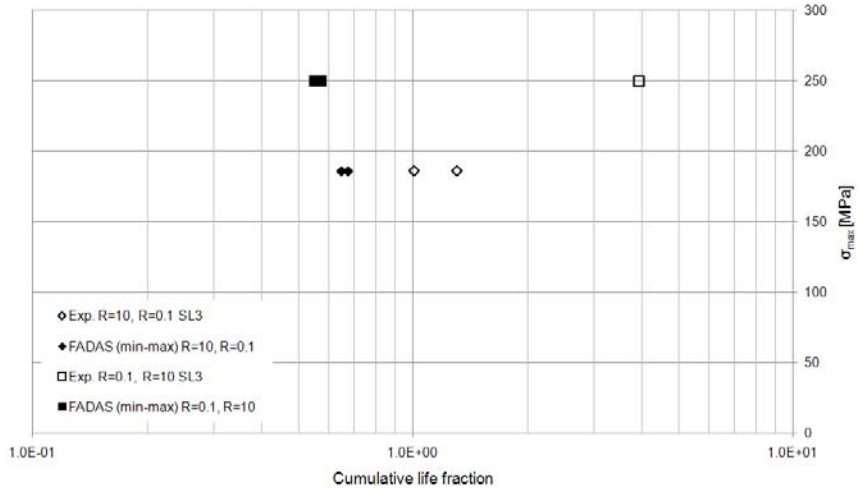

Fig. 91: Two-block tests, R=10, R=0.1 SL3

In the repeated two-block tests, the coupon was subjected to a sequence of alternating the two CA blocks, each for 1% of the nominal fatigue life. The cumulative life fraction is equal to one at 50 passes. These tests were simulated with the MATLAB implementation of FADAS, Fig. 92-97.

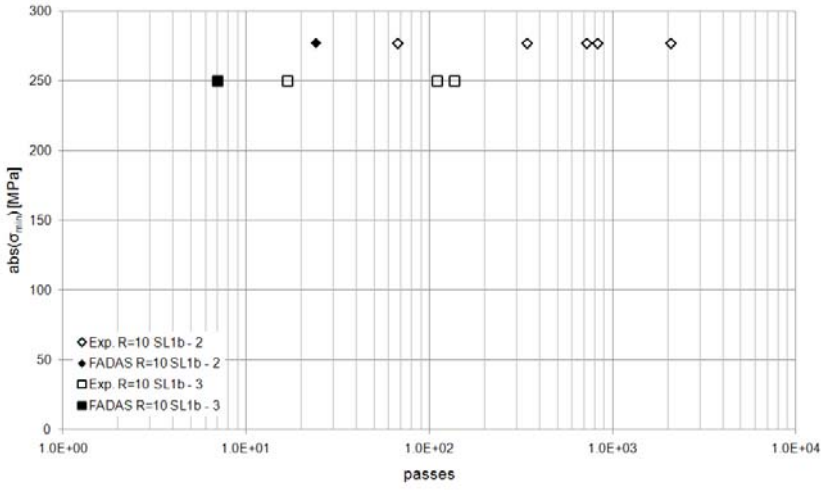

Fig. 92: Repeated two-block tests, R=10

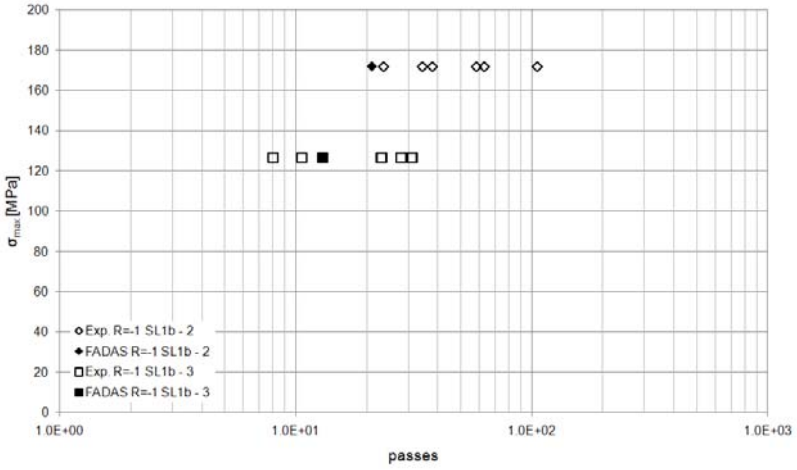

Fig. 93: Repeated two block tests, R=-1

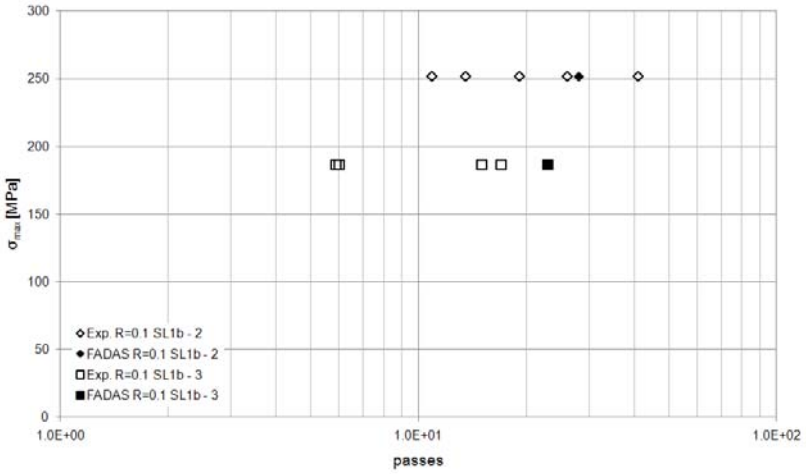

Fig. 94: Repeated two block tests, R=0.1

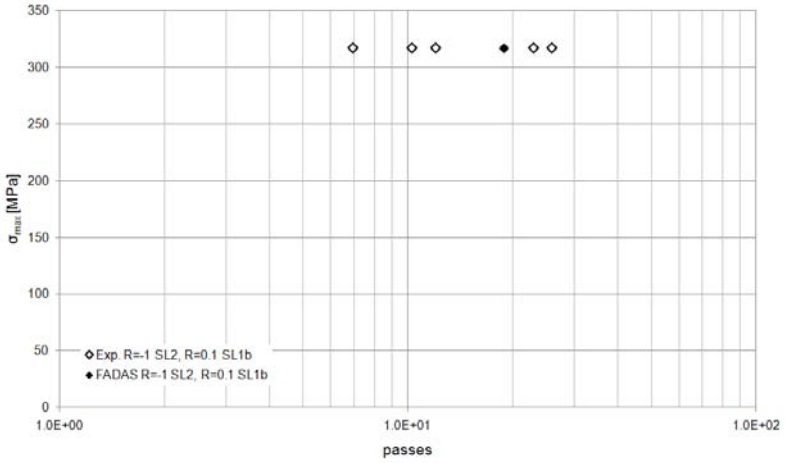

Fig. 95: Repeated two block tests, R=0.1 and R=-1

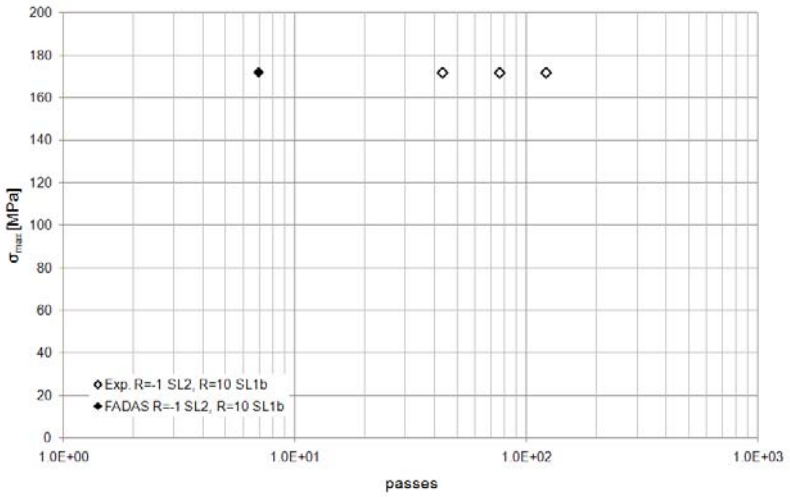

Fig. 96: Repeated two block tests, R=10 and R=-1

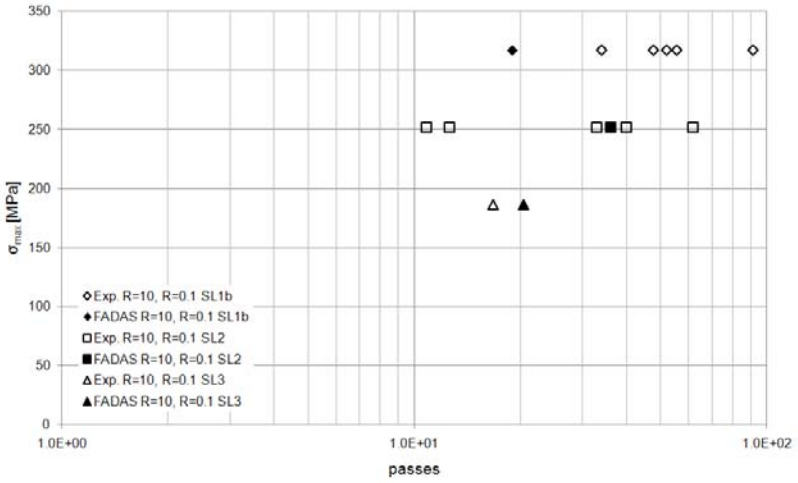

Fig. 97: Repeated two block tests, R=10 and R=0.1

The VA spectrum tests on the MD laminate $[(\pm 45/0)_4/\pm 45]_T$ [37], [63] were also simulated with the MATLAB implementation of FADAS. The results were compared to the tests and the Palmgren-Miner (PM) rule using a 3-R CLD for R=0.1, -1 and 10 in Fig. 98-101. Although the FADAS predictions are non-conservative, they are better than the results of the classic VA analysis using the 3-R CLD for the tension dominated spectra, Fig. 98-100, requiring the CLD of the MD laminate under consideration. In contrary, the results are worse (more conservative) for the compression dominated spectrum, Fig. 101.

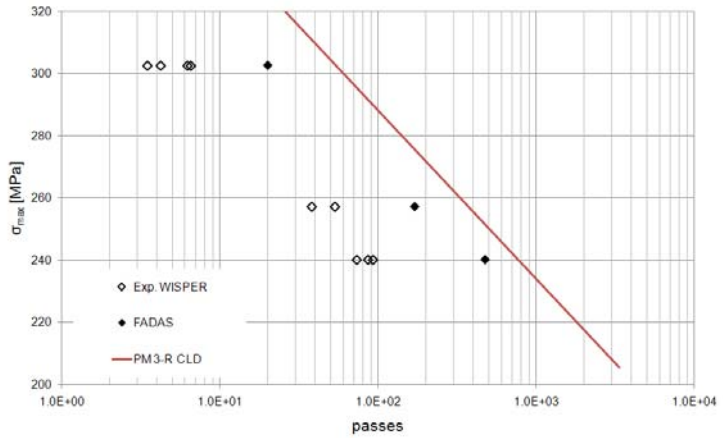

Fig. 98: Predictions of the VA tests, WISPER spectrum

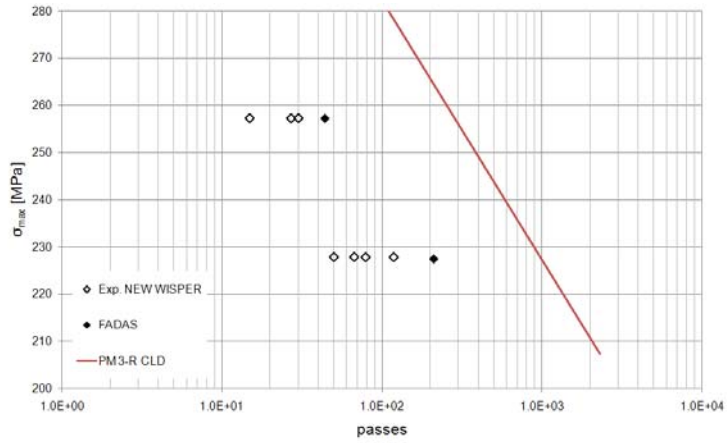

Fig. 99: Predictions of the VA tests, NEW WISPER spectrum

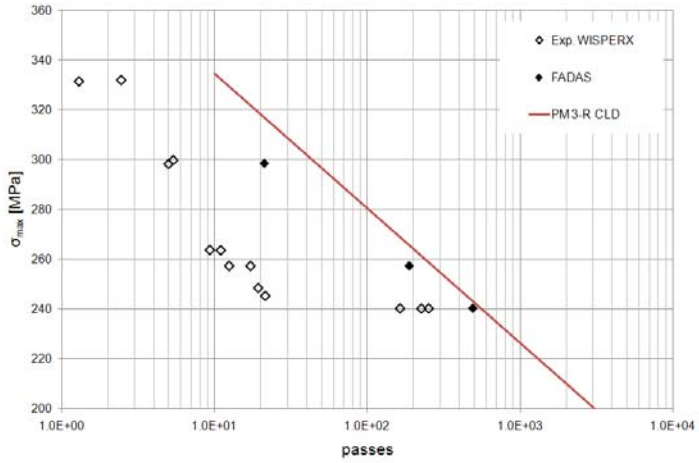

Fig. 100: Predictions of the VA tests, WISPERX spectrum

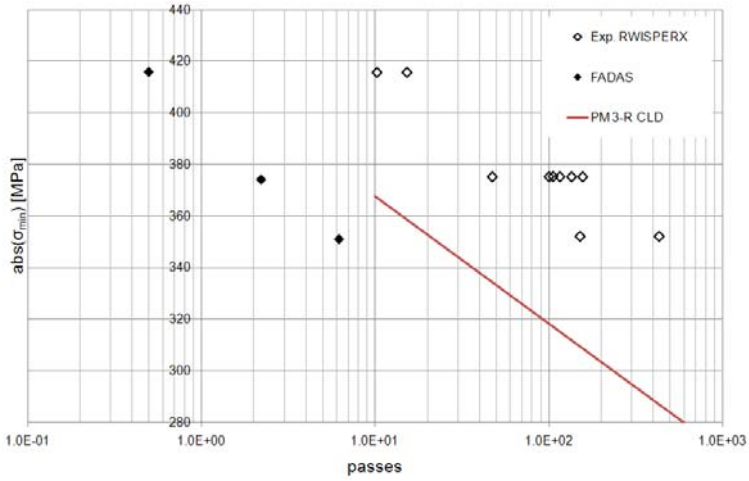

Fig. 101: Predictions of the VA tests, RWISPERX spectrum

6.4.1.8 VA tests on ISO 14129 $[\pm 45]_S$ coupons

The ISO 14129 $[\pm 45]_S$ coupon NEW WISPER tests [64] were simulated with the MATLAB implementation of FADAS and the results were compared to the tests in Fig. 102. The macroscopic prediction with the PM rule and the Broutman-Sahu residual strength model (BR) also appear in this figure.

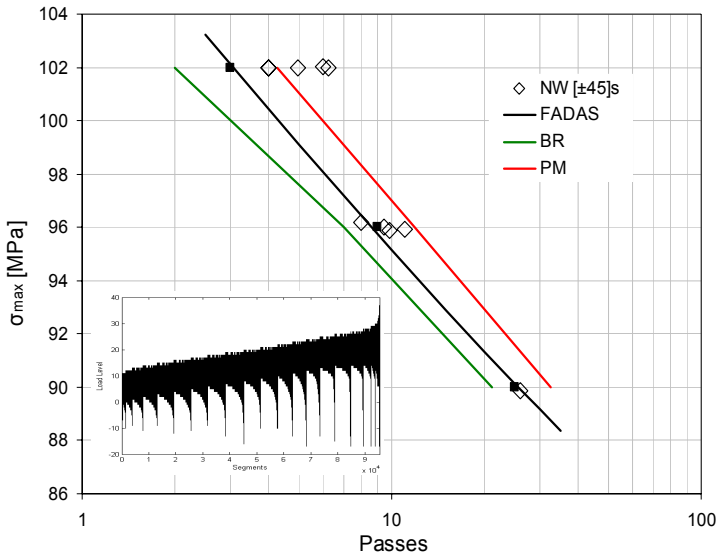

Fig. 102: Prediction of VA tests on ISO 14129 $[\pm 45]_S$ coupons

6.4.2 Tubular coupons

The UD ply thickness was set equal to 0.30 mm for the +45° and -45° layers of the tubular coupons [65], as they were made of the bidirectional stitched fabric of ±45 orientations, $[\pm 45]_{2T}$.

The tubular specimens were simulated for pure torsion CA loading, R=-1, with the ANSYS implementation of FADAS at four stress levels τ_{max}, namely 97.9, 85.6, 73.4 and 61.2 MPa. The results were compared to the tests in Fig. 103.

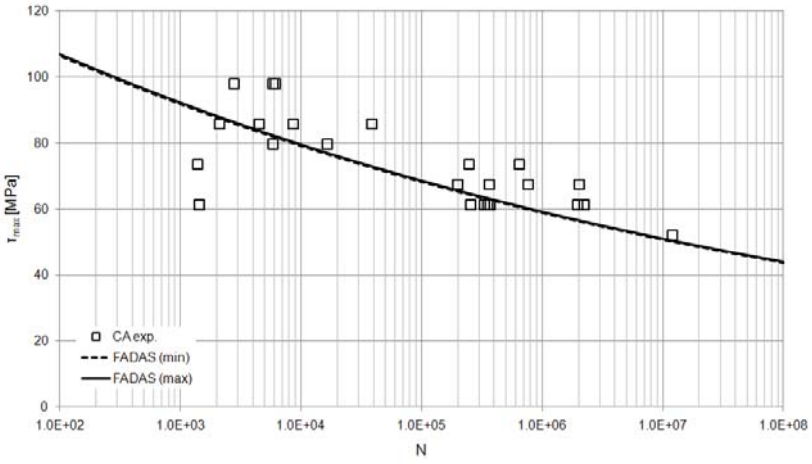

Fig. 103: Comparison between simulation results and exp. data, pure torsion, R=-1

The tubular coupons were also subjected to combined torsion-axial CA loading, R=-1. The numerical results, τ_{max}=52.0, 43.0, 36.9 and 30.7 MPa, appear in Fig. 104, (+) and (-) is the sign of the torsion, see [66], when the coupon was under tension. All tests were performed for a constant max axial stress to max shear stress ratio, σ_{max}/τ_{max}=0.7219.

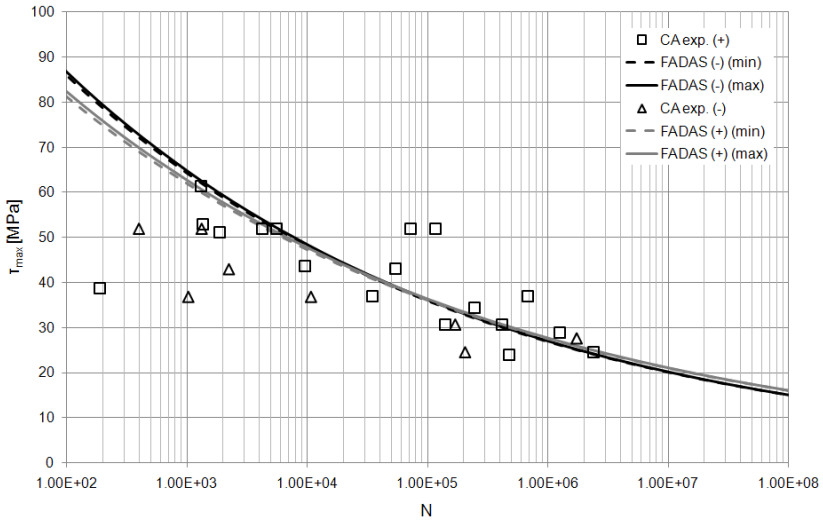

Fig. 104: Comparison between simulation results and exp. data, torsion-axial loading, R=-1

6.4.3 Cruciform coupons

The thickness of the UD plies of the cruciform coupons [51], [67] was the same as for the prismatic coupons. They were subjected to two different types of CA loading tests. The first was CA T-T loading in both directions, R=0.1, with the max load in the fibres direction, x, of the [0] plies being the same in all cases, F_{xmax}=30 kN. The second type was CA T-T loading (R=0.1) only in x direction, F_{xmax}=30 kN, and constant load in the transverse direction y, F_y=8.25 kN. The numerical results of all the above cases appear in Fig. 105.

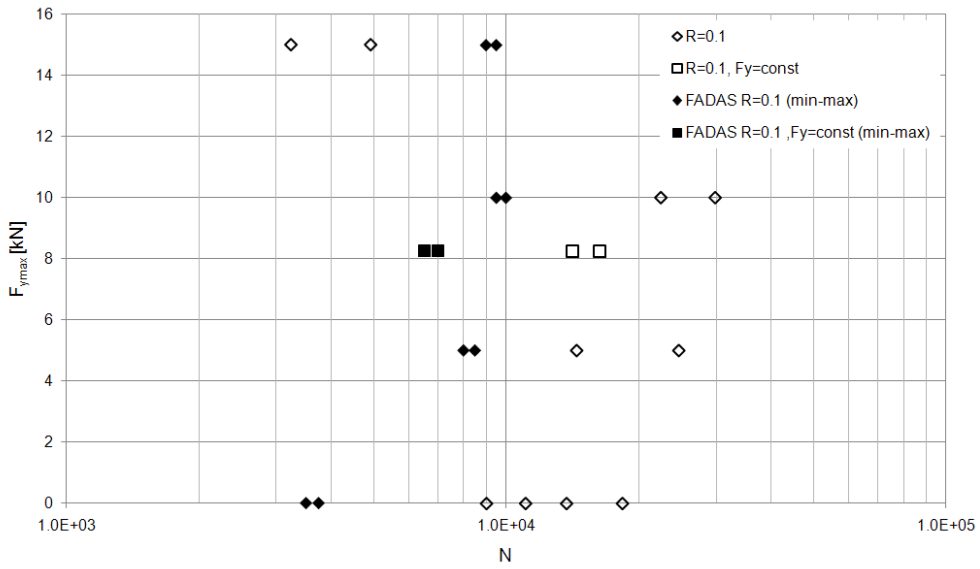

Fig. 105: Comparison between simulation results and exp. data, biaxial tests on cruciform coupons

7. Conclusions

An anisotropic non-linear constitutive model implementing progressive damage concepts to predict the residual strength/stiffness and life of composite laminates subjected to static or cyclic multi-axial loading was presented. In-plane mechanical properties of the material were fully characterized at the ply level while static or fatigue strength of any multidirectional stacking sequence was predicted.

The computational implementation of the theoretical model in MATLAB and ANSYS, simulating fatigue damage progression in a composite laminate by means of a ply-to-laminate approach, was presented as well. The in-plane residual strength of the UD layer was used as fatigue damage metric. Strength and stiffness degradation were modelled using simple and cost-effective schemes, while the failure criterion of Puck along with post failure behaviour of the material, has been implemented. The model was set up for a Glass/Epoxy material typical of the wind turbine rotor blade industry and has been verified through a series of constant and variable amplitude, uniaxial and biaxial fatigue tests on different lay-ups, simulating a variety of plane stress combinations and failure modes. Results from residual static strength and stiffness degradation prediction of coupons, previously loaded under cyclic stress, at various life fractions, were also validated by the experimental data.

These results indicate that the FADAS algorithm actually predicts satisfactorily fatigue strength under CA or spectrum loading and residual stiffness/strength of MD laminates made of the basic UD ply under multiaxial VA cyclic loading.

8. References

1. Philippidis TP, Vassilopoulos AP, Complex stress state effect on fatigue life of GRP laminates. Part I, Experimental, *International Journal of Fatigue* 2002; **24**(8), 813-823

2. Philippidis TP, Vassilopoulos AP, Complex stress state effect on fatigue life of GRP laminates. Part II, Theoretical formulation, *International Journal of Fatigue* 2002; **24**(8), 825-830

3. Philippidis TP, Vassilopoulos AP, Fatigue strength of composites under variable plane stress, in *Fatigue in Composites*, Ed. B. Harris, Woodhead Publishing Ltd and CRC Press, 2003, Chapter 18, 504-525

4. Philippidis TP, Vassilopoulos AP, Life prediction methodology for GFRP laminates under spectrum loading, *Composites: Part A* 2004; **35**(6), 657-666

5. Lee JW, Allen DH, Harris CE, Internal state variable approach for predicting stiffness reductions in fibrous laminated composites with matrix cracks. *Journal of Composite Materials* 1989; **23**, 1273-1291

6. Coats TW, Harris CE, Experimental verification of a progressive damage model for IM7/5260 laminates subjected to tension-tension fatigue. *Journal of Composite Materials* 1995; **29**(3), 280-305

7. Lo DC, Coats TW, Harris CE, Allen DH, Progressive damage analysis of laminated composite (PDALC). A computational model implemented in the NASA COMET finite element code. *NASA TM-4724,* 1996

8. Shokrieh MM, Lessard LB, Progressive fatigue damage modelling of composite materials, Part I: Modeling. *Journal of Composite Materials* 2000; **34**(13), 1056-1080

9. Shokrieh MM, Lessard LB, Progressive fatigue damage modelling of composite materials, Part II: Material Characterization and model verification. *Journal of Composite Materials* 2000; **34**(13), 1081-1116

10. Van Paepegem W, Degrieck J, Fatigue degradation modelling of plain woven glass/epoxy composites. *Composites A* 2001; **32,** 1433-1441

11. Van Paepegem W, Degrieck J, De Baets P, Finite element approach for modelling fatigue damage in fibre-reinforced composite materials. *Composites B* 2001; **32,** 575-588

12. Van Paepegem W, Degrieck J, A new coupled approach of residual stiffness and strength for fatigue of fibre-reinforced composites. *International Journal of Fatigue* 2002; **24**, 747-762

13. Van Paepegem W, Degrieck J, Coupled residual stiffness and strength model for fatigue of fibre-reinforced composite materials. *Composite Science and Technology* 2002; **62**, 687-696

14. Van Paepegem W, Degrieck J, Modelling damage and permanent strain in fibre-reinforced composites under in-plane fatigue loading. *Composites Science and Technology* 2003; **63**, 677-94

15. Van Paepegem W, Dechaene R, Degrieck J, Nonlinear correction to the bending stiffness of a damaged composite beam. *Composite Structures* 2005; **67**, 359-364.

16. Sihn S, Park JW, MAE: An Integrated Design Tool for Failure and Life Prediction of Composites, *Journal of Composite Materials* 2008; **42**(18), 1967-1988

17. Ladeveze P, A damage computational method for composite structures, *Computers and Structures* 1992; **44**(1-2), 79-87

18. Renard J, Favre J-P, Jeggy T, Influence of transverse cracking on ply behavior: introduction of a characteristic damage variable, *Composite Science and Technology* 1993; **46**, 29-37

19. Maire JF, Chaboche JL, A new formulation of continuum damage mechanics (CDM) for composite materials, *Aerospace Science and Technology* 1997; **4**, 247-257

20. Puck A, Schürmann H, Failure analysis of FPF laminates by means of physically based phenomenological models, *Composites Science & Technology* 1998; **58**, 1045-1067

21. Puck A, Schürmann H, Failure analysis of FPF laminates by means of physically based phenomenological models, *Composites Science & Technology* 2002; **62**, 1633-1662

22. Puck A, Kopp J, Knops M, Guidelines for the determination of the parameters in Puck's action plane strength criterion, *Composites Science & Technology* 2002; **62**, 371-378

23. Chang FK, Lessard BL, Damage tolerance of laminated composites containing an open hole and subjected to compressive loadings: Part I-Analysis, *Journal of Composite Materials* 1991; **25**, 2-43

24. Philippidis TP, Eliopoulos EN, Antoniou AE, Passipoularidis VA, Material Model Incorporating Loss of Strength and Stiffness Due to Fatigue. *UpWind project, Deliverable 3.3.1*, 2007, Contract No.: 019945(SES6)

25. Megnis M, Brøndsted P, Measurements of in-plane shear properties of GEV206 at ambient room conditions using V-notched beam test specimen. OB_TG3_R009, 2003. (http://www.wmc.eu/optimatblades.php)

26. Richard RM, Blacklock JR, Finite element analysis of inelastic structures. *AIAA* 1969; **7**, 432-438

27. Philippidis TP, Antoniou AE, Passipoularidis V, Assimakopoulou TT, Static tests on the standard OB unidirectional coupon Main test phase I (Static tensile tests). OB_TG2_R018, 2004. (http://www.wmc.eu/optimatblades.php)

28. Philippidis TP, Assimakopoulou TT, Passipoularidis VA, Antoniou AE, Static and fatigue tests on ISO standard ±45˚ coupons Main test phase I. OB_TG2_R020, 2004. (http://www.wmc.eu/optimatblades.php)

29. Philippidis TP, Assimakopoulou TT, Antoniou AE & Passipoularidis VA, Fatigue tests on OB standard coupons at 90^{o} Main test phase I. OB_TG2_R021, 2005 (http://www.wmc.eu/optimatblades.php)

30. Nijssen RPL, Knowledge Centre WMC, Wieringerwerf, The Netherlands, personal communication, 2007

31. Philippidis TP, Passipoularidis VA, Assimakopoulou TT & Antoniou AE, Fatigue tests in the fiber direction of UD OB standard specimen Main test phase I. OB_TG1_R013, 2006 (http://www.wmc.eu/optimatblades.php)

32. Hashin Z, Failure criteria for unidirectional fiber composites, *Journal of Applied Mechanics* 1980; **47**, 329-334

33. Philippidis TP, Passipoularidis VA, Residual strength after fatigue in composites: Theory vs. experiment, Int J Fatigue 2007; **29**, 2104-2116

34. Shokrieh MM, Lessard LB, Multiaxial fatigue behaviour of unidirectional plies based on uniaxial fatigue experiments-part I. Modelling, *International Journal of Fatigue* 1997; **19**(3), 201-207

35. Shokrieh MM, Lessard LB, Multiaxial fatigue behaviour of unidirectional plies based on uniaxial fatigue experiments-part II. Experimental evaluation, *International Journal of Fatigue* 1997; **19**(3), 209-217

36. Philippidis TP, Passipoularidis VA, Validated engineering model for residual strength prediction, *OB_TG5_R013,* 2006 (http://www.wmc.eu/optimatblades.php)

37. Nijssen RPL, Fatigue life prediction and strength degradation of wind turbine rotor blade composites, 2006, PhD Thesis, Faculty of Aerospace Engineering, T. U. Delft

38. Passipoularidis VA, Philippidis TP, Strength degradation due to fatigue in fibre dominated glass/epoxy composites: A statistical approach, *Journal of Composite Materials* 2009; **43**(9), 997-1013

39. Passipoularidis VA, Philippidis TP, A study of factors affecting life prediction of composites under spectrum loading, *International Journal of Fatigue* 2009; **31**(3), 408-417

40. Broutman LJ, Sahu S, A new theory to predict cumulative fatigue damage in fibreglass reinforced plastics, *Composite materials: Testing and design (2nd conference)* ASTM STP 497, 1972, 170-188

41. Harris B, A Parametric Constant-Life Model for Prediction of the Fatigue Lives of Fibre-Reinforced Plastics. In: Fatigue in Composites, Ed. Harris B, Woodhead Publishing Ltd and CRC Press, 2003, Chapter 3, 546-568

42. Philippidis TP, Eliopoulos EN, A progressive damage mechanics algorithm for life prediction of composite materials under cyclic complex stress, in *Fatigue life prediction of composites and composite structures,* ed. A. P. Vassilopoulos, Woodhead Publishing Ltd and CRC Press, 2010, Chapter 11, 390-436

43. Eliopoulos EN, Philippidis TP, A progressive damage simulation algorithm for GFRP composites under cyclic loading. Part I: Material constitutive model, Compos Sci Tech (2011), doi: 10.1016/j.compscitech.2011.01.023

44. Eliopoulos EN, Philippidis TP, A progressive damage simulation algorithm for GFRP composites under cyclic loading. Part II: FE Implementation and model validation, Compos Sci Tech (2011), doi: 10.1016/j.compscitech.2011.01.025

45. Passipoularidis VA, Philippidis TP, Brøndsted P, Fatigue life prediction in composites using progressive damage modeling under block and spectrum loading, Int J Fatigue 2011; **33**, 132-144

46. Schaff JR, Davidson BD, Life Prediction Methodology for Composite Structures. Part II-Spectrum Fatigue, *Journal of Composite Materials* 1997; **31**(2), 158-181

47. Eliopoulos EN, Numerical simulation of damage progression in GFRP composites under cyclic loading, 2007, Draft version of PhD thesis, University of Patras

48. Release 11.0 documentation for ANSYS, 2007 SAS IP, Inc.

49. Guide to ANSYS programmable features, ANSYS Release 6.1, 2002

50. Antoniou AE, Kensche CW, Philippidis TP, Mechanical behavior of glass/epoxy tubes under combined static loading. Part II: Validation of FEA progressive damage model. Compos Sci Tech 2009; **69**(13), 2248–55

51. Antoniou AE, Van Hemelrijck D, Philippidis TP, Failure prediction for a glass/epoxy cruciform specimen under static biaxial loading. Compos Sci Tech 2010; **70,** 1232-41

52. Philippidis TP, Assimakopoulou TT, Antoniou AE, Passipoularidis VA, Residual strength tests on ISO standard ±45° coupons, OB_TG5_R008, 2005 (http://www.wmc.eu/optimatblades.php)

53. Philippidis TP, Assimakopoulou TT, Antoniou AE, Passipoularidis VA, Residual strength tests on ISO standard ±45° coupons, Main test phase II, OB_TG2_R037, 2006 (http://www.wmc.eu/optimatblades.php)

54. Philippidis TP, Antoniou AE, Assimakopoulou TT & Passipoularidis VA, Fatigue tests on OB unidirectional & multidirectional off-axis coupons Main test phase I. OB_TG2_R030, 2006 (http://www.wmc.eu/optimatblades.php)

55. Krause O, Kensche C, Summary fatigue test report. OB_TG1_R026, 2006 (http://www.wmc.eu/optimatblades.php)

56. Nijssen R, van Wingerde A, Residual strength tests-data and analysis, OB_TG5_R007, 2006 (http://www.wmc.eu/optimatblades.php)

57. Dutton AG, Robertson SJ, Canfer SJ, Blanch MJ, Residual strength testing of OPTIMAT MD specimens−tests by CCLRC-RAL, OB_TG5_R012, 2006 (http://www.wmc.eu/optimatblades.php)

58. Lekou DJ, Rossis K, RESIDUAL STRENGTH TESTS ON STANDARD OB SPECIMENS, OB_TG5_R016, 2006 (http://www.wmc.eu/optimatblades.php)

59. Krause O, Philippidis TP, General test specification, OB_TC_R014, 2005 (http://www.wmc.eu/optimatblades.php)

60. Philippidis TP, Vassilopoulos AP, Fatigue of composite laminates under off-axis loading, Int J Fatigue 1999; **21,** 253-262

61. Philippidis TP, Antoniou AE, Assimakopoulou TT, Passipoularidis VA, Static tests on the standard OB UD and MD off-axis coupons, OB_TG2_R022, 2005 (http://www.wmc.eu/optimatblades.php)

62. Nijssen R, Krause O, Kensche C, Block tests Results and analysis of simple load spectrum tests, OB_TG1_R025, 2005 (http://www.wmc.eu/optimatblades.php)

63. Nijssen R, (NEW) WISPER(X) load spectra Test results and analysis, OB_TG1_R024, 2005 (http://www.wmc.eu/optimatblades.php)

64. Philippidis TP, Passipoularidis VA, Assimakopoulou TT, Antoniou AE, Variable Amplitude Cyclic Tests on Standard OB UD Coupon and ISO $[\pm 45]_S$ performed at UP Main Test Phases I & II. OB_TG2_R031, 2006 (http://www.wmc.eu/optimatblades.php)

65. Kensche C, Final report on tube testing, OB_TG2_R038, 2006 (http://www.wmc.eu/optimatblades.php)

66. Antoniou AE, Kensche CW, Philippidis TP, Mechanical behavior of glass/epoxy tubes under combined static loading. Part I: Experimental, Compos Sci Tech 2009; **69**(13), 2241–47

67. Makris A, Ramault C, Van Hemelrijck D, Biaxial fatigue testing of cruciform composite specimens, *UpWind project,* 2010

9. Appendix: Experimental Data from L-U-R cyclic tests

9.1 Tensile L-U-R tests on the $[0_4]_T$ laminate

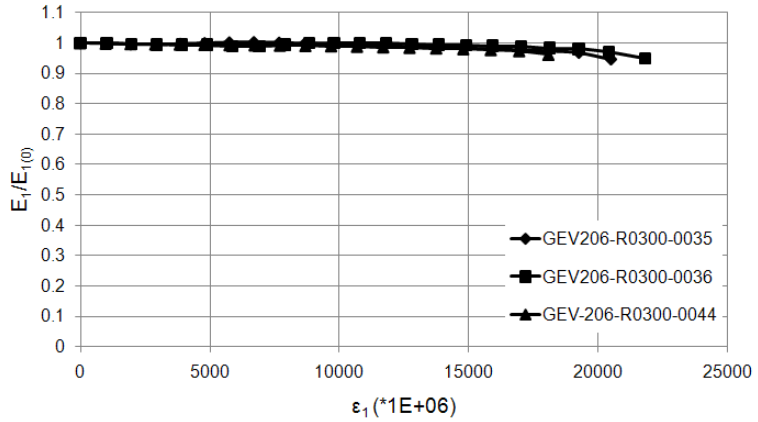

Fig. 106: Modulus degradation parallel to the fibres due to tensile L-U-R cycles vs. the strain level previously reached

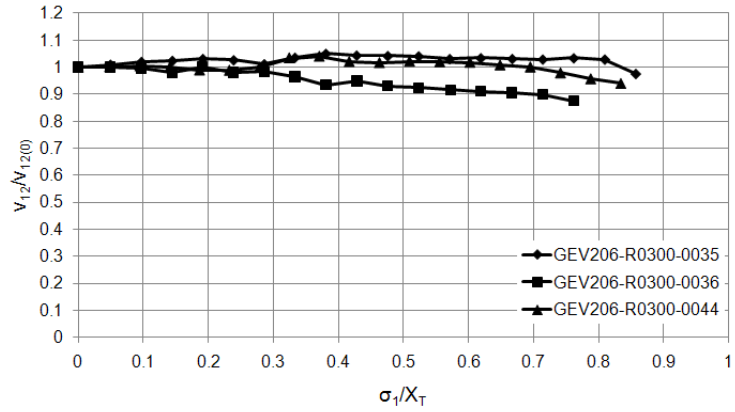

Fig. 107: Major Poisson ratio during the tensile L-U-R tests parallel to the fibres

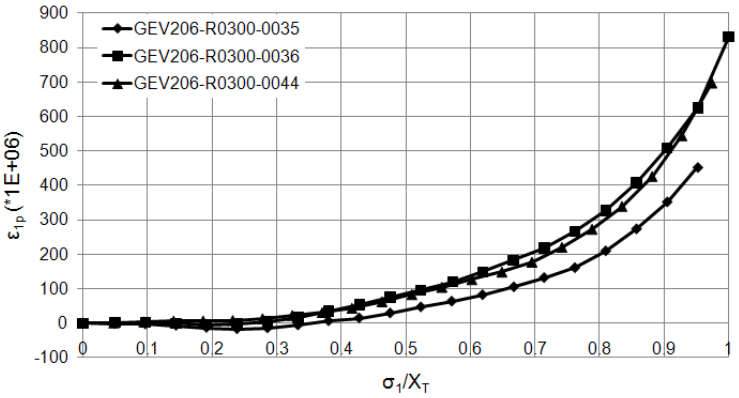

Fig. 108: Permanent strain due to tensile L-U-R cycles parallel to the fibres

9.2 Compressive L-U-R tests on the $[0_4]_T$ laminate

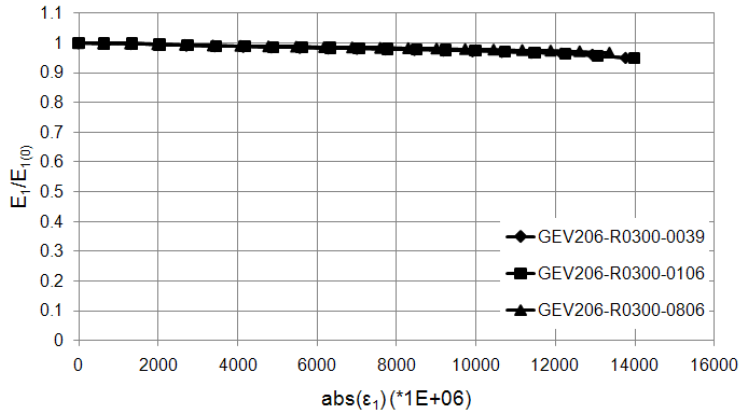

Fig. 109: Modulus degradation parallel to the fibres due to compressive L-U-R cycles vs. the strain level previously reached

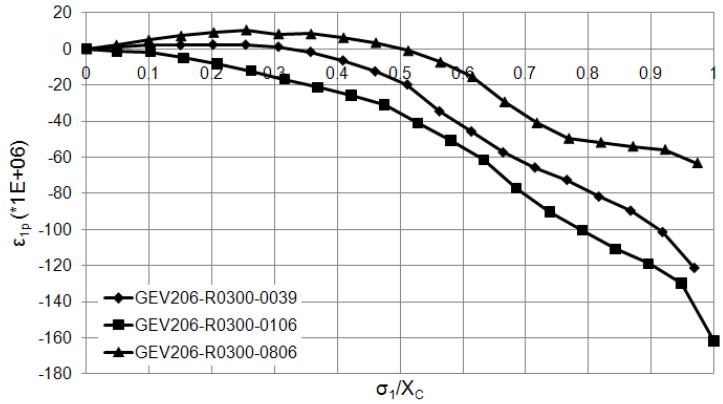

Fig. 110: Permanent strain due to compressive L-U-R cycles parallel to the fibres

9.3 Tensile L-U-R tests on the $[90_7]_T$ laminate

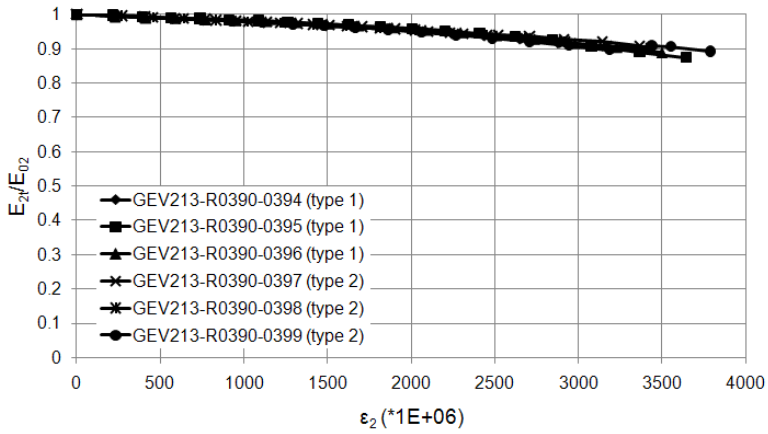

Fig. 111: Modulus degradation transversely to the fibres due to tensile L-U-R cycles vs. the strain level previously reached

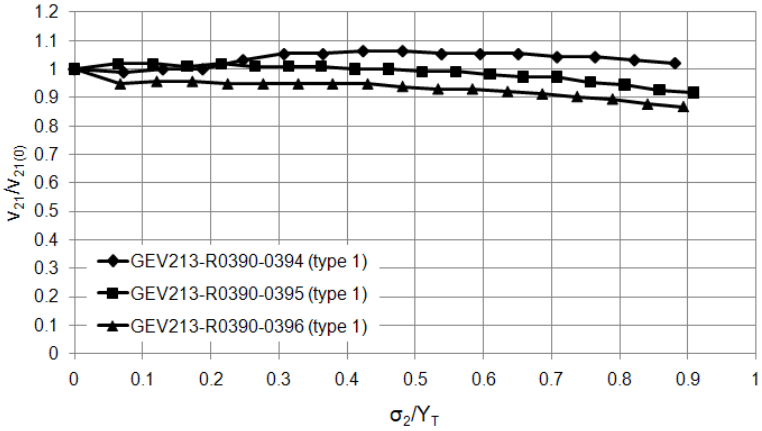

Fig. 112: Minor Poisson ratio during the tensile L-U-R tests transversely to the fibres

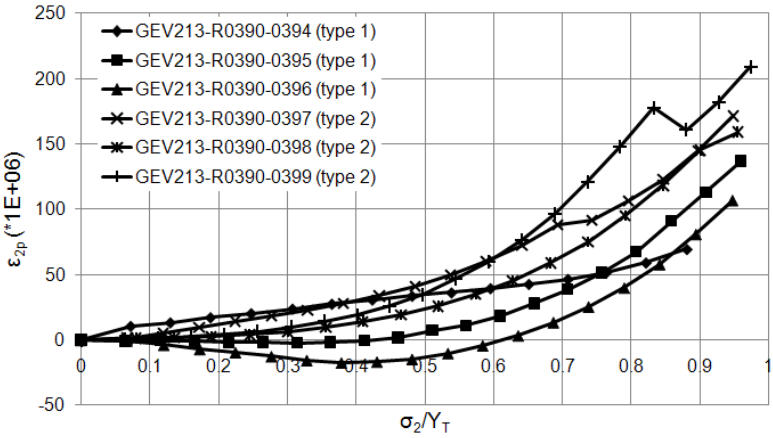

Fig. 113: Permanent strain due to tensile L-U-R cycles transversely to the fibres

9.4 Compressive L-U-R tests on the $[90_7]_T$ laminate

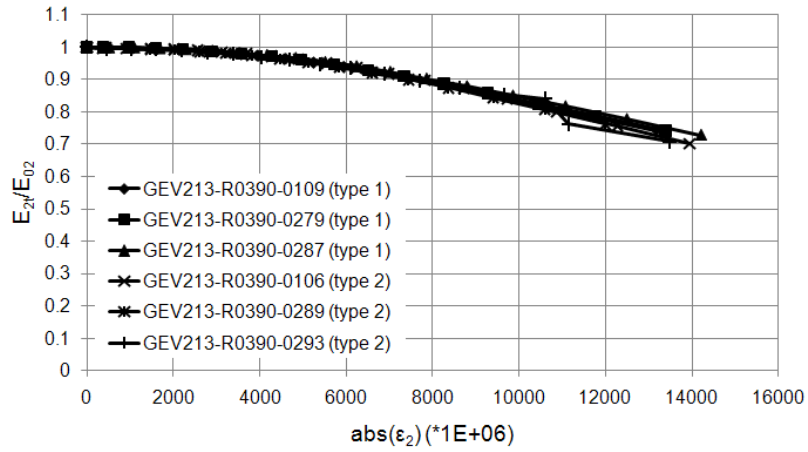

Fig. 114: Modulus degradation transversely to the fibres due to compressive L-U-R cycles vs. the strain level previously reached

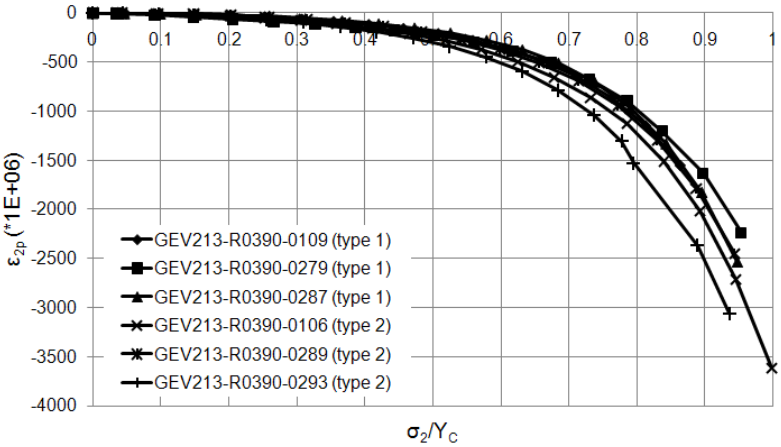

Fig. 115: Permanent strain due to compressive L-U-R cycles transversely to the fibres

9.5 Tensile L-U-R tests on the ISO 14129 $[\pm 45]_S$ coupons

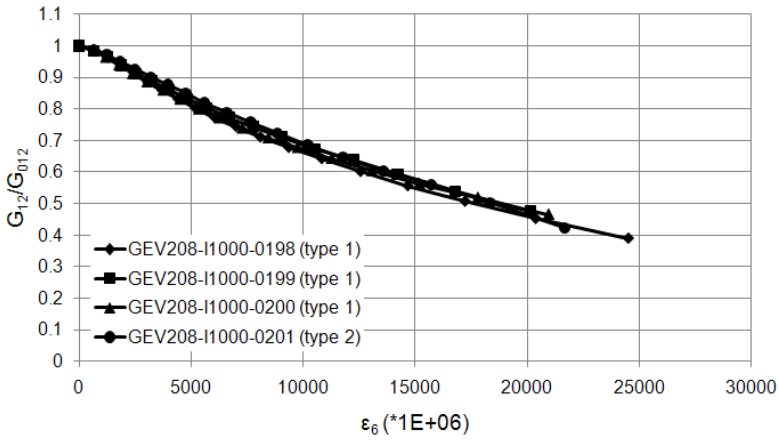

Fig. 116: Shear modulus degradation due to L-U-R cycles vs. the strain level previously reached

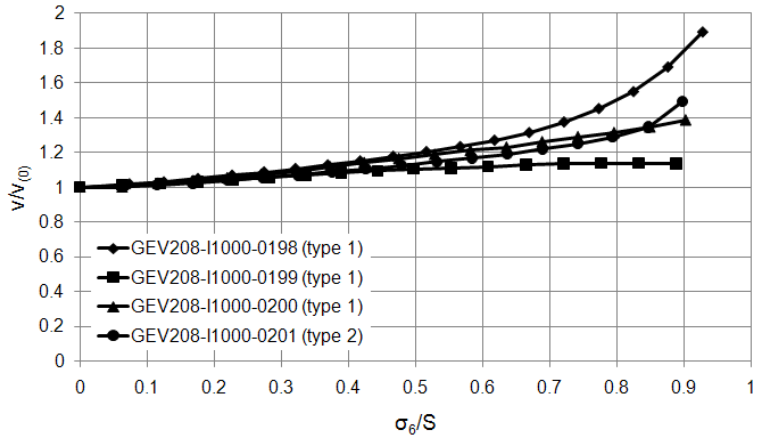

Fig. 117: Poisson ratio during the tensile L-U-R tests on the ISO 14129 $[\pm 45]_S$ coupons

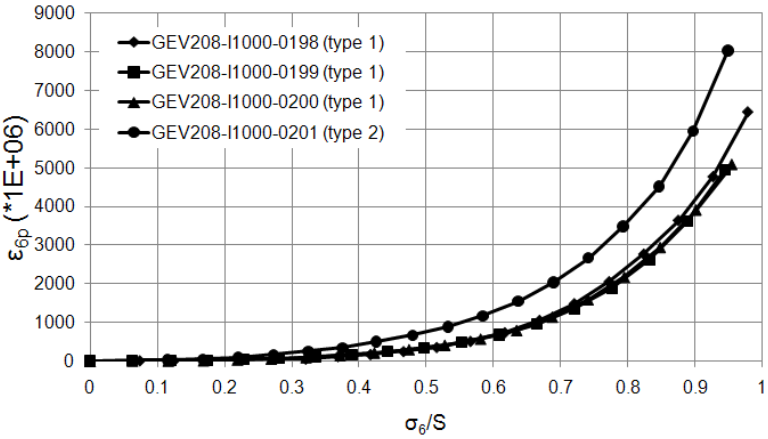

Fig. 118: Permanent shear strain due to L-U-R cycles